CHARACTERIZATION OF CATALYTIC MATERIALS CONTAINING ZEOLITES USING *n*-HEXANE CRACKING REACTION

BY

YUNUSA UMAR

A Thesis Presented to the

DEANSHIP OF GRADUATE STUDIES

KING FAHD UNIVERSITY OF PETROLEUM & MINERALS

DHAHRAN, SAUDI ARABIA

In Partial Fulfillment of the
Requirements for the Degree of

MASTER OF SCIENCE

In

CHEMISTRY

MAY 2001

ProQuest Information and Learning Company
300 North Zeeb Road
P.O. Box 1346
Ann Arbor, MI 48106-1346

KING FAHD UNIVERSITY OF PETROLEUM AND MINERALS

DHAHRAN, SAUDI ARABIA

DEANSHIP OF GRADUATE STUDIES

This thesis, written by **Yunusa Umar** under the direction of his thesis advisor and approved by his thesis committee, has been presented to and accepted by the Dean of Graduate Studies, in partial fulfillment of the requirements for the degree of **MASTER OF SCIENCE IN CHEMISTRY**.

Thesis Committee

Dr. Sami A. I. Barri
Thesis Advisor

Prof. Abdul Rahman A. Al-Arfaj
Member

Dr. Zaki Shakir Seddigi
Member

Dr. Adnan M. Jarallah Al-Amer
Member

Dr. Assad A. Al-Thukair
Department Chairman

Prof. Osama A. Jannadi
Dean, College of Graduate Studies

Date: 30/5/2009

Dedicated to
My Parents,
Brothers and Sisters

ACKNOWLEDGMENT

Gratitude and praise be to Almighty Allah for making it possible for me to accomplish this work successfully.

I wish to register my gratitude and unreserved appreciation to Dr. Sami A. I. Barri who severed as my thesis advisor. The success of this work is credited to his tireless support and priceless idea. I wish to thank the other members of my thesis committee, Prof. Abdul Rahman A. Al-Arfaj, Dr. Zaki Seddigi and Dr. Adnan Jarallah Al-Amer for their constructive suggestion and contribution towards the success of the work and Dr Pasl A. Jalil for his sincere help and contribution.

I am indebted to the chairman of chemistry department Dr. A. A. Al-Thukair for his assistant and help especially in the most difficult times. My special thanks to all faculty members and staff of chemistry department for their support in one way or the other.

My sincere appreciation to the following brothers and friends not only for the moral support and kindness but also for their concern and encouragement in the course of my studies; Bashir A, Tijani J, Mu'azu Abujiya, A Nasir Tukur, Yushau B, Dr. Usman, Dr. Umar A, Shuiab B G, Abdulkareem M, Suleiman Edah, Dr. Umar Y, Shazali A, Danjuma N, Idowu Kasumu, Dr. Kamurudeen A, Abdulkareem B, Salman Y. O, AbdulHameed B, Adeleke H, Adewusi S, Ayinde T, Abiola T, Aman H, El-Rayees Ali, Mazhar M. H, Uwais B, Abdul Hameed, AbdulAziz S, Saeed A, Izzat K, Shafique A.

My profound gratitude and appreciation to my mother, uncles, sisters, brothers, friends and the entire family of Ndace Sunkuso for their affection and concern. Finally, I wish to thank King Fahd University of Petroleum and Minerals for the assistantship and support of this research.

TABLE OF CONTENTS

LIST OF TABLES

LIST OF FIGURES

THESIS ABSTRACT

NAME: **Yunusa Umar**

TITLE: **Characterization of Catalytic Materials Containing Zeolites using *n*-Hexane Cracking Reaction.**

MAJOR FIELD: **Chemistry.**

DATE: **May 2001**

ZSM-5 zeolites precursors were synthesized by hydrothermal crystallization method from aluminosilicate gels in the presence of organic templates: - tetrapropyl ammonium bromide, and diethanolamine at temperatures of 175°C under autogeneous pressure. The materials were characterized by powder X-ray diffraction, Infrared spectroscopy, and benzene adsorption. The course of crystallization was followed by examining the X-ray diffraction pattern of the calcined samples and the optical density ratio of the bands at 550cm^{-1} and 450cm^{-1} in the mid IR region of the structure spectra as a function of crystallization time. For a well crystalline material, the optical density ratio is 0.70; this ratio was found to be less if amorphous silica is present in zeolite.

The catalytic activity of the samples has been evaluated for the *n*-hexane cracking in tubular fixed bed reactor at the temperature range of 300°C to 500°C. The Cracking Mechanism Ratio (CMR) calculated reveals that the n-hexane cracking reaction over the catalyst tested proceeds predominantly via protolytic route and catalytic activity of the TPABr-mediated samples increases with crystallinity. Apparent activation energies are remarkably similar in spite of differences in relative level of activity.

The X-ray, IR and n-hexane cracking activity data suggests that these zeolite precursors are microcrystalline solid material in amorphous matrix with structures similar to that of ZSM-5. The infrared spectroscopy results were correlated with other structural data obtained by X-ray diffraction, adsorption measurements, and also with the results of catalytic test.

MASTER OF SCIENCE DEGREE
KING FAHD UNIVERSITY OF PETROLEUM AND MINERALS
DHAHRAN SAUDIA ARABIA

خلاصة الرسالة

الاســـــــــــم : يـــونـــس عـمـر

عنوان الرسالة : دراسة خواص مواد حفازه محتويه على الزيولايت بواسطة تفاعل تكسير الهكسان .

التـــخـــصـــص : كيمياء

الـــتـــاريـــخ : مايو ٢٠٠١

تم تحضير الزيولايت ZSM-5 بطريقة التبلر الهيدروحرارى من سليكات الألومينوم في وجود مواد عضويه مثل : "Diethanolamine, tetrapropylammonium bromide" عند درجـــة حرارة ١٧٥°م ، وتم دراســـة خواص المواد باستخدام حيود أشعـــة اكس الأطياف تحت الحمراء وامتزاز البنزين ، تم متابعة عمليه التبلر بواسطة حيود أشعة اكس وبالكثافة الضوئية للقم عند ٤٥٠ $^{-1}$سم ، ٥٥٠ $^{-1}$سم في منطقة وسط الأشعة تحت الحمراء ، وقد وجدت الكثافة الضوئية للمادة المتبلره تماماً تساوى ٧ر٠ وتقل بوجود مواد غير متبلره في الزيولايت .

وقد تم دراسة النشاط الحفزى للمواد عن طريق تكسير الهكسان عند درجات حرارة من ٣٠٠°م إلى ٥٠٠°م . وتم حساب CMR ، والتي أثبتت أن التكسير يتم من خلال انتقال بروتونى ووجد أن النشاط الحفزى يزداد بزيادة التبلر .

نتائج حيود أشعة اكس والأطياف تحت الحمراء والتكسير الحفزى للهكسان تشير إلى أن هذا الزيولايت يوجد في وسط غير متبلر ويشبه في تركيبه إلى ZSM-5 .

درجة الماجستير في العلوم
جامعة الملك فهد للبترول والمعادن
الظهران – المملكة العربية السعودية

CHAPTER 1

INTRODUCTION

Microporous (pore diameter ≤ 20A°) inorganic materials such as zeolites admit molecules below a certain size into their extensive internal space, which makes them of considerable interest as heterogeneous catalyst and sorbents[1]. Zeolites, which are widely used in separation, purification, catalysis, ion-exchange processes and organic synthesis for the production of specialty chemicals [2-6] are still finding the potential for more applications. The introduction of amorphous silica-alumina as a solid catalyst[1, 7] was a significant step in the field of heterogeneous catalysis. This materials, with either 13 or 25% Al_2O_3 content was widely used and is still being used today in few cracking and hydrocracking units to produce gasoline, diesel and jet fuel. However, the largest revolution in heterogeneous catalysis occurred at the end of 1960's, when crystalline aluminusilicate (zeolites) were prepared in the acid form and showed a remarkable activity and selectivity for acid catalyzed processes[8, 9]. Since then, the numbers of new development in the field of zeolites as catalyst have grown very quickly.

Natural zeolites were found in vugs and vesicles of basaltic lava, in specific kinds of rocks and in volcanic ash deposits. At least forty species of natural zeolites have been found, however, the difficulty in the purification of natural zeolites hindered their application in industrials processes[10]. It was not until 1950's that the synthetic zeolite became available commercially with the successful development of low temperature synthesis method. Most commercial zeolites are synthetic product made in high purity using inorganic preparative methods.

Zeolites are generally known as crystalline aluminosilicate with tetrahedral framework containing microporous structure with cavities occupied by cations and water molecules both of which have freedom of movement to permit cation exchange and reversible dehydration[11]. According to their structure, zeolites may be classified into one, two or three dimensional pore structure systems with mordenite, ZSM-5 and type A as the representative examples. Zeolites possess distinct characteristics that make them of especially interesting for heterogeneous catalyst and introduce many versatile applications.

The microporous structure is one of the reasons for zeolites to be excellent adsorbents and the uniformity of the pore size of molecular dimension posses the "molecular sieving effect" for the separations[12]. The unique ion-exchange capability of the cations, which are necessary to preserve electric neutrality in the structure, makes it possible to modify the catalytic properties and sorption properties towards a specific application. Their active sites, such as acid sites for instance can be generated in the framework and their strength and concentration can be tailored towards a particular application. The possibility to be regenerated (e.g. by burning carbonaceous material) after deactivation by coke deposition makes them to have special interest in the field of catalysis. All these aforementioned distinct properties of zeolites, which are of paramount important in catalysis, are ultimately dependent on their high thermal and hydrothermal stability. High thermal stability is important since many hydrocarbon reactions require elevated temperatures in order to proceed, while high hydrothermal stability is needed in the regeneration of deactivated catalysts since water vapor is produced in the oxidation of coke deposits.

Zeolite Socony Mobil 5(ZSM-5), a prominent member of high silica zeolite shows outstanding properties as a catalyst for a number of industrial processes dealing with hydrocarbons. The framework structure of this five membered ring zeolite was studied by Kokotailo et al[13] and the general name "pentasil" was proposed for these types of zeolites. The shape selective ZSM-5 zeolite finds applications in various catalytic processes like conversion of methanol to gasoline, xylene isomerization, distillate dewaxing, toluene disproprotioanation, ethylbenzene synthesis.[14, 15] Over the last several years it has been used as an additive in some FCC catalyst for the enhancement of gasoline produced[16].

It has been shown that these zeolites may be modified in various ways to influence reaction selectivity[17], one way of doing so depends on the variation of the crystal size. Small crystals provide less diffusion resistance to reactants and products and as a result, the level of conversion for the catalytic reaction may be enhanced. Whereas large crystals often provide high degree of reaction selectivity because of their small external surface area and the long diffusion path for the product molecules. Almost a decade ago, Jacob[18] reported the synthesis of very small zeolite crystals by interruption of the synthesis process before the onset crystallization stage of this synthesis process. The material was below the detection limit of X-ray powder diffraction but was shown by infrared spectroscopy to consist of microcrystalline zeolitic solid that is similar in structure to ZSM-5. However, more recently Bellusi et al[19] have claimed the material to be mesoporous and show it to have interesting catalytic properties. Therefore it is of interest to further investigate this zeolite precursor in order to establish whether it could be used, as for the ordered mesoporous alumino-silicates, for reactions involving large organic molecules. The scope of this thesis is to synthesis these materials and study their

physicochemical and catalytic properties in order to access their structural and catalytic properties.

1.1 Background

1.1.1 Zeolite Molecular Sieve

Zeolites are hydrated crystalline aluminosilicates with fully cross-linked open framework structure made up of corner-sharing SiO_4 and AlO_4 tetrahedral. The first zeolite, stilbite, was discovered by Cronstedt in 1756[20] who found that the mineral losses water rapidly on heating and thus seems to boil. This observation led to all other minerals that showed this property to be called zeolites, which is derived from the Greek words Zeo meaning "to boil" and lithos meaning "stone". A representative empirical formula of zeolite is

$$\mathbf{M_{2/n}O.Al_2O_3.YSiO_2.ZH_2O}$$

where $Y \geq 2$ according to Lowenstien's rule[21], Al^{3+} does not occupy adjacent tetrahedral site. M represents the exchangeable cation of valence n. M is generally a group II ion, or I although other metal, non-metal or organic cations may also balance the negative charge created by the presence of Al in the structure. Compositionally, zeolite framework can be visualized as being made up of SiO_4 tetrahedral linked together by sharing of oxygen ions. Substitution of Al for Si generates a charge imbalance, necessitating the inclusion of cation. The framework may contain cages and channels of discrete size, which are normally occupied by water molecules[22]. The water may be removed reversibly, generally by application of heat, which leaves intact the crystalline host structure permeated with micropores that may account for greater than 50% of the micro crystal volume.

Considering the channel size, zeolites are conventionally defined as large (12-membered), medium (10-membered), and small (8- membered) pore materials depending on the smallest number of oxygen or T atoms that limit the pore aperture of their largest channel and whose diameter varies between 5 and 20A°. With these well-defined channels and cages, the zeolite may be classified as a molecular sieve.

The term molecular sieve was coined by McBain (1992) to describe a material with selective adsorption properties capable of separating components of a mixture on the basis of a difference in molecular size and shape. Since then nomenclature of this kind of porous material seems to be ambiguous. The success of synthetic crystalline aluminosilicates, in particular the emergence of the new family of aluminophospahate[23] ($AlPO_4$) and silicoaluminophospahate[24] (SAPO), metal-containing aluminophospahate[25] (MeAPO), and metal containing silicoaluminophospahate[26] (MeASO), made the concept of zeolite and molecular sieves more intricate. In broad sense, zeolites are molecular sieves. Strictly speaking zeolites are crystalline aluminosilicates with molecular sieve properties.

Although zeolites were first identified as a class of minerals in 1756, attempts artificially to synthesize zeolitic materials did not begin until 1862. Early attempts concentrated on simulating the high temperature and pressure (T>200°, P>100bar) of geological conditions under which natural zeolites were believed to form. However, it was not until 1948 that Barrer[27] reported the successful synthesis of a zeolitic material without the natural counter part. The first large scale methodologies for the synthesis of zeolite was pioneered by Milton et. al at the Union Carbide Laboratories in the late 1940's who developed hydrothermal zeolite synthesis at low temperature (100°C) and low autogenous pressure using alkaline metal aluminosilicate. The next major advance in zeolite synthesis

occurred in 1961, when Barrer and Deny[28] reported the synthesis of several already-known zeolite structures including zeolite A, using organic alkylammonium cations instead of alkali metal cations. Also in 1961, Keer and kokotailo[29] reported the synthesis of a zeolite designated ZK-4 that is isostructural with zeolite A (SiO_2/Al_2O_3 = 2.0) but whose SiO_2/Al_2O_3 is 3.4. It was later disclosed that this zeolite was synthesized from a reaction mixture that contained both tetra methyl ammonium ions and sodium ions[30].

The use of organic cation which allowed the synthesis of zeolite with much higher Si /Al ratio increased rapidly, this research efforts directed at the use of organic cation led to the discovery of many new zeolites[31, 32]. The most commercially interesting of these is the high siliceous material designated as ZSM-5 (Zeolite Socony Mobil number 5) developed by Mobil scientist[33]. ZSM-5 has been synthesized over a range of silica-alumina ratio (of about 10 to greater than 8000) from a reaction mixture containing sodium and tetrapropyl ammonium ions at temperatures above 100°C. For the more siliceous varieties, Falanigen and co-workers[34] named their material silicalite even though it has the same frame work structure as ZSM-5.

Most of the shape selective reactions used by the industries involves catalyst-containing zeolite having diameter between 0.5 and 0.6nm. However, the necessity for treating heavier feeds, as well as for synthesizing large molecules used as commodities and fine chemicals, created an ever-growing interest in expanding the pore sizes of zeolite material. Following this line, Wilson and co-worker[23] disclosed the synthesis of the first so-called ultra large pore crystalline micro porous aluminophosphate AlPO4-8 which contain 14-membered rings about 8.0nm diameter. This stimulated further investigation on the other ultra large pore molecular sieves such as VPI-5 (Davis et al 1988)[35], colverite[36] (Etermenn et al 1991), JDF-20[37] (Jones et al) and UTD-1[38]. However, these

materials suffer from limited thermal stability and negligible activity because their framework is electrically neutral.

Pillared clays another class of microporous solids; with rectangular pores about $0.8A^{\circ}$ x 1.4 nm in size were studied as possible component of catalyst[39]. Pillaring reagents and drying agents can be manipulated to obtain expanded clay minerals that contain both micropores and mesopores[40]. Following the definition[41] accepted by IUPAC, porous materials are divided into three classes: microporous (<2nm), mesoporous (2 – 50nm) and macroporous (>50nm). Table 1 shows some zeolites and molecular sieves with variable pore sizes.

Attempts to increase the activity of the existing microporous materials for the processing large molecules were also undertaken. This approach involves the generation of mesopores in the crystallites of the microporous zeolite. Cartlidge et al. and Bayerlain et al. reported the formation of the mesopores of mixed sizes in the range 10 – 20nm during the dealumination of zeolite Y and CSZ-1[42, 43]. Further investigation by Croma[44] reveals that dealumination by $SiCl_4$ generates little mesoporousity and preserved must of the microporousity. Whereas the dealumination by steam produced many more mesoporous area within the material while some of the microporousity was destroyed. Catalytic activity for the normal heptane cracking of zeolite Y samples dealuminated by $SiCl_4$ treatment was found to be higher than those dealuminated by steam. However, when the two series of the dealuminated Y zeolite were used to crack vacuum gas oil, containing molecules too large to penetrate deep into the micropores system, the steam dealuminated samples, which contain a greater portion of mesoporousity gave a higher conversion. This method of formation of secondary mesoporous system by steaming the microporous solid can only be adequate for special cases. Low temperature reactions that

require moderate temperature for catalyst regeneration gives good selectivity and activity due the formation of mesopores by steam treating zeolite during activation. While the generation of the catalyst at high temperature changes the mesoporousity of the catalyst in an uncontrollable way. Thus other general solution needs to be explored. Recently Yanagiswa et al[45] reported the synthesis of the mesoporous silica with uniform pore sizes. Shortly after, researchers at Mobil Corporation discovered a new family of mesoporous crystalline alumino silicates designated as M415[46, 47] which resulted in worldwide resurgence in heterogeneous catalysis. One of the members of this family called MCM-41 shows a hexagonal array of uniform mesopores ranging between 2 and 10nm diameter depending on the template and synthesis conditions used.

1.1.2 Fundamentals of Zeolite Structure

The framework of molecular sieves, zeolite in particular, is an extensive three-dimensional network composed of joined $[SiO_4]^{4-}$ and $[AlO_4]^{5-}$ coordinated polyhedron. By definition, these tetrahedra are arranged such that the oxygen at each tetrahedral corner is shared with that of identical tetrahedral containing either Si or Al in its center. The tetrahedral form cages and channels of molecular dimensions and the –2 oxidation state of each oxygen is accounted for. Each silicon ion has its +4 charge balanced by the four tetrahedral oxygens and the silica tetrahedral are therefore electrically neutral while each aluminium tetrahedral as a residual charge of –1 since the trivalent aluminium is bonded to four oxygen anions (fig 1.1a). To maintain electrical neutrality, this negative charge on aluminium tetrahedral are compensated by the cations (usually sodium) present during the synthesis and kept in the interstices of the structure upon crystallization. These cations can

Table 1. Pore Definition of Zeolites and Molecular Sieves[48].

Pore Size (A°)	Definition	Typical material	Ring Size	Pore Diameter (A°)
>500	Macroporous			
20-500	Mesoporous	MCM-41		15-100
<20	Microporous			
	Ultra large pore	Cloverite	20	6.0 x 13.2
		JDF-20	20	6.2 x 14.5
		VPI-5	18	12.1
		$AlPO_4$-8	14	7.9 x 8.7
	Large pore	Faujisite	12	7.4
		$AlPO_4$-5	12	7.3
		ZSM-12	12	5.5 x5.9
	Medium pore	ZSM-48	10	5.3 x 5.6
		ZSM-11	10	5.1 x 5.5
		ZSM-5	10	5.3 x 5.6
				5.1 x 5.5
	Small pore	CaA	8	4.2
		SAPO-34	8	4.3

easily be exchange for other cations. Ion exchange therefore represents the most direct and useful method for the alteration of zeolite properties.

The primary building unit of zeolite is the individual tetrahedral unit combined into a more complicated secondary building units (SBU)[49]. These are inter connected to form a wide range of polyhedra, which are in turn connected to form the infinitely extended frame works of the various specific zeolites structure. The distribution of tetrahedra in a crystal is not entirely random in amorphous and crystalline aluminosilicates. According the so called Lowenstein[21] rule Al-O-Al linkages in zeolite framework are forbidden, as a result, all aluminate tetrahedra must be linked to four silicate tetrahedra, but a silicate tetrahedron may have five different possible environment: Si (0Al, 4Si), Si (1Al, 3Si), Si (2Al, 2Si), Si (3Al, 1Si), Si (4Al, 0Si).

The framework of ZSM-5 contains a novel configuration of linked tetrahedra as shown in fig1.1b and consist of eight five member rings, These ZSM-5 units join through edges to form chains as shown in fig1.1b, the chains which extended to Z- axis to form sheets and the linking of the sheets lead to a three dimensional framework structure. Rings consisting of five O atoms are evident in this structure; the name *pentasil* is therefore used to describe it.

According to Kokotailo et al[50] ZSM-5 crystallizes in the ideal orthorhombic system with space group Pnma and lattice constant a= 20.1, b = 19.9, and c = 13.4A°; monoclinic symmetry has also been observed. The ZSM-5 framework contains two intersecting channel system, one sinusoidal 10-ring tunnel system runs along the a-axis [001] and has a near circular (5.4 to 5.7A°) opening. The other 10 ring tunnel runs straight along the b-axis [010] and have elliptical openings (5.1 x 5.7A°)[51, 52] indicated in fig 1.1d. the channel intersection have a diameter of about 9A° and are probably the locus of strong

acid site and the catalytic activity on ZSM-5[53]. The size of these openings is between that of the large pore, 12-membered ring opening of faujasite and the small pore, 8-membered ring opening of zeolite A.

Zeolites ZSM-5 and ZSM-11 are structurally related to one another[54]. Aluminosilicate sheets composed of connected chains of 5-member rings joined together through an inversion center will structurally define the ZSM-5 zeolite. These sheet of connected chains of 5-member rings, if joined together not through a center of inversion but through a mirror plane, will generate to ZSM-11 structure.

1.1.3 Microporous System in Zeolites

Shape selectivity provided by micro porous structures of zeolites are of great importance in hydrocarbon transformation. Both product distribution and rate of coke deactivation largely depend on shape selectivity, since zeolites with different crystalline structure can be synthesized, the shape selective properties can be altered to great extend. In heterogeneous catalysis the reaction proceeds through several steps: diffusion and adsorption of the reactant, formation of the activated intermediate, reaction and finally desorption and diffusion of the product. The shape selectivity principle is based on these different steps and result to different types of shape selectivity observed over zeolites[55].

Reactant selectivity: resulting in exclusion of molecules too large to diffuse into the zeolite pore. Since the active centers are located within the cavities or channels, the reactant should diffuse within the channels through the zeolite pores. Therefore only molecules which size is small enough penetrate the cavities and thus will interact with the active site. This type of selectivity is due to sieving properties of zeolites. An example is the selective cracking of linear with respect to branched paraffins in zeolites A (fig1.2a).

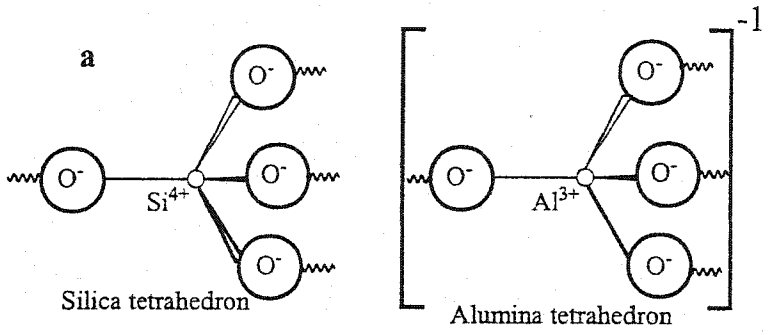

Primary Building Blocks of Zeolites

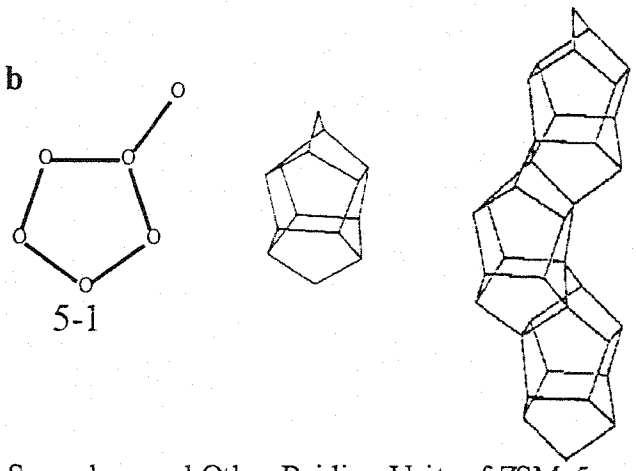

Secondary and Other Buiding Units of ZSM-5

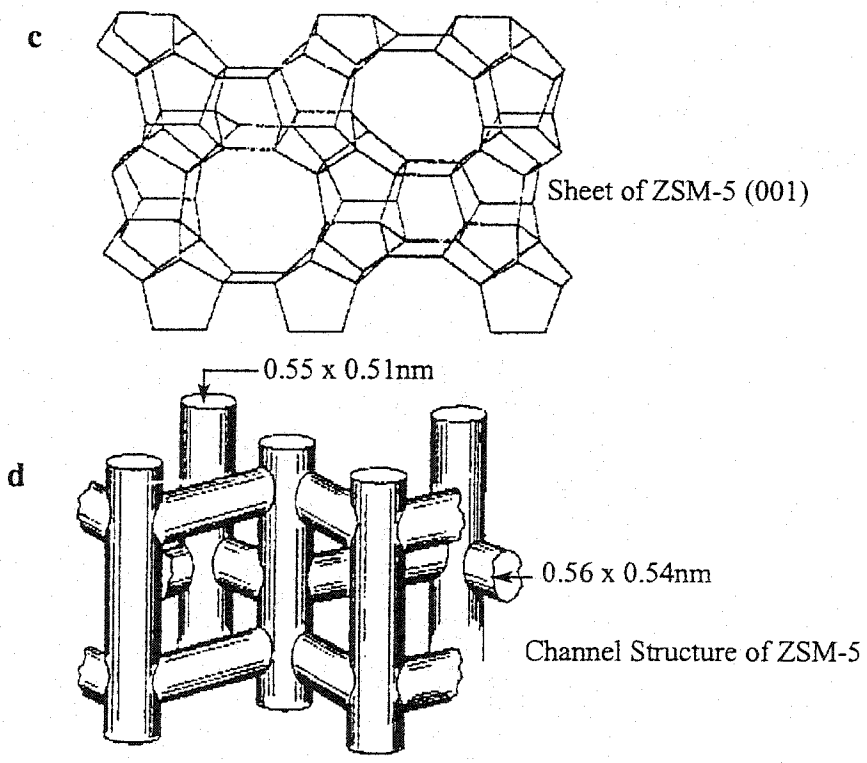

Figure 1.1 Building units and structures of ZSM-5[13, 51]

Product selectivity: - allows only sufficiently small molecules formed during the reaction to diffuse out side the pores, while the molecules that are bulky to diffuse out side the pores are either converted to less bulky molecules, e.g. through equilibrium reaction or they transformed into polymers or coke that eventually deactivate the catalyst. An example is the alkylation of toluene with methanol on ZSM-5 zeolite (fig1.2b). The selectivity of the para isomer is enhanced due to its three orders of magnitude large diffusivity with respect to the ortho and meta isomers. Similarly, when the catalytic reaction within the pores or channels produces large or bulky molecules the slow diffusion of the product out of the small zeolite pores might hinder the reaction. Indeed the slow diffusion will increase the contact time which either will allow a further transformation of the product into a less bulky one or will degrade totally leading to catalyst deactivation. This type of shape selectivity has been called " Reversed molecular size selectivity".[55]

Restricted transition state selectivity: - occurs when certain reactions are prevented because the corresponding transition state would require more space than available in the cavities or pores. Neither the reactant or product molecules are prevented from diffusing through the pores. Reactions requiring smaller transition state proceed unhindered. An example is the bimolecular transalkylation reaction of dimethylebenzenes, in which the formation of the 1,3,5-isomer is hindered, due to size of the reaction intermediate, which overcomes the pore diameter (fig1.2c).

Molecular traffic control selectivity[56]: - occurs when the reactant can diffuse inside preferentially through a given type of pore and the product diffuses through another type of pores, according to their molecular size. This type of selectivity is exhibited by zeolites possessing two types of channel systems (e.g. ZSM-5), having different pore

openings and geometry. In some cases this can minimize the effect of counter diffusion, so enhancing reaction rate. The shape selectivity in zeolite is often characterized by its "constraint index," which is the ratio of the cracking rate constant of for n-hexane and 3-methylpentane. Large pore zeolites, such as zeolites X, Y, B, or L have constraint indices smaller than 1; medium-pore zeolites such as ZSM-5, ZSM-11, or ZSM-22 have constraint indices between 1 and 12. A high constraint index is indicative of higher shape selectivity[57]. The constraint index increases with increase in tempreture[58, 59].

1.1.4 Ion Exchange and Acidity of Zeolites

The concept that solid surface may be acidic arose from the observation that hydrocarbon reactions such as cracking that are catalyzed by acid treated clays or silica alumina, give rise to a much different product distribution than those obtained by thermal reaction. These solid catalyzed reactions exhibit features similar to reactions catalyzed by mineral acids. An acid site may be of the Bronsted type, in which it donates a proton to an unsaturated hydrocarbon, or Lewis type, in which it acts as an electron acceptor, removing a hydride ion from hydrocarbon.

To produce the zeolite acid catalyst, it is necessary to replace the cations present in the freshly synthesized material with protons. At first glance the most obvious way to replace the alkali metal or quaternary ammonium cations in a zeolite with a proton is to simply treat the zeolite with aqueous acidic solutions. This treatment, however, dissolves at least a portion of the aluminum framework[60-65]. Another approach for the preparation of hydrogen zeolite consists of thermal decomposition of ammonium form to produce ammonia and the hydrogen zeolite.

As synthesized ZSM-5, which generally contains sodium and tetrapropyl,

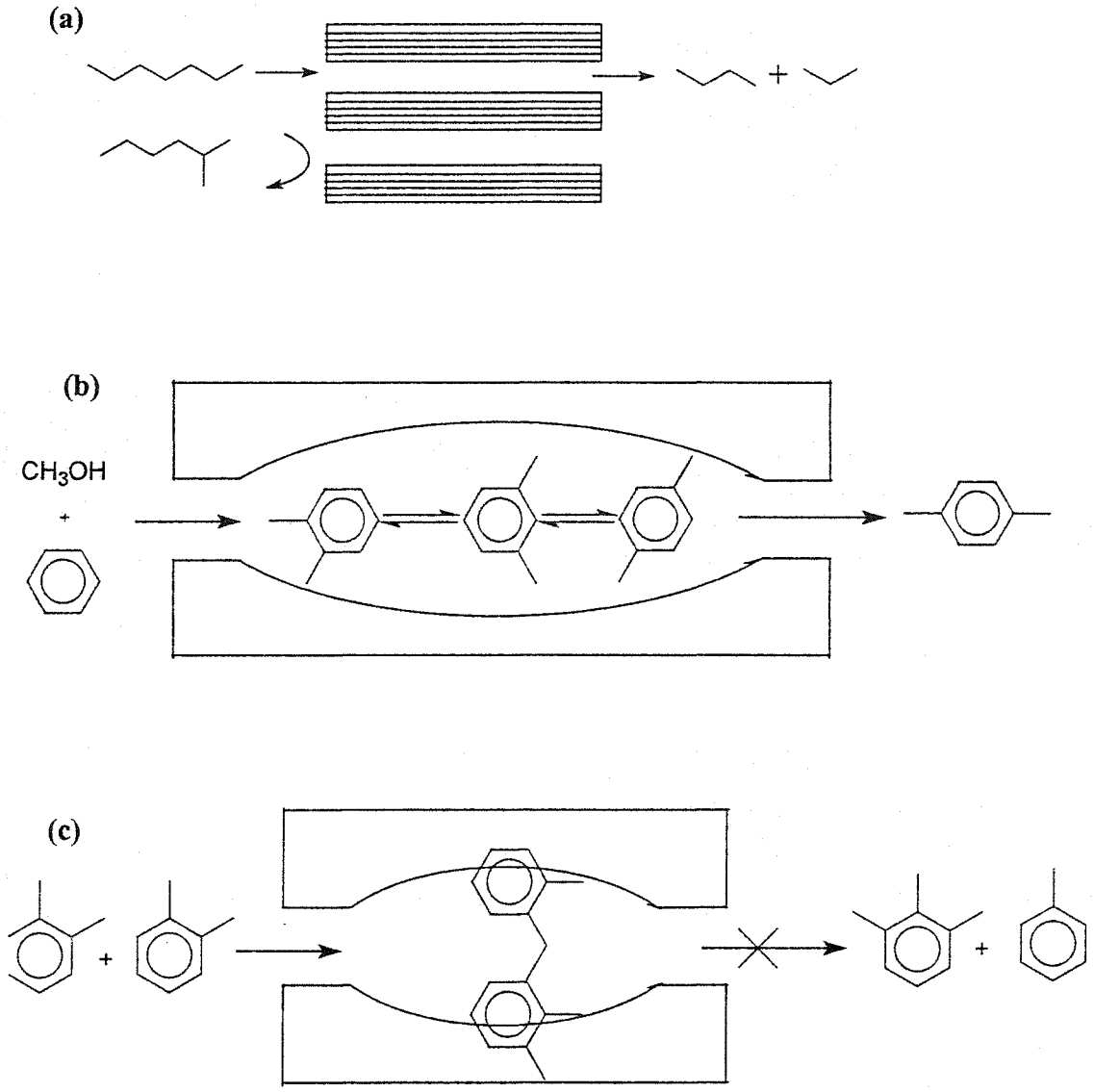

Figure 1.2: Diagram depicting the three types of selectivity[54]: (a) reactant selectivity, (b) product selectivity and (c) restricted transition-state selectivity.

ammonium ion is not readily susceptible to ion exchange. The tetrapropyl ammonium cation is too large to be exchange from the zeolite so it is thermally degraded and the degraded and degradation products are purged from the zeolite to yield the sodium and the hydrogen zeolite, which is then converted to ammonium form by simple cation exchange. Inui et al. reported that after calcinations to remove tetrapropyl ammonium cations, ZSM-5 contains about 17% protons with the remainder of the cations being sodium. The remaining sodium cations can be removed through exchange treatments, which produce the complete protonated material. Subsequent ion exchange is normally done with an aqueous ammonium salt to produce the ammonium ion form. This can be calcined further to produce the acid form[60, 66-69]. The proton is rendered acidic through the interaction between the unshared pair of electrons on the oxygen atom and the unoccupied orbital of the aluminium atom[70], which weakens the bond between the oxygen atom and proton coordinated to it so that the proton has donor acidity[71].

One of the first methods of preparation of acidic zeolite was based upon treatment with ammonium chloride vapor at about 300°C[72-73]. When ammonium exchanged zeolite was subsequently heated in vacuum and treated with oxygen at 350°C, it oxidizes to form acidic zeolite, nitrogen and water. Study conducted by Inui et al. on acidity of ZSM-5 treated with aqueous nitric, hydrochloric and sulphuric acids, as well as ammonium salts of these acids, revealed that 1.0M ammonium nitrate produced the best catalyst having the greatest acidity. This treatment was determined to have the largest amount of strongly bound ammonia and the degree of proton exchange was 89%. Some investigators however, reported that higher degrees of exchange could be obtained by repeating batch wise exchange treatment[62-68, 74].

The final step in producing acidic zeolite involves thermal decomposition of ammonium form into ammonia leaving proton as the counter ions. Deammoniation of zeolite ZSM-5 is typically accomplished at temperatures around 500°C, but it can be done at 300 to 340°C under vacuum[75]. Generally, heat treatment influences the state and localization of aluminium in zeolites. When the temperature of treatment is lower or equal to 300°C, essentially Bronsted acid sites are generated by calcinations of the ammonium form of zeolites. At higher temperatures, however, e.g. 500°C, dehydroxylation take place resulting in the formation of one Lewis sites from two Bronzed sites. Figure 1.3 shows possible types of structures to be present at various stages of treatment of silica rich zeolite.

1.2 Objective

Solid precursor to the synthesis of ZSM-5 was reported to have interesting catalytic properties. Jacobs[18] suggested that it is microcrystalline ZSM-5 and supported his claim with characterization by infrared spectroscopy. Bellusi et al[19]., however claimed that it is mesoporous material and provided the catalytic performance of the precursor in propene oligomerization and liquid phase alkylation of benzene with propene as evidence for this material. Normal hexane cracking reaction is very useful in evaluation of catalyst performance; it is therefore the objective of this work to synthesize these solid precursors and assess their catalytic performance using n-hexane cracking. The present work will contribute to the understanding of the nature of this.

Succinctly, the research work has focused on the following outline.

- Synthesize a series of material on the crystallization curve of ZSM-5

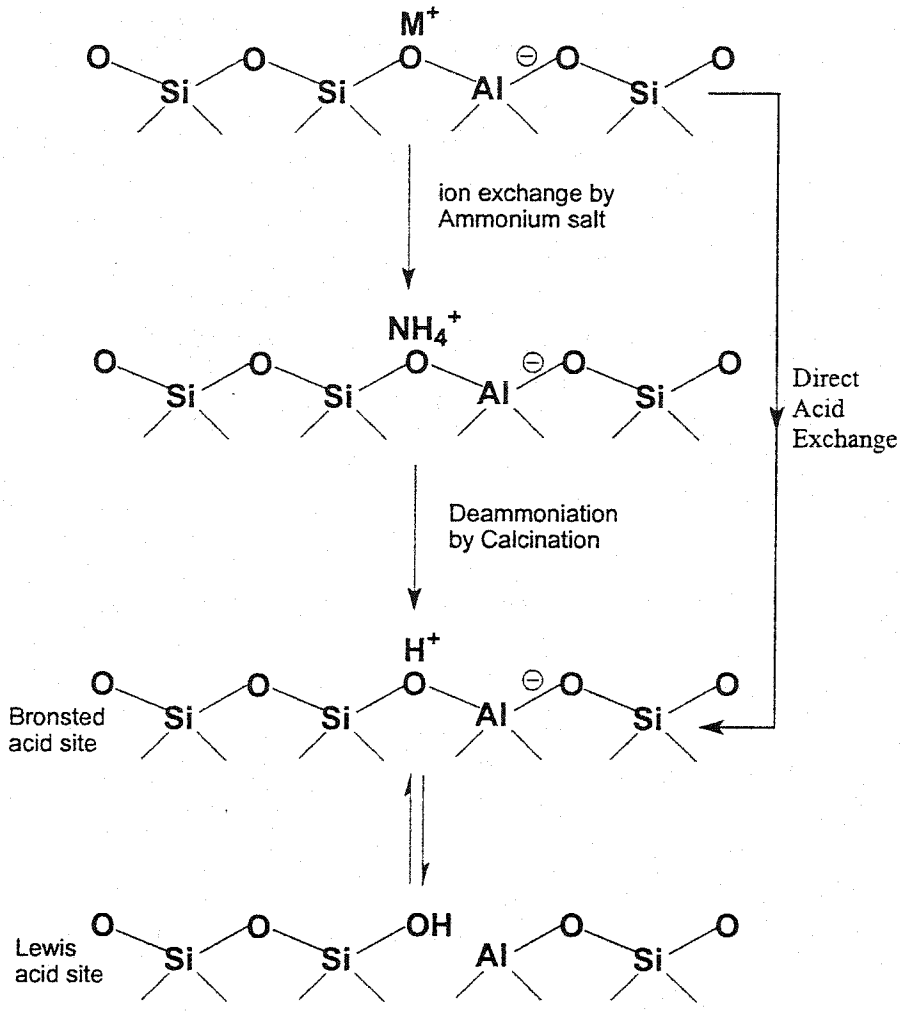

Figure 1.3: Diagram showing surface of zeolite framework[80]

- Characterize these materials with X-ray diffraction, FTIR spectroscopy, and adsorption measurement.
- Evaluate their catalytic performance using n-hexane cracking reaction test.
- Analyze the data to compare the catalytic performance of the precursor material and its physiochemical properties with those of ZSM-5.

CHAPTER 2

LITERATURE REVIEW

2.1 Synthesis of Microporous Materials

Though zeolites can be prepared from non-aqueous synthesis mixture[76], they are almost exclusively synthesized under mild hydrothermal condition, and under autogeneous pressure, from a solution containing silicon and aluminium compound in the presence sodium salt. Such conditions are typical of those found in the earth's crust where some zeolites are found naturally. The versatility of the hydrothermal technique derives from extremely solvating ability of water under these conditions. This allows the dissolution and mixing of the reagents to form an inhomogeneous gel in the initial stages of the reaction. At the later time the nucleation centers are formed which subsequently grow as the reaction proceeds to form the final crystalline product[10]. The precise zeolite formed is determined by the reactants and the particular synthesis conditions used, such as temperature, time, PH, particularly critical is the templating ion. The templating ion is usually organic cation around which the aluminusilicate lattice is formed, so that the tunnel size is determine by the templating cation.

The formation of the ZSM-5 phase as been reported[77-80] to depend on the SiO_2/Al_2O_3, TPA^+/SiO_2, and OH/SiO_2, as well as duration and temperature of synthesis. Since the discovery of ZSM-5 in 1972, it has been synthesized over a wide range of SiO_2/Al_2O_3 ranging from 15 to infinity[33,34,31]. However attempt to prepare zeolite ZSM-5 of SiO_2/Al_2O_3 ratio less than 15 resulted in the crystallization of mordenite or other less

silica rich phases. Several workers[82-85] have investigated the influence of the aluminum content on the rate of ZSM-5 crystallization, all other factors remained unchanged. They reported that crystallization rate for the formation of ZSM-5 structure increases as the aluminum content of the gel decreases, with a rapid increase in rate above SiO_2/Al_2O_3 of 100. This however, is opposite to the normal hydrothermal behavior of such systems; higher Si/Al ratio gives a system with higher viscosity of the solution and lower reaction rate.

An immediate application of the effect of the Si/Al ratio on the crystallization rate was reported Chen et al.[86] who demonstrated that a much faster crystallization will be expected if instead of adding aluminum at once to the synthesis mixture it is added gradually. In fact, the synthesis time when Aluminum is added gradually is reduced to one tenth of the time required for a synthesis in which aluminum is added at once.

Zeolite materials are meta-stable phases, which are thermodynamically unstable with respect to dense oxide phases. It is therefore clear that the formation of zeolitic material can not be rationalized on the basis of thermodynamics alone, kinetics must play a large part in determining which particular phases are formed. Time is therefore also important factor governing the product formed in zeolite synthesis. The synthesis of zeolitic material obeys Ostwald's law of successive reaction[10]. This state that an initial meta-stable phase successively converted into a thermodynamically more stable phase until the most stable is produced. A typical example is the crystallization sequence reported Dai et al[77] in the preparation of ZSM-5 from organic free system. He obseverd that the initially formed ZSM-5 transformed into mordenite phase, followed by the appearance of quartz phase with further crystallization time. The temperature, however, can also influence the type of product to crystallize. Increasing temperature will give rise

to more dense products, as the fraction of water in the liquid phase, which has to stabilize the porous products by filling the pores, will drop. Therefore the existence of an upper limit for the formation zeolites is to be expected. The temperature range for the crystallization increases with increasing Si/Al ratio in the zeolite, from 20°C to 125°C for the aluminum rich zeolites, A and X zeolites, from 100°C to 150°C for intermediate Si/Al zeolites, L, omega and mordenite and from near 125°C to 200°C for high-silica zeolite as exhibited by ZSM-5.[87-88]

Kulkarani et al.[89] discussed the role of PH on the aluminum distribution in the framework of ZSM-5 and experimentally showed that PH of 6.7 was the lowest limit for the crystallization of ZSM-5. Obviously a longer period of time for crystallization at this PH was required. However, the minimum autoclaving time (60hours) was found for the PH range 8.6-11.0, it was observe that the final PH of the reaction is always higher than the initial PH.

Argauer and Landolt[33] were the first to systematically investigate the formation of medium pore ZSM-5 zeolite from aqueous alumina-silica gel using tetra propylammonium (TPA) as template molecule. The concept that the organic molecule (template) used in molecular sieve synthesis were not simple acting as charge balancing cations, and were in fact playing an active role in directing the synthesis of a particular molecular sieve structure, was first suggested because of the close correlation that was often seen between the size and the shape of the template. In the synthesis of ZSM-5 using tetra propylammonium cation, it was found that the cation is located at the intersecting channel system, with the four alkyl chains lying along the four individual channels[34]. These and other observation lead to the suggestion that the organic molecules were acting as templates and building the molecular sieves structure around themselves by

directing the condensing oxide tetra hedral into a particular geometry[90-91]. However, it is clear that the situation is very much complex than originally suggested. For example it is true that NPr_4^+ is an effective structure directing agent for the synthesis of ZSM-5 zeolite, but ZSM-5 was latter synthesized from mixture containing other quaternary ammonium cations such as amines, alcohols, ethers, or certain transition metal complexes. The synthesis of ZSM-5 in the absence of any organic compound has been reported.[77]

Araya[92] examined the relative role of various agents in the synthesis of ZSM-5 starting with the aluminosilicate composition of $10Na_2O$-Al_2O_3-$30SiO_2$-10organic-$3000H_2O$, the crystallization of ZSM-5 was observed at 100°C with the following organic reagents: tetra propylammonium bromide (TPABr), hexane-1, 6-diamine (HXDM), hexane-1, 6-diol (HXDL), piperazine (PIPZ), and no organics. Only TPABr appears to be a true templating agent and stabilizes the ZSM-5 structure. Such a stabilization effect was derived from PH measurements. The PH increase during the crystallization is highest for TPABr templated synthesis; similar to the template free synthesis is the case of HXDL and the PIPZ and intermediate for HXDM. Such studies illustrate the fact that most of the organic agents in ZSM-5 synthesis do not play the active role of true templates but are only passive void fillers accommodated in micropores. This studies was further completed by van Santel et al.[93] who show both a faster crystallization in the presence of TPAOH and high stability of ZSM-5 in the mother liquor in the presence of the organic reagent. The dual role of the TPA^+ is illustrated here: it increases the nucleation rate (template effect) and its incorporation in the network of micropores stabilizes the hydrophobic molecular sieve to such extend that no further transformation is observed.

Another important variable that determine the type of zeolite obtained is silica and alumina source. Mostowicz and Sand[94] examined the crystallization of ZSM-5 using four

different sources of silica; they reported that the crystallization using either colloidal sol (Ludox) or silicate produced a very sharp crystallization due to rapid nucleation of the desired structure after five hours. However, precipitated silica (QUSO-F-20) resulted in a lengthening of the induction period before crystals were observed. Crystallization was observed to be completed after 15hours using Cabosil (fumed silica) and beyond 25 hours QUSO, while the Ludox and silicate produced crystalline material within 6 to 8 hours.

2.2 Mechanism of Zeolite Crystallization

Conceptually, the crystallization of zeolitic material can be considered to follow an idealized process involving three states. Initial dissolution of the starting reagents by the solvent water to form a randomly distributed array of reaction components followed by an ordering of some of these components on the microscopic level (i.e. formation of nucleation site) and finally the growth of these nucleation sites to form the final material in which long range order is observed i.e. formation of crystal[95].

Several mechanisms for the zealite crystallization were proposed[96-102], however, the solution mediated transport and the solid hydrogel transformation mechanistic processes comprises the two extremes of the range. Zhadanov et al.[103-104], Sand et al.[99], Kacirek and Lechert[105] presented evidences for crystallization by solution mediated transport mechanism. This involves dissolution of the reagent in the solution phase followed by transport of the dissolved silicate/phosphate species via solution- mediated diffusion to the nucleation sites where crystal growth takes place. More recently, a convincing evidence of this mechanistic process are provided by Ueda et. al[95] who crystallized zeolites Y, S, and P from clear solutions and Testa et al[106] who crystallized

zeolites ZSM-5 and ZSM-11 from similar solutions. In these cases the possibility of solid-solid transformation appears to be ruled out.

The solid hydrogel transformation mechanism which is thought to involve the re-organization of the solid phase from the initially amorphous state to one with long-range order (crystallized zeolite) was reported by Breck and Flanigen[107] and McNicol[108]. This type of mechanism was demonstrated by Xu et al.[109] in the synthesis of ZSM-5 and ZSM-11 by first dehydrating an amorphous aluminosilicate set at 550°C, and then treating this mixture with liquid triethylamine and ethylene diamine in the absence of water at 160°C. They observe no silicate or aluminate species in the liquid phase during the crystallization of the zeolite indicating that a solid phase transformation must be occurring.

The existence of these extreme mechanisms was also ascertained to occur in the case of the nucleation and growth of the (NH_4^+, NPr_4^+) ZSM-5 zeolite in the absence of cation[110-111]. This was later experimentally confirmed by Gabelica et al.[112] However, Derouane et al[113] have earlier on suggested that both the solution-mediated mechanism and the solid hydrogel transformation mechanism are important in studying the synthesis of ZSM-5 zeolite depending on the silica source and the gel formulation. Iton et al.[114] and Bodart et al.[115] have reported that ZSM-5 can be synthesized via either of the two extreme reaction mechanisms depending on the source and the concentration of the reactants and the reactions conditions. It is therefore clear, that in any particular case, the true mechanism of zeolite crystallization could lie somewhere between these two extremes, or could proceed via combination of both mechanism.

In general, synthesis mechanisms of typical low silica zeolite are apparently different from the high silica zeolite. Flanigen[116] suggested that in the synthesis low silica

zeolite, the crystallization mechanism is controlled by the solution chemistry of aluminosilicate tetrahedra and aluminosilicate species. Nuclei are formed consisting of alkali metal ion complexes of aluminosilicate species structural units consisting of four-membered rings, six membered rings and cages coordinated with cation are thought to be involved in the nucleation and crystallization. In high silica zeolite, the mechanism appears to be templating type where alkyl ammonium cation complexes with silica via pre-organization of the silica species around the organic cation prior to zeolite crystallization. Gies and Marler[117] suggested that this interaction was primarily due to Van der Waals contacts. The formation of ZSM-5 in the presence of NPr_4^+ has long been considered to be a classical example of structure direction in the formation of zeolites, based on the close correspondence between the shape of the cation and the intersection of the channels in ZSM-5, and the tight enclathration of the NPr^+ within the zeolite post synthesis.

Burkett and Davis's[118] work provide the most direct evidence of pre-organized organic-inorganic composite structures during the synthesis of Si-ZSM-5, and is consistent with a mechanism of structure direction in which these organic-inorganic composite structure from the precursor to the formation of the ZSM-5 channel intersection. They subsequently suggested that the formation of the organic-inorganic composite species is initiated by overlap of the hydrophobic hydration spheres around the NPr_4^+ cation[119] and hydrophobically hydrated domain of soluble silicate species as shown in figure 2.2.

Muller[120] described hydrophobic hydration as the reorientation of water molecules in the vicinity of a hydrophobic solute species in order to accommodate them whilst still maintaining a fully hydrogen bonding. This allows the establishment of favorable van der

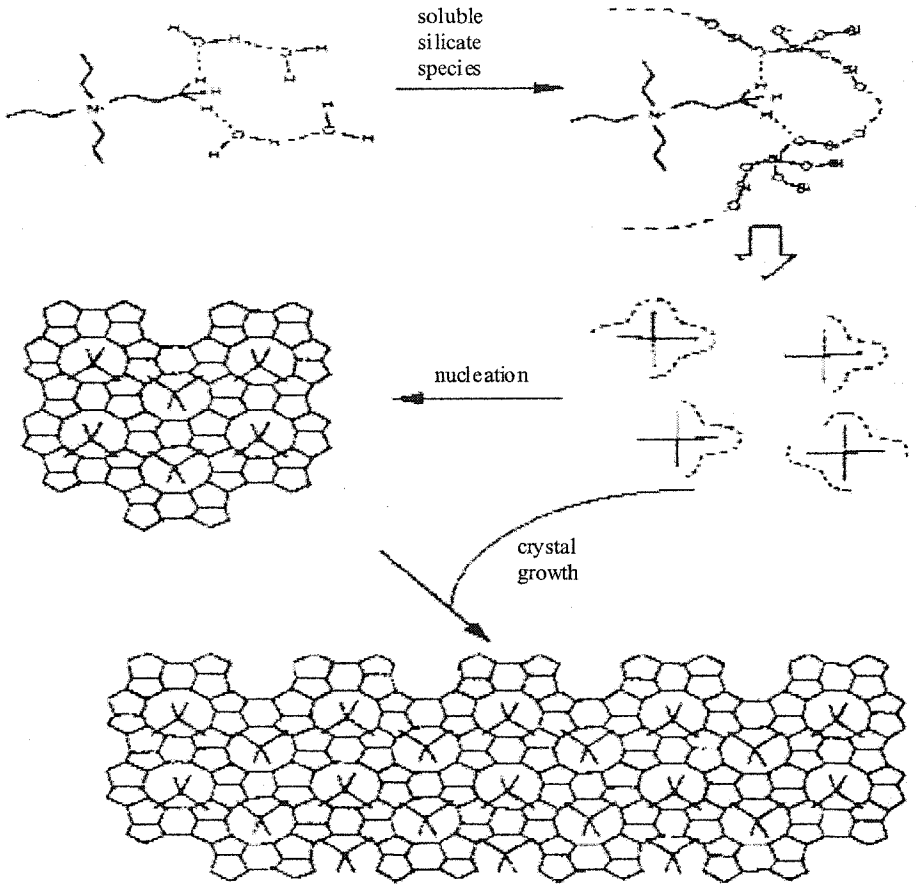

Figure 2.1a: Schematic of the proposed mechanism of structure direction and the growth involving inorganic-organic composite species in the TPA-mediated synthesis of ZSM-5[118]

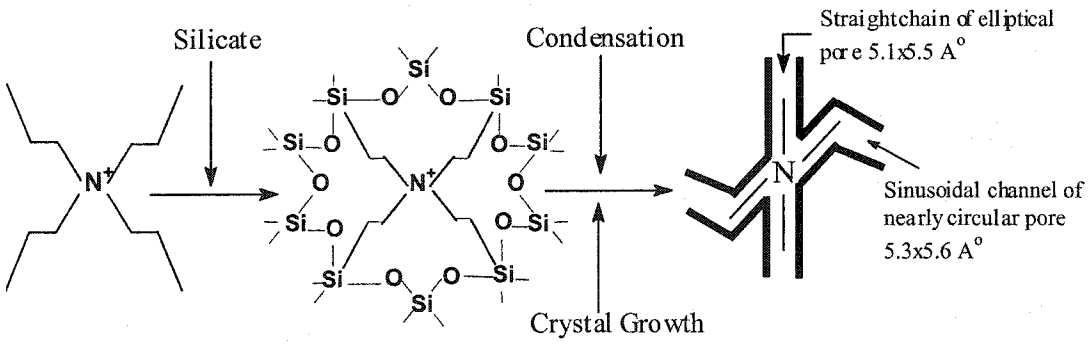

Figure 2.1b: Mechanism of the formation model for the templating by single TPA^+

Waals contacts between the alkyl chains of the NPr_4^+ and the hydrophobic silica species, whilst at the same time allowing the release of the water molecules from the ordered hydration spheres around the NPr_4^+ and the silica species.

2.3 Crystallization Kinetics of Zeolite

Typical kinetics curves of crystallization are characterized by regions of nucleation and crystal growth. The conventional nucleation region could be subdivided into two periods.[121] induction period when no crystal phase is found, and transition period, involving a slow growth of the crystal phase. A region of a relatively rapid crystal growth follows. Experimental crystallization curves, giving yield of crystalline material in time, usually exhibit sigmoid shape profile[10, 105,122,123]. A method of analyzing the nucleation and crystallization part of such S-shaped curves was developed by Zdhanov and Samulevich[123] in the case of zeolite Na-X. The activation energy E_n and the pre-exponential factor (lnA_n) of the nucleation can be determine from the crystallization curves at various temperature with the same batch of composition. Assuming that the formation of nuclei of a size stable enough not re-dissolve but grow into a crystal is an energetically activated process is rate determining during the induction period, E_n can be calculated by;

$$\ln (1/t_o) = \ln A_1 - E_n/RT$$

where t_o is the induction time i.e. the point on the crystallization curve where conversion to the crystal phase is just starting[124]. The apparent activation energies for zeolite (MFI) nucleation and for crystal growth are usually lower in the absence of alumina and the induction period before crystal appear that are detectable by X-ray diffraction techniques

is also much shorter for the aluminum free silicate system respectively. Chao and Co-workers[125] reported apparent activation energy for nucleation of ZSM-5 estimated at 34 and 25kJmol^{-1} for the aluminosilicates system with SiO_2/Al_2O_3 = 70 and aluminum free silicate system respectively.

Similarly, study conducted by Mintova et al[121] on the crystallization kinetics of zeolite ZSM-5 synthesized from TPABr and pyrolidine organic templates reveal that the nucleation energy for the systems is approximately the same i.e. 35 and 34kJmol^{-1}. The difference is in the values of the pre-exponential factor, which could de connected to the number of active nucleation centers, geometric orientation and steric hindrance[126]. The resulted high value of pre-exponential factor in the synthesis with TPABr was interpreted to be due to more effective interactions leading to the formation of more nuclei. This is evidence of the different mechanism of action of the two templates during induction period.

After nucleation, a phase of accelerated formation of crystals start, i.e. the nuclei will grow by addition or condensation of precursor species towards fully-grown crystals. Experimental crystallization curves can be described by Kholnogorov's equation[123].

$$\alpha = 1 - \exp(-k.t^n)$$

where α and t are the fractional conversion and the time respectively and n and k are constant. This equation describes the evaluation of the ration (Z) of the mass formed at time t to the mass in the final product. The value of constant n contains information of the nucleation kinetics of the crystallization; $n > 4$, increasing in nucleation rate, $n < 4$, decreasing nucleation rate; $n = 4$ is characteristic for a constant nucleation rate. Seeding i.e. the introduction of seed crystal or pre crystal nuclei could induce Crystal growth.

Using this procedure the induction period is eliminated, and crystal starts immediately, so that the crystallization of the desired zeolite may be completed before the nucleation of zeolitic impurity reaches a stage at which growth commences[98].

Nowadays, there seems to general agreement that zeolite crystal growth occurs in solution[127] more especially, it is believed that crystal growth occurs at the crystal plane-solution interface; a direct transition of the solid phase of the gel into crystalline product through solid-solid transformation seems to be very unlikely[105]. Most probably, crystals growth occurs by condensation of dissolved species (secondary units or extended species) onto the growing crystal surface[10, 128].

In general, temperature and time have a positive influence on zeolite crystallization process; rising temperature will increase both nucleation rate and linear growth rate (expected as k = 0.5 $\partial I/\partial t$ with I = crystal size); the crystallinity of samples normally increases with time. This however, is only partially true. As far as time is concern, zeolite synthesis is governed by the occurrence of successive phase transformation (Ostwald rule of successive phase transformation). The thermodynamically least favorable phase will crystallize first, and will be successively replaced in time by more stable phases[10]. Therefore, leveling off of the crystallization curves after a period of crystal growth indicates complete crystallization of that phase. Depending on the system under investigation, a decline in the crystallinity of the initial product sometimes may be observed, with subsequent formation of a second, more stable, phase. For example, mordenite was reported to be stable than ZSM-5, the crystallization to mordenite of the ZSM-5 initially formed is observed, with α-quartz beginning to appear with further crystallization time[77].

ZSM-5 crystallization always occurs after an induction period. During this period, it was shown however, that already small ZSM-5 nuclei were formed that showed, because of their small size, an amorphous appearance to X-ray diffraction[18]. These X-ray amorphous nuclei" were shown to exhibit typical properties of X-ray crystalline ZSM-5. Using ^{29}Si and ^{27}Al MAS-NMR, IR, thermal and textual analysis Scholle and co-workers[129] confirmed the presences of increasing amount of TPA-ZSM-5 unit cell at early stages of the crystallization. The concentration of these nuclei can be followed using the intensity of the lattice vibration at $550cm^{-1}$, specific to ZSM-5 zeolite[18, 130].

One can follow the course of a crystallization by stopping the crystallization at various time and sampling the batch, by taking a sampling while the crystallization is progressing, or by running the crystallization in a series of identical crystallization vessels charged from the same batch of starting gel. Each method will provide information on the progress of the crystallization. However, there are difficulties associated with each technique[80]. Stopping the crystallization to take a sample can change the course of the crystallization, as the system is perturbed in the act of taking the sample. Taking the sample while the crystallization is ongoing is possible at low temperatures; however, at elevated temperatures and pressures generally encountered in most of the synthesis processes, this method become extremely difficult. The final technique, simultaneous crystallization in several identical type vessels using the same batch of starting gel, has been utilized extensively to obtained much of the reported crystallization data, and is thought to provide a good representation of the crystallization system at various points during the crystallization.

2.4 Catalytic Cracking of Paraffins

The characterization of the active component of cracking catalyst, the understanding of the complex reaction net work occurring during cracking of the industrial feed stocks and the use of test reaction for the evaluation of catalyst performance has received considerable interest in the recent years. Catalytic cracking of paraffins is frequently used for the characterization of the catalytic properties of various zeolites. While the criteria such as α-test, β-test, the constraint index, paraffin/olefin ratio, cracking mechanism ratio (CMR) has been used to explain the predominant mechanism involved in the course of paraffin cracking reaction[131-135]. Small hydrocarbon such as n-propane, n-butane, n-pentane, 3-methlypentane, n-hexane and n-heptane are often used as reactants due to the limited number of possible reactions and products inherent in the catalytic cracking process of these compounds which makes the chemical analysis both easier and accurate.

From the very beginning, when natural clays were still used as cracking catalyst, it was obvious, then that an acidic surface was the agent responsible for the cracking process. Two types of acidic site were thought to be involved in catalytic cracking of alkanes: Lewis center, very aprotic acidic species with vacant orbitals, which are capable of removing H^+ from alkane molecules and converting them into carbenium ions $[C_nH_{2n+1}]^+$ [7, 136-138]. And Bronsted centers, strong protic acidic species, which either protonate alkane molecule to non-classical carbonium ions $[C_nH_{2n+3}]^+$ with penta coordinated carbon atoms[139-142] or directly protolyze C-C bonds in alkane and produce smaller alkane and carbenium ions.[132, 143, 144]

The catalytic cracking of hydrocarbons in a chain reaction that is believed to follow the carbonium theory developed by Whitmore[145]. This chain reaction mechanism involves three elementary steps: Initiation, Propagation, and Termination. The initiation step is represented by the attack of an active site on the reactant to produce the activated carbocation complex. Bronsted acid site are normally regarded as the active species involve in the initial step of olefin cracking, even relatively weak acids can protonate olefin molecules[146]. However, for the cracking of paraffins, the initial step has been widely debated. It was first thought that the presence of olefins, even at trace level, was necessary to initiate the cracking of paraffins[7, 147]. In this mechanism, the traces of olefins are readily protonated and the carbenium ions formed are able to abstract a hydride ion from paraffin, generating the carbenium ion necessary for the to keep reacting.

It was also claimed that the olefin necessary to initiate the cracking of paraffins could be formed by the direct attack of a proton on an H-C bond of the paraffin to give H_2 and an olefin in a similar way as occurs in the presence of liquid super acids[148]. The formation of the first surface carbenium ion was also proposed to occur by abstraction of a hydride ion by a Lewis acid site of the catalyst[149, 150].

$$R-CH=\!=CH-R' \xrightarrow{H^+} R-\overset{\oplus}{C}H-CH_2-R'$$

$$R-\overset{\oplus}{C}H-CH_2-R' + CH_3(CH_2)_4CH_3 \longrightarrow R-CH_2-CH_2-R' + CH_3-\overset{\oplus}{C}H-(CH_2)_3-CH_3$$

In all cases regardless of the active site involved, it was always proposed that the cracking of paraffins on solid acids occurred through formation of carbenium ion as the initial step. This remained so until 1984, when the Haag and Dessau[140] proposed (fig 2.2) that also on solid acids the cracking of paraffins could be initiated by the attack of

Bronsted site on C-C bond forming surface carbonium ion type activated complex. When this carbonium ion is formed it can be crack via protolytic cracking or even give hydrogen if the proton attack take place at a C-H bond. Using 3-methyl pentane and hexane as reactants, Haag and Dessau proposed the reaction and the active sites for the initiation step in the cracking of paraffins shown in figure 2.3.

Moreover, it has been suggested[147-149] that the presence of Lewis acid or electron acceptor sites in many solid acids and certainly in zeolite where they are associated with partially coordinated framework Al or extra framework Al (EFAL) species[151] can enhanced the hydrogenation of paraffins, thus forming olefins that can initiate or at least enhances, the cracking reaction. It is therefore obvious, that the current knowledge certainly suggests that Bronsted active site intervene in the initiation step of for the cracking olefins and protolytic cracking of paraffins.

Regardless of the initiation and cracking mechanism, when the carbon-carbon is broken a carbenium like ion is left on the surface. This can either desorb, giving one olefin or one paraffin if it involves in a hydride abstraction reaction. It has been traditionally proposed that chain propagation will occur when a carbenium abstracts an hydride ion from a reactant paraffin and while the former will desorbs as a paraffin, the reactant molecule will be converted into a carbenium ion that will be able to either isomerize and or crack, therefore propagating the reaction. At this point it should be possible to write a general mechanism for paraffin cracking in which the initiation step occurs through a monomolecular reaction where the 'carbocation' is formed. This will be followed by a bimolecular chain transfer reaction that corresponds to the hydride transfer between an adsorbed 'carbenium' and a reactant molecule. The chain transfer is terminated when the surface 'carbenium ions' are desorbed and the Bronsted acid site of

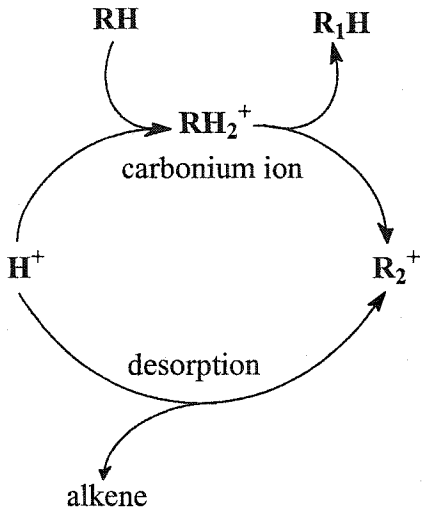

Figure 2.2: Haag-Dessau cracking mechanism for the alkane molecule (RH) proceeding via carbonium ion transition state[140].

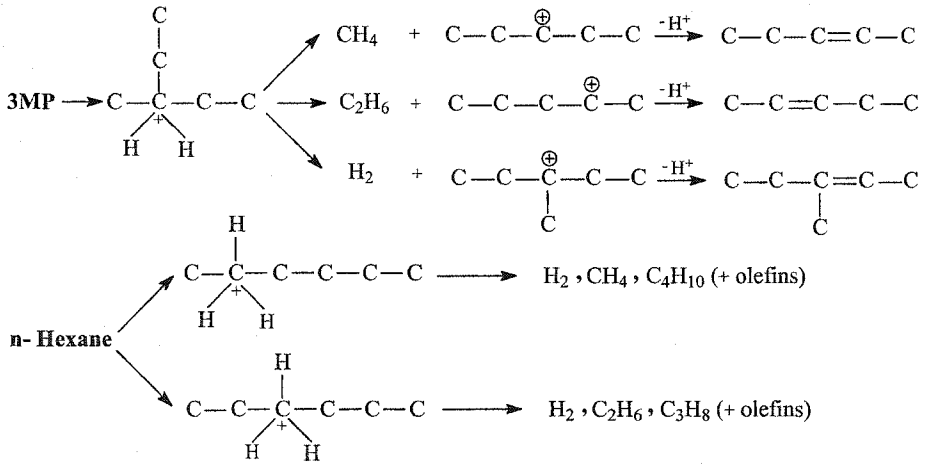

Figure 2.3: Protolytic cracking of 3-methylpentane and *n*-hexane via pentacordinated carbonium ion[140].

the catalyst is regenerated[141, 152]. This step is just the reverse of the adsorption of one olefin and could be written as:

$$C_3H_7^+ \longrightarrow C_3H_6 + H^+$$

With this simple set, the cracking chain mechanism is completed.

2.5 *n*-Hexane Cracking

It is generally accepted that n-hexane cracking reaction on the zeolites proceeds via monomolecular and bimolecular mechanism[133, 140,153-155]. The bimolecular mechanism is the classical carbenium ion chain mechanism (β-cracking) involving the activation of n-hexane followed by β-scission and isomerization of the newly formed carbenium ions. The monomolecular (protolytic cracking) pathway involves direct protonation of alkane form high-energy transition state pentacoordinated carbonium ions, which subsequently decomposes to lower linear paraffins or hydrogen. The two reaction mechanism are illustrated in fig 2.4 below.

In the first case, the rate-determining step of the reaction is concluded to be the hydride transfer following the initial generation of the carbenium ion, in later case the rate is determined by carbonium ion formation or their subsequent decay. Though the two cracking routes are believed to be integrated in the course of a cracking reaction and hence referred to as chain mechanism[156]. However, the prevalence of one of the two mechanisms is governed by the reaction temperature and the surface concentration of the reactants (determined by temperature, reactant pressure, and the concentration of the acid sites)[140].

The cracking rate was found to be first order with respect to the partial pressure of n-hexane and second order to the Al content of the zeolite[154,155]. However, the protolytic

route is claimed to be favored by increasing temperature, decrease in aluminium content and decrease in pore dimension[157]. Haag and Dessau[140] reported that the activation energy was higher for the protolytic than the β-cracking mechanism. Thus, it can be expected that the molecular mechanism will predominate at high temperatures. This was supported by Riekert and Zhou[158], who observed an induction period during the paraffin cracking (which is typical of bimolecular reactions) only at temperature below 200°C. Consistent with this, was the report of Lukyanov et. al[134] who observed an important contribution of the hydride transfer on the cracking on n-hexane with ZSM-5 at the reaction temperature below 400°C.

The product distribution observed during the cracking of paraffins depends on the relative contribution of the two mechanisms. If most of the cracking occurs through a bimolecular β-scission mechanism, high yield of branched product will be obtained. On contrary, if protolytic-cracking mechanism dominates, then more linear paraffins, methane, ethane, and ethylene and hydrogen will be produced. The criterion used to determine the relative contributions of each cracking route include.[131-135]

- Paraffin/Olefin ratio (P/O)
- Cracking mechanism ratio CMR defined as CMR = $(C_1 + \Sigma C_2)/i\text{-}C_4$
- β-test, which is the ratio of propane formation rate in the hydrogen transfer steps to the propene concentration of n-hexane cracking.
- Constrain index, which is the ratio of the first order rate constant for the conversion of n-hexane and 3-methyl pentane.

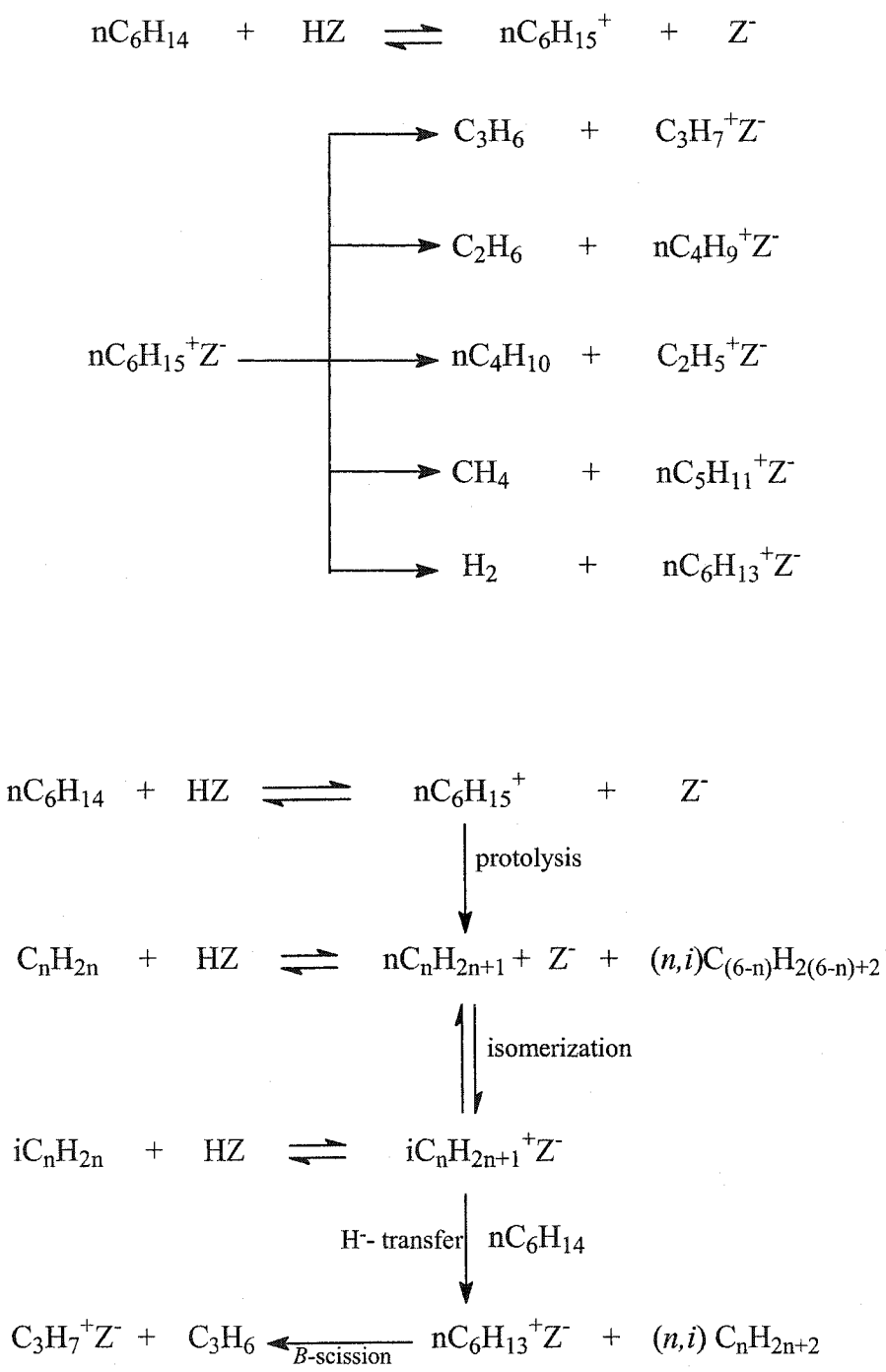

Figure 2.4: General reaction scheme for the protolytic and β-cracking route[155].

The paraffin/olefin ratio was found to increase with the pore dimension, as a result of hydride transfer reaction, which increasingly become more important due to the larger dimension of the transition state complex of the intermediate in the bimolecular route. A CMR value greater than unity reflects a significant contribution of the protolytic route, whereas a value below one is an indication of classical carbenium ion chemistry and cracking through β-scission reaction. The presence of two adjacent acid sites is required for hydride transfer reaction in bimolecular reaction mechanism, while the mono-protolytic cracking route require isolated acid sites. Hence mono-protolytic cracking route is favored as the Si/Al ratio increases[156].

CHAPTER 3

EXPERIMENTAL METHODS

3.1 Catalyst Synthesis

Two batches of catalyst samples of nearly identical composition were hydrothermally synthesized from different systems by varying the organic molecule functioning as template. Technical sodium aluminate (BDH) containing 51% of Al_2O_3 and 39% Na_2O was used as the alumina source, and colloidal silica (Ludox AS-40 DuPont) containing 40% by weight SiO_2 was used as silica source. Other chemicals used in the synthesis include sodium hydroxide (Fluka AG) as additional source of Na^+ and mineralizing agent, distilled water as the solvent while diethanolamine (Baker), and tetrapropylammonium bromide (Aldrich), served as the template. The crystallization was performed in 150ml teflon lined autoclaves under autogeneous pressure at 175°C for various periods (1hours to 20hours). After the stipulated time, the autoclaves were progressively removed from the oven in order to obtain materials with increase in crystallinity. After cooling to room temperature, the resulting solids product were recovered by filtration on a Buchner funnel, washed thoroughly with distilled water, and dried overnight at 100°C for further treatments. The teflon vessels were usually cleaned with sodium hydroxide solution carefully prior to the succeeding experiments in order to avoid the seed effects.

3.1.1 As Synthesis of Tetrapropyl Ammonium Bromide Mediated Samples.

Hydrogel molar composition:

$2.5Na_2O$: 14TPABr: Al_2O_3: $30SiO_2$: $400H_2O$

The synthesis mixtures were prepared by dissolving 1.332g of sodium aluminate ($NaAlO_2$), 0.667g of sodium hydroxide, and 7.102g of tetrapropyl ammonium bromide (TPABr) in 30.00g of distilled water. 30.00gram of the colloidal silica (Ludox AS-40) was added drop wise under continues stirring. The resulted gel was stirred to homogeneity under magnetic stirring for another five minutes. Then, the homogeneous gel, the preparation of which was carried out in a beaker, was then transferred into a 150ml teflon lined stainless autoclaves for the hydrothermal crystallization. The autoclaves are then mounted in the heat furnace maintained at 175°C and are continuously rotated at 20rpm (rotation per minute) under autogeneous pressure. The crystallization time was varied between 1hour to 20hours. After the stipulated time, the pressure vessels were progressively removed from the oven and cooled in a stream of cold water from the tap. The as-synthesized materials were recovered by filtration, washed with distilled water and dried at 373K over night.

3.1.2 As Synthesis of Diethanolammine (DEA) Mediated Samples.

Similarly, five gel samples with molar composition:

$2.5Na_2O$: 15DEA: Al_2O_3: $30SiO_2$: $400H_2O$ were synthesized following the procedure described above using 10.52g of diethanolammine template molecule in place of tetrapropylammonium bromide.

3.2 Catalyst Preparation

The organic template molecules used in the synthesis were removed in a calcination step before the as-synthesized material could be investigated in any catalytic application. The template molecules are strongly adsorbed in the zeolite lattice and often

located in positions having limited accessibility. Consequently, removal of the organic template by calcinations in air is a strongly activated process. All the samples were prepared for use as catalyst by first calcining in air at 500°C for 24hours in a furnace with temperature increase of 1.0°C per minute from room temperature. This was followed by ammonium ion exchange with 20.0ml of aqueous ammonium nitrate (1M NH_4NO_3) solution per gram of the catalyst under reflux for 1hour, cooled and decanted. The ion exchange was repeated twice, washed and filtered. The ammonium form finally obtained were dried at 100°C and calcined again at 500°C for 24hours for deammoniation and to obtain the protonated form of the TPABr and DEA mediated samples (fig 3.1).

3.3 Structural Characterization of the Catalyst.

Knowledge of catalyst structure is essential to the understanding of the chemistry actually occurring in catalysis, this makes structure characterization crucial throughout the life cycle of the catalyst, from the preparation step to the use in reaction conditions. Various physical techniques were used in the characterization of the as-synthesized materials in order to understand their structural characteristics.

3.3.1 Powder X-Ray Diffraction.

The crystallinity and phase purity of synthesized zeolites can be obtained using powder X-ray diffraction (PXRD), since every crystalline material has it own characteristic XRD pattern. The powder XRD involves the use of collimated beam of X-rays, with wavelength Cu $K_\alpha \sim 0.5\text{-}2A^\circ$, incident on a specimen, which is diffracted by the crystalline phased in the specimen according to well known Bragg's equation($n\lambda=2d\sin\theta$).

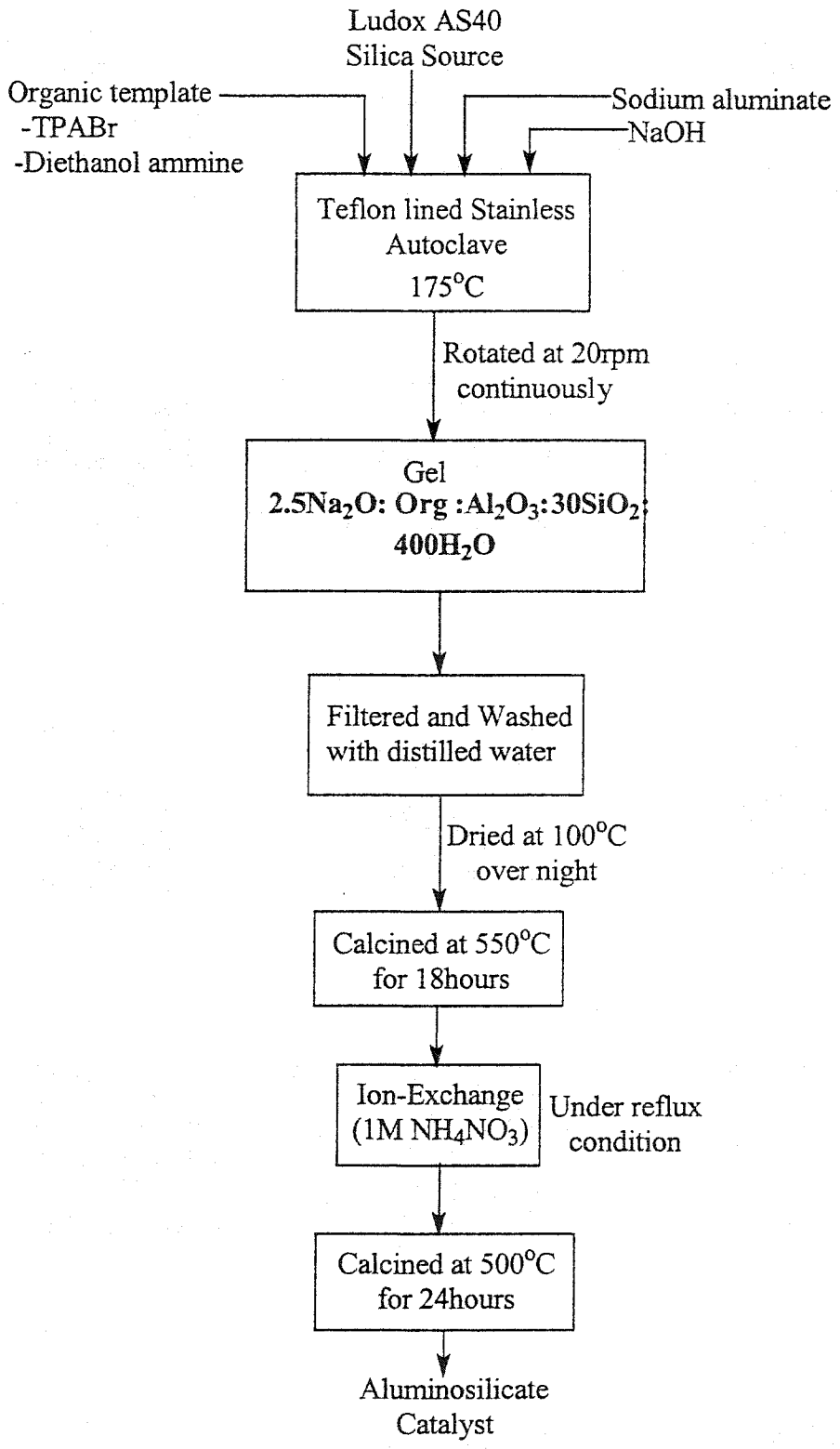

Figure 3.1: Showing the preparation of diethanolammine and tetrapropylammonium bromide templated catalyst.

Each sample was gently grounded in an agar pestle and morter. The fine powder was packed into a sample holder having diameter of ~25mm and depth of ~3 mm. The surface of the packed sample was smoothed with a flat glass and then powder X-ray diffraction spectra samples were then recorded on Siemen D5005 X-ray defractometer under the following operation conditions.

- Copper K X-ray radiation (λ =1.541A°) from a broad focus tube at 40 KV and 30mA
- Autodivergence slit with no scatter slit and a receiving slit of 0.1mm
- Scanning speed and interval of data collection was 0.01 degree 2θ/sec
- Angle scanned are from 0.5 – 50 degree 2θ.
- A graphite monochromator was used.

3.3.2 Infrared Spectroscopy

The mid-infrared absorption region of zeolites, which contains fundamentals vibrations of the framework of silica-alumina tetrahedral, can be used in characterization of zeolite type. These vibrations include symmetric and asymmetric stretching and bending mode of Si $(Al)_4$ tetra hedral, and double ring vibration. The mid infrared spectra of the as-synthesized materials were recorded on a Perkins Elmer 61F PC spectrometer using the KBr pellets technique. About 0.5mg of the as-synthesized zeolite sample was grounded with 200mg of KBr in a small ball mill mortar. The mixture was transferred into a die (pellet maker) of 8mm in diameter, and the pressed for few minutes at about 10,000 psi under vacuum to obtain transparent pellets. The spectra were then recorded by taking 20scans with a resolution of 4.0cm^{-1} and a scan range of 350 to 1400cm^{-1}.

3.3.3 Adsorption Measurements.

After dehydration, the zeolite is a crystalline solid permeated by micropores. A property that has been extensively utilized in characterizing molecular sieve materials is the ability to adsorb selected molecules. From examination of adsorption properties, substantial structure information can be discern about molecular sieve material. Adsorption of different size gives direct information about the dimensions of the pore system. Generally, the adsorption isotherm (the amount of gas adsorbed as function of the partial pressure of the gas at constant temperature gives information about the pore structure. Adsorption measurements were carried out on a Hiden Analytical IGA system (gravimerical measurement). Aliquots of the sample being measured (~100mg) was loaded and evacuated at ca. 10^{-7} bar. The temperature was then raised to 450°C at the rate of 3°C/minute for the furnace temperature. However because of the high vacuum, the sample temperature only rose to 350°C.

After at least three hours at the final temperature and high vacuum making sure the sample weight stabilized, the sample was cooled to ambient and then to 15°C using circulating chilled liquid system. When the conditions equilibrated, small pulses of benzene vapor were introduced periodically via gas admittance valve, which was electronically controlled to obtain adsorption steps of 2% by weight. At each period of pressure, the equilibrium was attained before another pulse of the adsorbate was introduced. The sample weight was recorded on a highly accurate microbalance and the pressure of adsorbate was measured using a set of pressure transducers, each calibrated to measure the pressure at a specific range. The conditions (pressure and temperature), operation, and data processing were handled by specifically designed software on a local computer

3.4 Catalytic Evaluation by *n*-Hexane Cracking

3.4.1 Reaction Apparatus and Parameters

The experimental set up used in evaluation of the synthesized catalysts consist of feed system i.e. containing n-hexane (99.67% purity), carrier gas system containing high purity nitrogen gas as the feed carrier (diluent), preheating zone, tubular stainless reactor, and the glass tubes as the product trap system. Other apparatus include of temperature controlled water bath, ball gas flow meter and temperature controller system for controlling the reactor temperature. A bubbler system which was used to introduce *n*-hexane into to the reactor was operated at 0°C to ensure a constant partial pressure of n-hexane (6.0kPa) at atmospheric pressure The reactor is 21cm long stainless tube with an internal diameter of about 1.05cm.fig 3.3 shows the diagram of the experimental set up. The feed consist of 6.0 kPa partial pressure n-hexane at 0° C, and 95.3 kPa nitrogen (99.99% purity). The catalytic reactions were carried out over about 1.00g of the catalyst under atmospheric pressure and temperature range of 200 ° C to 500° C. The flow rate was randomly varied from 15.0ml/min to 65.0ml/min.

3.4.2 Catalytic Test.

The catalytic activity of the synthesized materials in n-hexane cracking between 250 and 500°C was investigated using a fixed bed micro-reactor system operating at atmospheric pressure. The catalysts were first prepared into granules by subjecting the powder form of each catalyst into a tablet under about 15bar pressure. The tablets are crushed and sieve through a 1.18mm top and 500micron as a bottom (BSS) mesh to obtain granules of 0.5 to 1.0mm diameter range. In all catalytic runs, about 1.00g granules of the catalyst were used. The catalyst granules were sandwiched between the quartz wool at the

isothermal region of the reactor, and the remaining part of was filled with carborandom inert silicon carbide granules. Purified nitrogen gas at a predetermined rate was bubbled through an n-hexane saturator at 0^{o} C into a preheating zone with a temperature 100^{o}C through a flow meter before being finally passed into the reactor. The reactor effluent was collected in a series of airtight glass tubes and analyzed using Chrompack gas chromatograph equipped with a flame ionization detector and Al_2O_3/KCl 100m capillary column. From the GC results, the n-hexane fractional conversion (x) was obtained, and for each catalyst tested, the rate constant (k) was obtained from the slope of the first order plot of -ln (1-x) against contact time at a given reaction temperature. The activation energy E_a was calculated from an Arrhenius plot of ln k against T^{-1}. The absence of thermal cracking was confirmed with blank experiment using carborandom inert silicon carbide granules in placed of the catalyst.

3.4.3 Catalyst Activation.

The catalysts loaded in the reactor were activated under airflow (at about 8.0ml per minute) by raising the temperature of the reactor from room temperature to 500^{o} C and maintaining this temperature for at least 6 hours and cooled to the desired temperature. The desired reaction temperature was maintained for 1 hour prior to the introduction of n-hexane. At the end of each reaction run, the catalyst was reactivated at 500^{o} C for at least 3 hours under airflow and cooled to the stipulated temperature for the next run. The experimental setup used for the evaluation of catalyst in this study is shown schematically in fig 3.3. The reactor was heated electrically and the temperature of the catalyst bed was measured by thermocouple connected to the fixed bed reactor. The

temperature of the reactor could be controlled by means of temperature controller with a variation of ± 1.0°C.

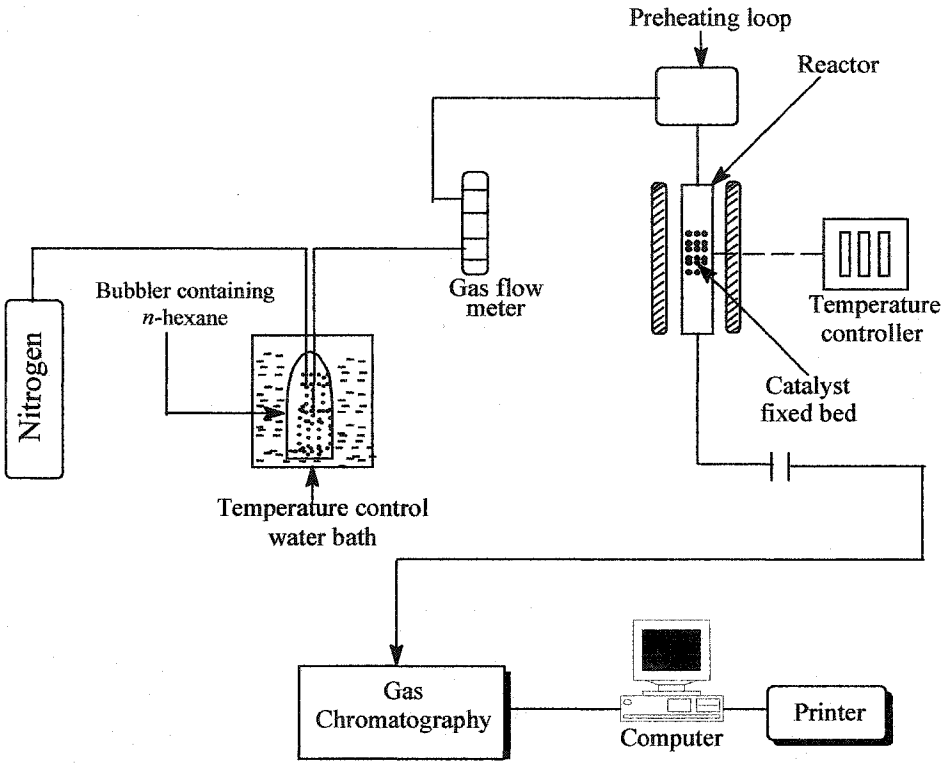

Figure 3.2: Schematic representation of the experimental setup for the n-hexane cracking reaction

CHAPTER 4

RESULTS AND DISCUSSION

4.1 Synthesis of Zeolitic Material

The molar compositions of the gels employed in the present study are summarized in table 4.1. The crystallization temperature was maintained at 175°C during the synthesis of both TPABr and DEA mediated samples. The phases identified were, complete amorphous, microporous aluminosilicate with structure similar to ZSM-5, and fully crystalline ZSM-5 materials. At lowest synthesis time of TPABr and DEA templeted systems, amorphous materials were produced with no evidence of the formation of microcystalline material.

Regions of nucleation, crystal growth and full crystallization generally characterized the synthesis. There was induction period of less than three hours during the synthesis of TPABr templeted samples before any crystallization material was detected while the DEA templeted sample synthesis exhibited an induction period as long as nine hours. The differences in the induction period may be attributed to better structure directing ability (templating effect) of TPA^+ than diethanolammine. TPA^+ are recognized to form complexes with aluminosilicate and silicate species and subsequently causes replication of the framework structure via stereospecific interaction. The induction period is defined as the time necessary for the sufficient amount of large enough crystals to be formed so as to be detected by X-ray diffractometer scan or infrared spectroscopy. Sometimes material may be amorphous to X-ray but are shown by infrared spectroscopy

Table 4.1: Gel composition and the crystallization kinetics of the material synthesis under hydrothermal conditions

Code	Molar composition of the starting gel	Synthesis time	Phase identified
T-1	$2.5Na_2O:14TPABr: Al_2O_3:30SiO_2:400H_2O$	1hour	Amorphous
T-2.5	,,	2hrs:30min	Amorphous
T-3	,,	3hours	MFI plus amorphous
T-3.4	,,	3hrs:15min	MFI plus amorphous
T-3.5	,,	3hrs:30min	MFI plus amorphous
T-345	,,	3hrs:45min	MFI plus amorphous
T-4	,,	4hours	ZSM-5
T-5	,,	5hours	ZSM-5
T-10	,,	10hours	ZSM-5
T-15	,,	15hours	ZSM-5
T-20	,,	20hours	ZSM-5
	$2.5Na_2O:15DEA: Al_2O_3:30SiO_2:400H_2O$		
E-1	,,	1hour	Amorphous
E-3	,,	3hours	Amorphous
E-5	,,	5hours	Amorphous
E-10	,,	10hours	MFI plus amorphous
E-15	,,	15hours	ZSM-5
E-20	,,	20hours	ZSM-5

to consist of microcrystalline zeolitic solid material. In our case, there is close correlation between powder X-ray crystallinity and relative crystallinity estimated from the infrared spectroscopy.

4.2 Infrared Spectral Analysis of the synthesized material

In practice the framework structure in the mid-IR region ($1400cm^{-1} - 300cm^{-1}$) is useful for zeolites characterization since it contains the fundamental vibrations of the framework silica-alumina tetrahedral. A typical spectrum of well crystallized ZSM-5 zeolite (figure 4.1a) contains absorption band at 1100(S), 800(W) and 450(S) cm^{-1}, which coincide with that of silica alumina (figure4.1b) and have been assigned to[159] the asymmetric stretching and the bending modes of the $Si(Al)O_4$ tetrahedral respectively. In addition, distinct absorption bands that are structural sensitive are observed at $1225cm^{-1}$ and 550 cm^{-1}, also reported by Jansen et al[160], these two bands, observed in zeolite with five member rings, are vital importance as they help in differentiating zeolite type.

The first structure sensitive band at $1225cm^{-1}$ due to external asymmetric stretching vibration is clearly present in IR spectra of ZSM-5 zeolite with four chains of five member rings arranged around two-fold screw axis of the zeolite framework. According to Jacob et al[161], Vadrine et al[130], the second structure sensitive absorption band at $500cm^{-1}$ is caused by double 5-membered ring blocks of tetrahedral in the framework, which are known to be precursors of some zeolitics structure. This absorption peak appeared with a weak intensity in the spectra of TPABr templated sample after 2.5 hours. Its intensity increases with time (fig 4.3), similar trend were also observed for DEA

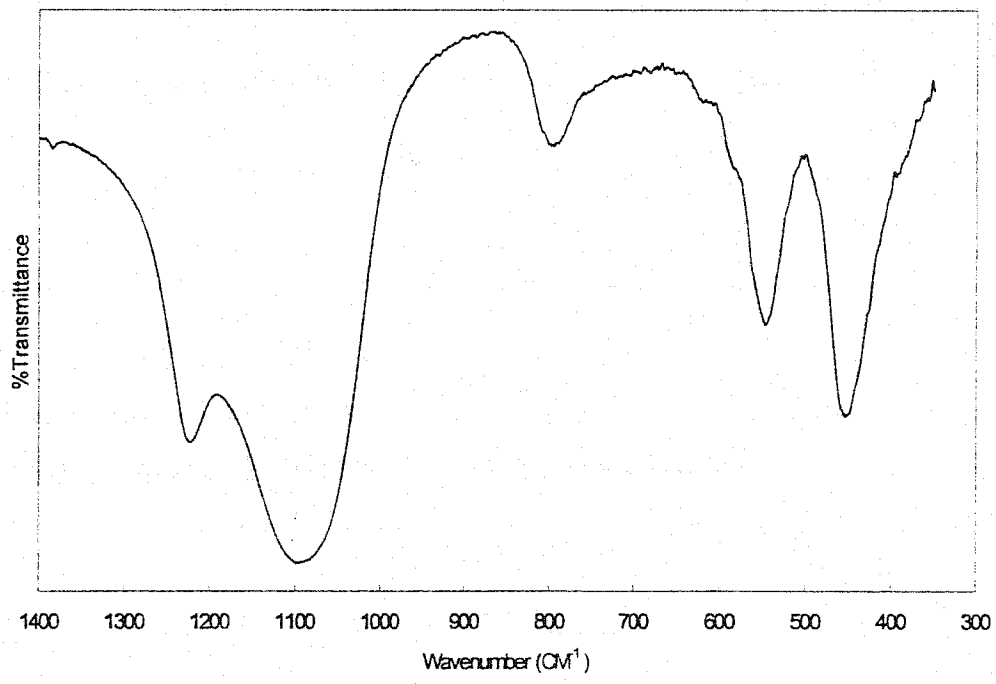

Figure 4.1a: A typical IR spectrum of the framework region (1400-300cm^{-1}) of ZSM-5.

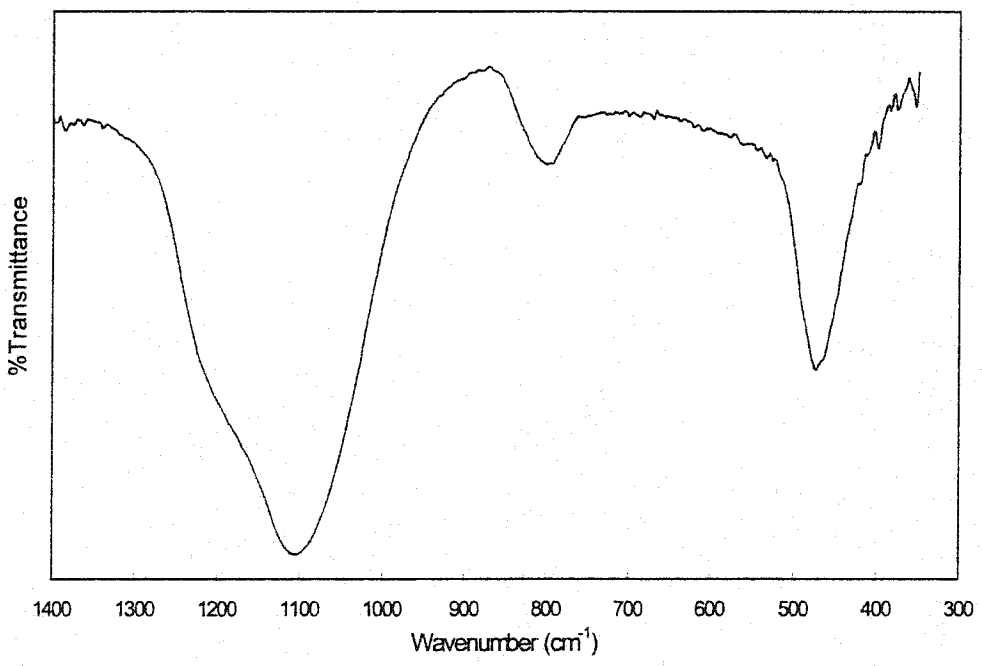

Figure 4.1b: A typical IR spectrum of the framework region (1400-300cm^{-1}) of Silica-alumina

templated samples. The position of the main absorption of amorphous silica (figure 4.1b) at around 1090, 800 and 400cm^{-1}coincide with that of ZSM-5 corresponding peaks. Some of the spectra we obtained especially at long crystallization time exhibit absorption peaks typical of ZSM-5 while those synthesized at short time of crystallization exhibit absorption peaks characteristic of amorphous material. The mid-infrared spectra as function of synthesis time of the as-synthesized material are provided in figure 4.2.

Since all pentasil contain the same type and number of characteristic 5-membered ring per unit cell, and as silica does not show absorption band near 500 cm^{-1}, it was however possible to appreciate their crystallinity from optical density ratio at 550 and 450 cm^{-1}. This ratio increases with crystallinity. Literature gives different values for this ratio in the case of well crystalline ZSM-5 sample (0.80, 0.70)[162, 130]. In our case, the value of 0.70 is the most suitable for both TPABr samples and DEA templated samples. The IR spectra in the framework absorption region are shown in figures 4.3 while the ratio of the optical densities of the A (500-650) and B (440-480) cm^{-1} bands are given in table 4.2

4.3 X-Ray Spectral Analysis of the Synthesized Material

Zeolites being crystalline solids with a regular structure have a characteristic diffraction pattern; this can be used to identify the material, determine the degree of crystallinity of the material and to determine possibly the presence of other crystalline impurities. Amorphous material can be detected by the nature of the baseline; very broad low base line absorption usually indicates amorphous material. Quantitative analysis are much more difficult to make. First, because there is no absolute 100% zeolite standard, peak intensities can only be compared to an arbitrary defined standard. This crystallinity percent can only be determined relatively and not absolutely.

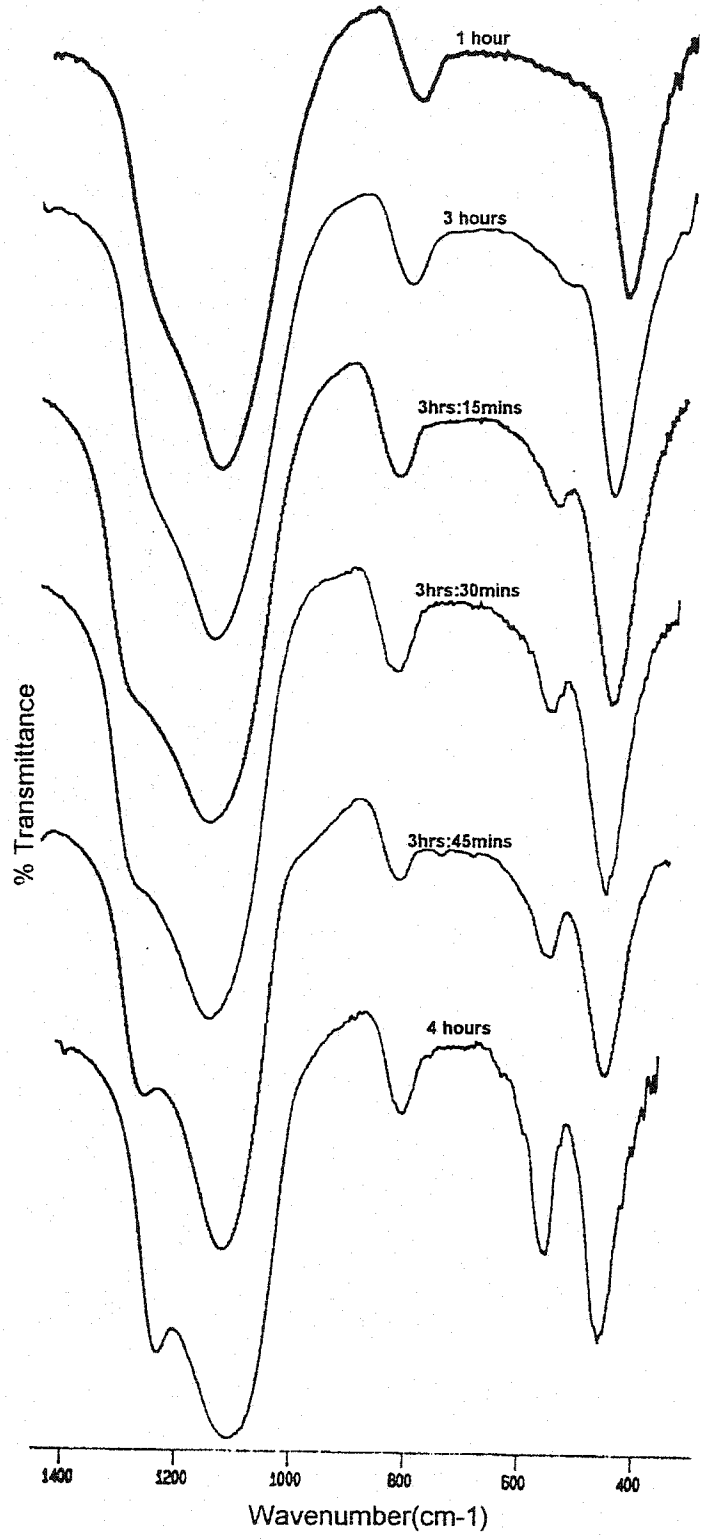

Figure 4.2a: Mid IR spectra of the framework region TPABr-mediated samples.

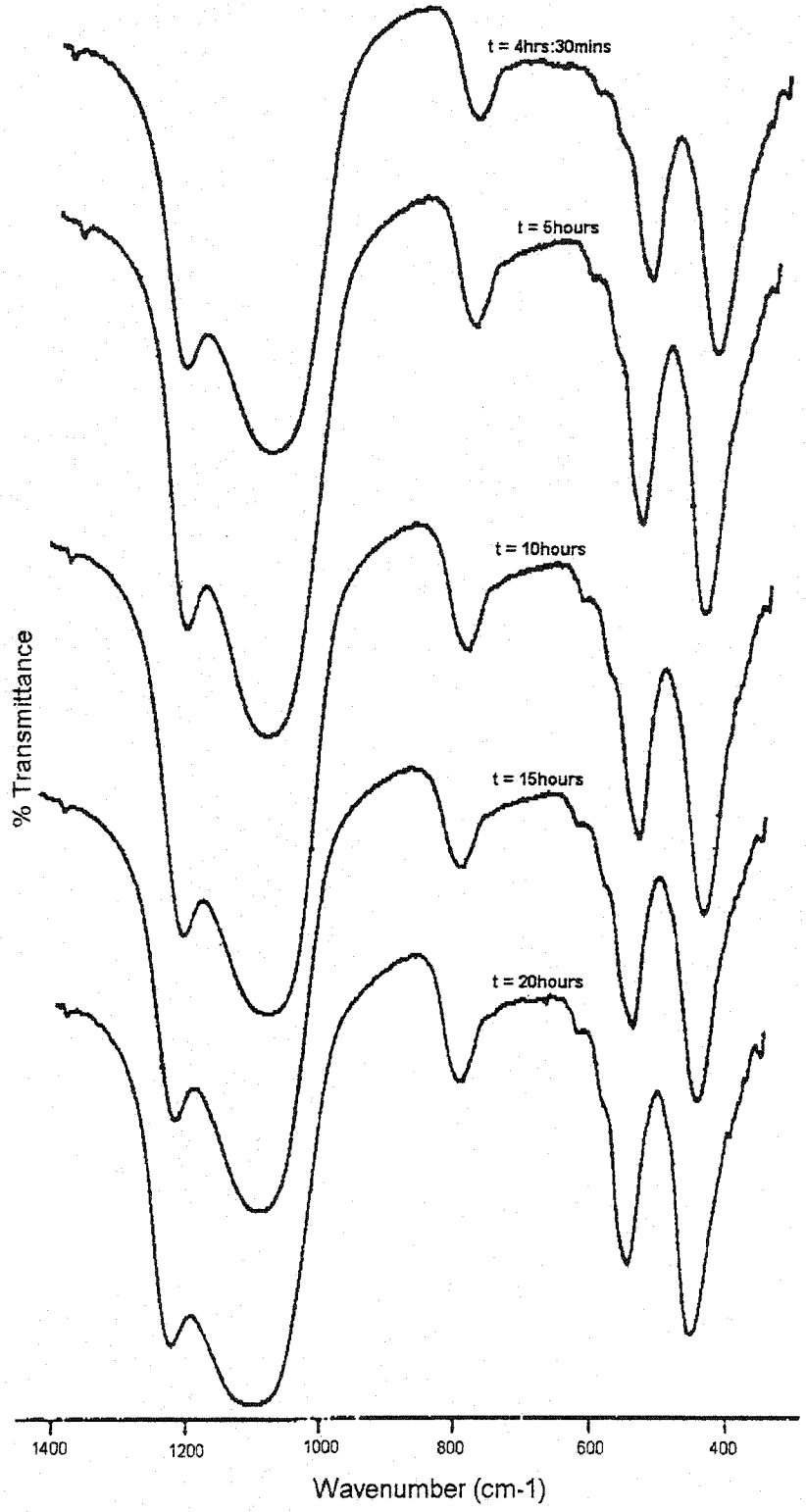

Figure 4.2b: Mid IR spectra of the framework region of fully crystalline TPABr-mediated samples.

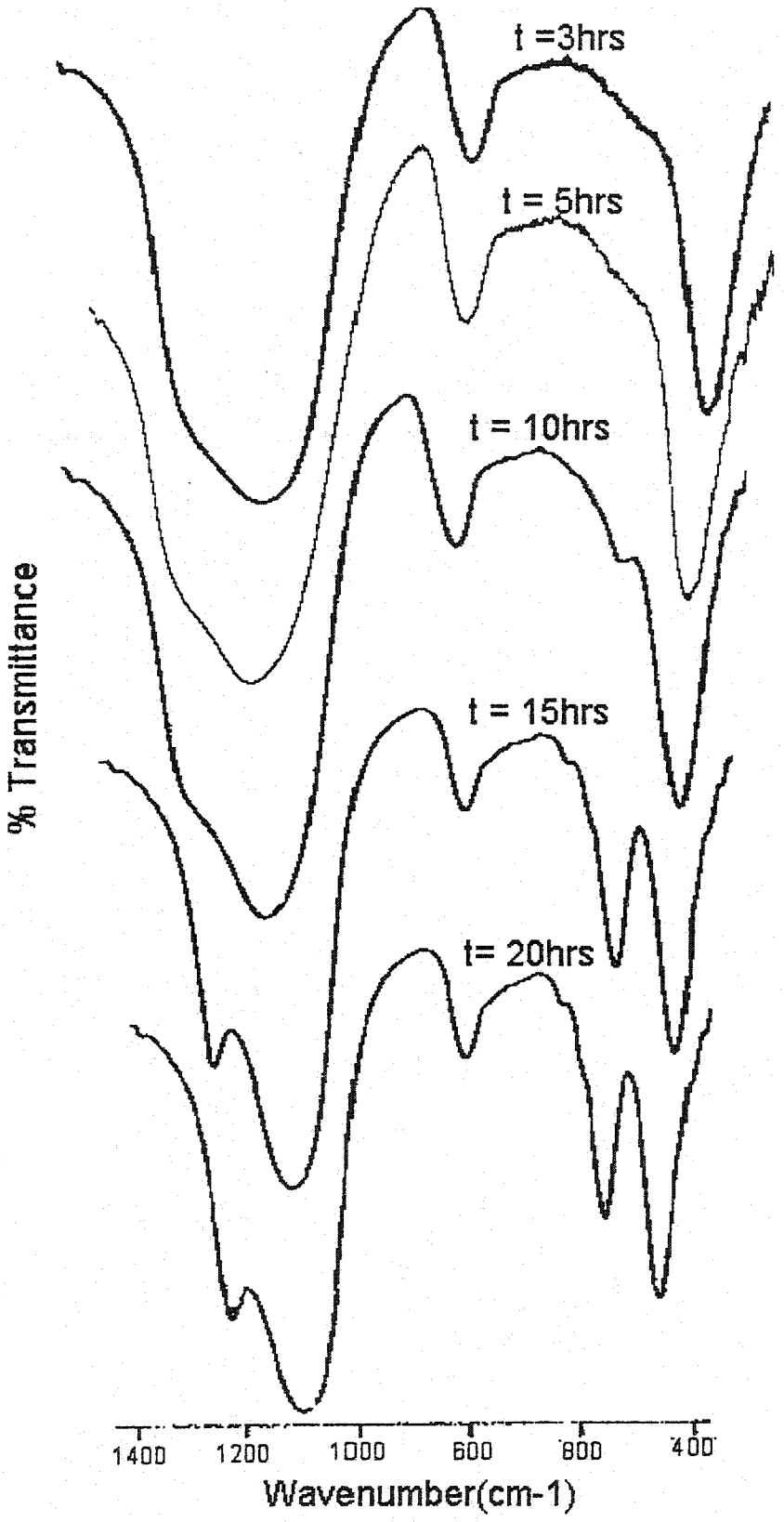

Figure 4.3: Mid IR spectral region of the framework of DEA mediated samples.

Table 4.2a: IR Spectroscopic measurements of TPABr templated samples.

Sample Code	Crystallization Time	$\frac{A_{550}}{A_{450}}$
T-1	1hrs	0.00
T-3	3 hrs	0.35
T-3.4	3hrs: 15mins	0.42
T-3.5	3hrs: 30mins	0.46
T-345	3hrs: 45mins	0.64
T-4	4hours	0.67
T-4.5	4hrs: 30mins	0.70
T-5	5hours	0.70
T-10	10 hours	0.70
T-15	15 hours	0.70
T-20	20 hours	0.69

Table 4.2b: IR Spectroscopic measurements of DEA templated samples.

Sample Code	Crystallization Time (hour)	$\frac{A_{550}}{A_{450}}$
E-1	1	0.00
E-3	3	0.00
E-5	5	0.00
E-10	10	0.38
E-15	15	0.70
E-20	20	0.70

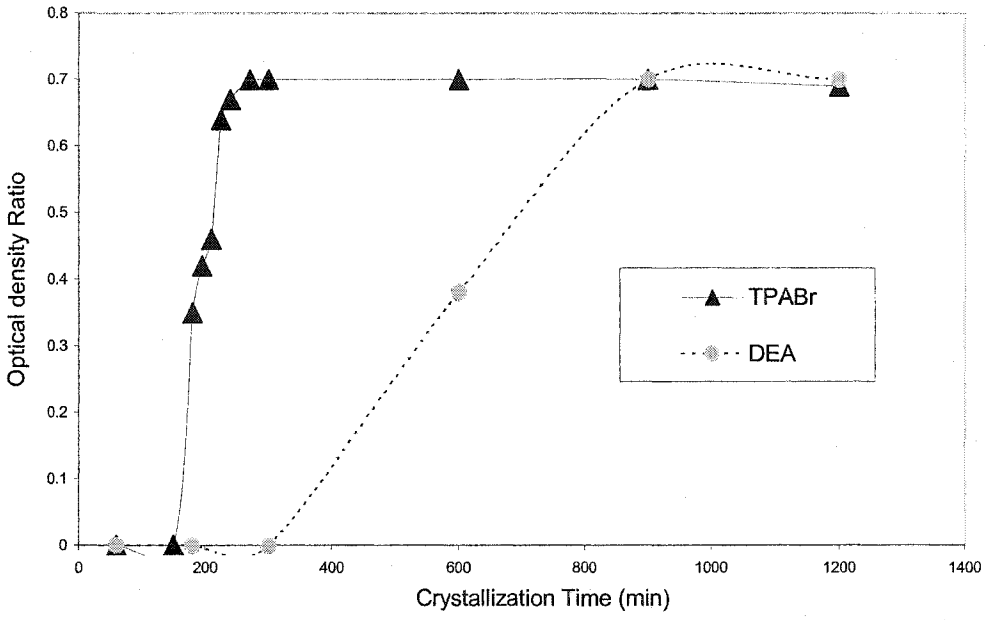

Figure 4.4: Crystallization curve of TPABr and DEA templated samples

The peak intensities also vary markedly with degree of hydration of the samples, and thus zeolites equilibrated to the same degree of hydration should be compared[80].

Figure 4.4, shows the X-ray diffraction pattern of as-synthesized materials as function of crystallization time for the TPABr and DEA templated samples. The TPABr templated samples show a broad signal characteristic of amorphous material for the samples crystallized at 2.5 hours and shorter time, broad baseline X-ray diffraction pattern is also observed from the DEA samples crystallized shorter than 9hours. The line width of this signal increases with crystallization time, indicating that the regularity increases and relative amount of amorphous decreases. A well-resolved XRD pattern characteristic of ZSM-5 zeolite (figure 4.5) is observed after 4hours and 10hours for the TPABr and DEA templated samples respectively.

Since these weak intensities observed in the X-ray diffraction pattern of some of our samples are typical of ZSM-5 material, it can be inferred that these materials may consist of microcrystalline zeolitic solid that is similar in structure to ZSM-5. It can be concluded from both infrared and X-ray measurements that the bonds giving the characteristic framework vibrations of ZSM-5 zeolite are already formed in the initial stage (from 3 hours and 10hours reaction time for the TPABr and DEA mediated samples respectively) and the total amount of IR and X-ray crystalline ZSM-5 zeolite increases with crystallization time. It was also observed that by increasing the time of crystallization beyond 15 hours, there was no change in both IR and X-ray crystallinity. Therefore, these methods of preparations prevent the formation of quartz phase even at long crystallization time, as confirmed from powder X-ray diffraction pattern. This is due to the presence of template in the crystallized zeolite, thus stabilizing their structure relative to quartz.

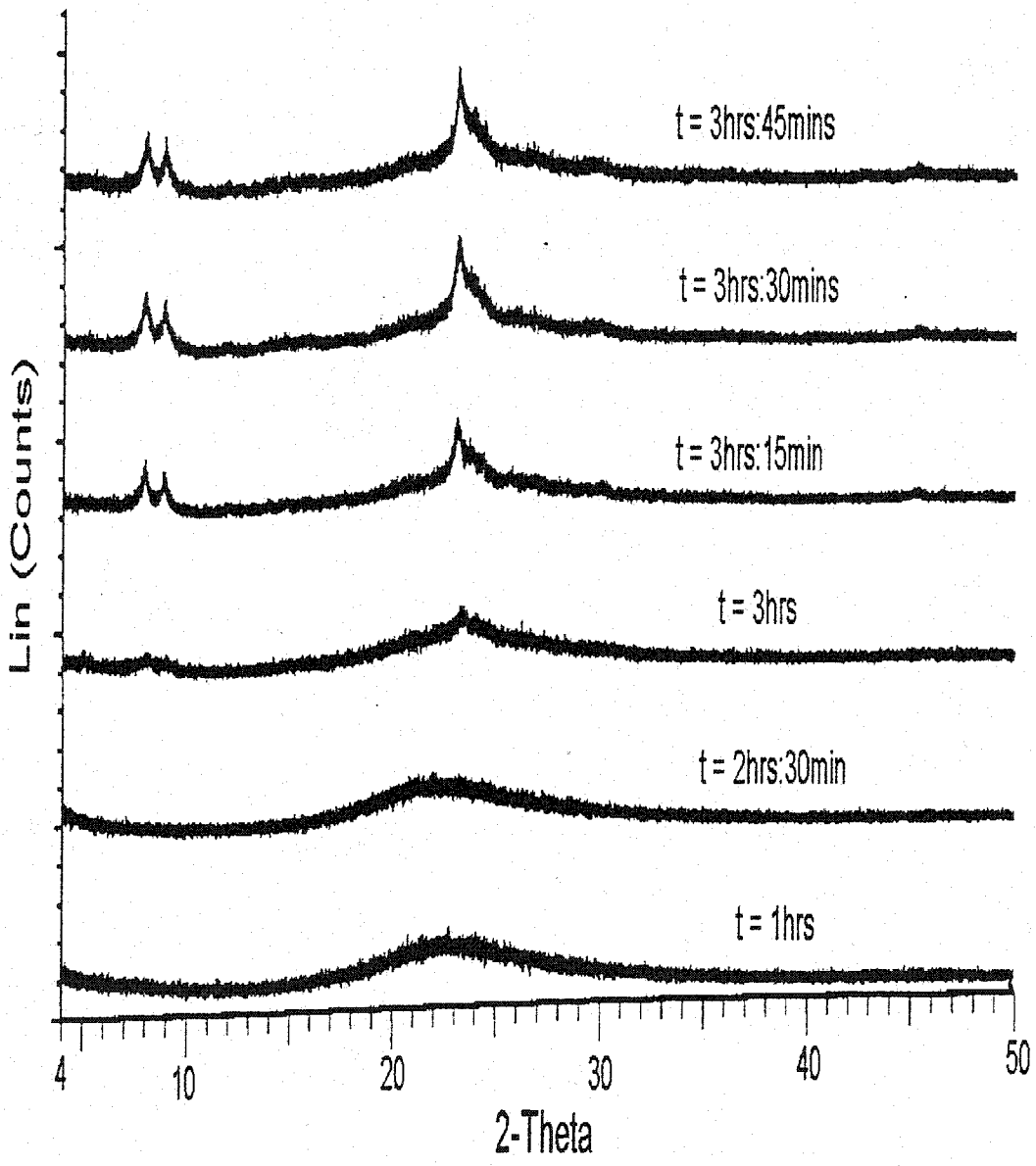

Figure 4.5a: Powder X-ray diffraction pattern of TPABr templated samples

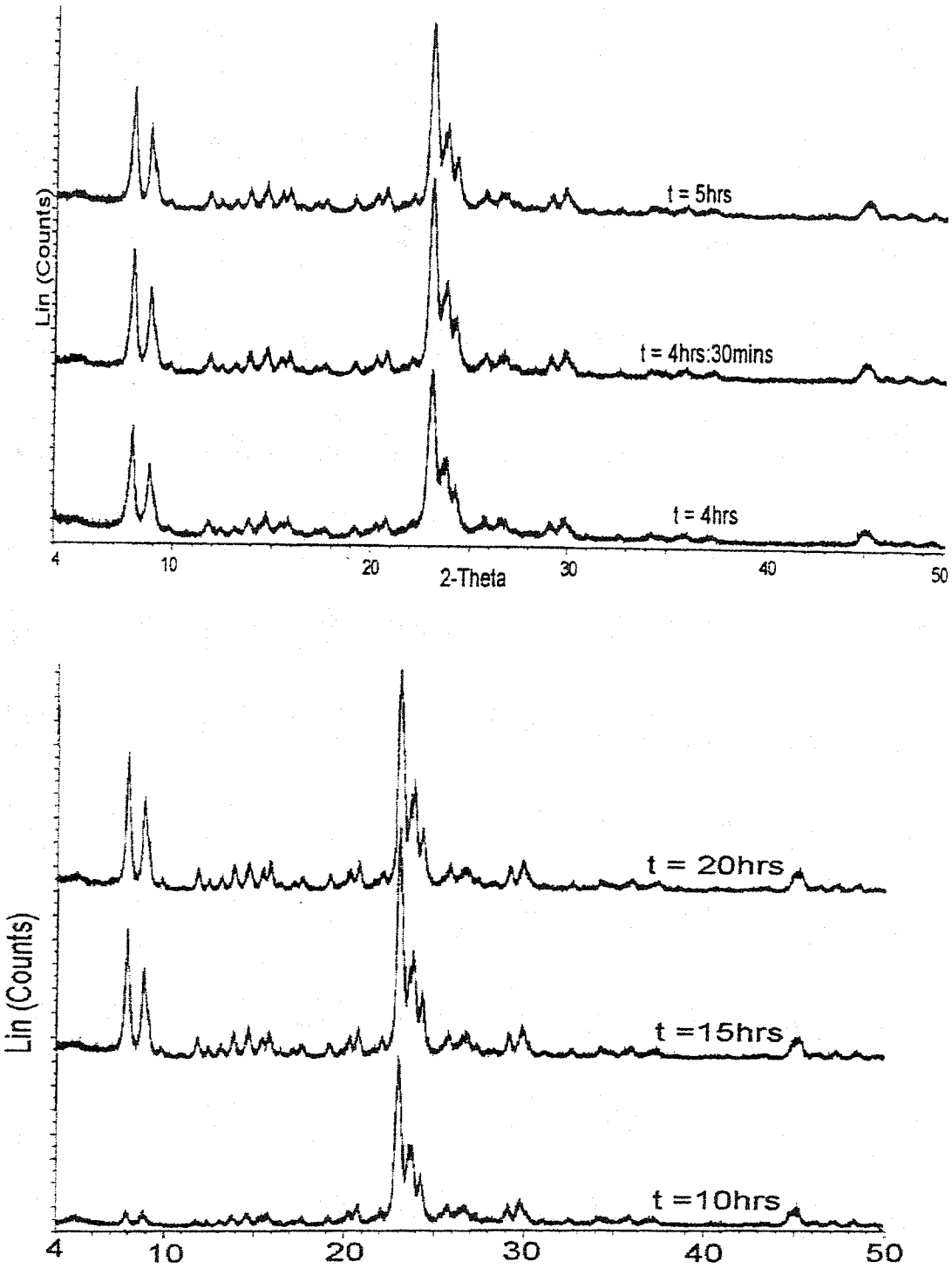

Figure 4.5b: Powder X-ray diffraction pattern of TPABr templated samples

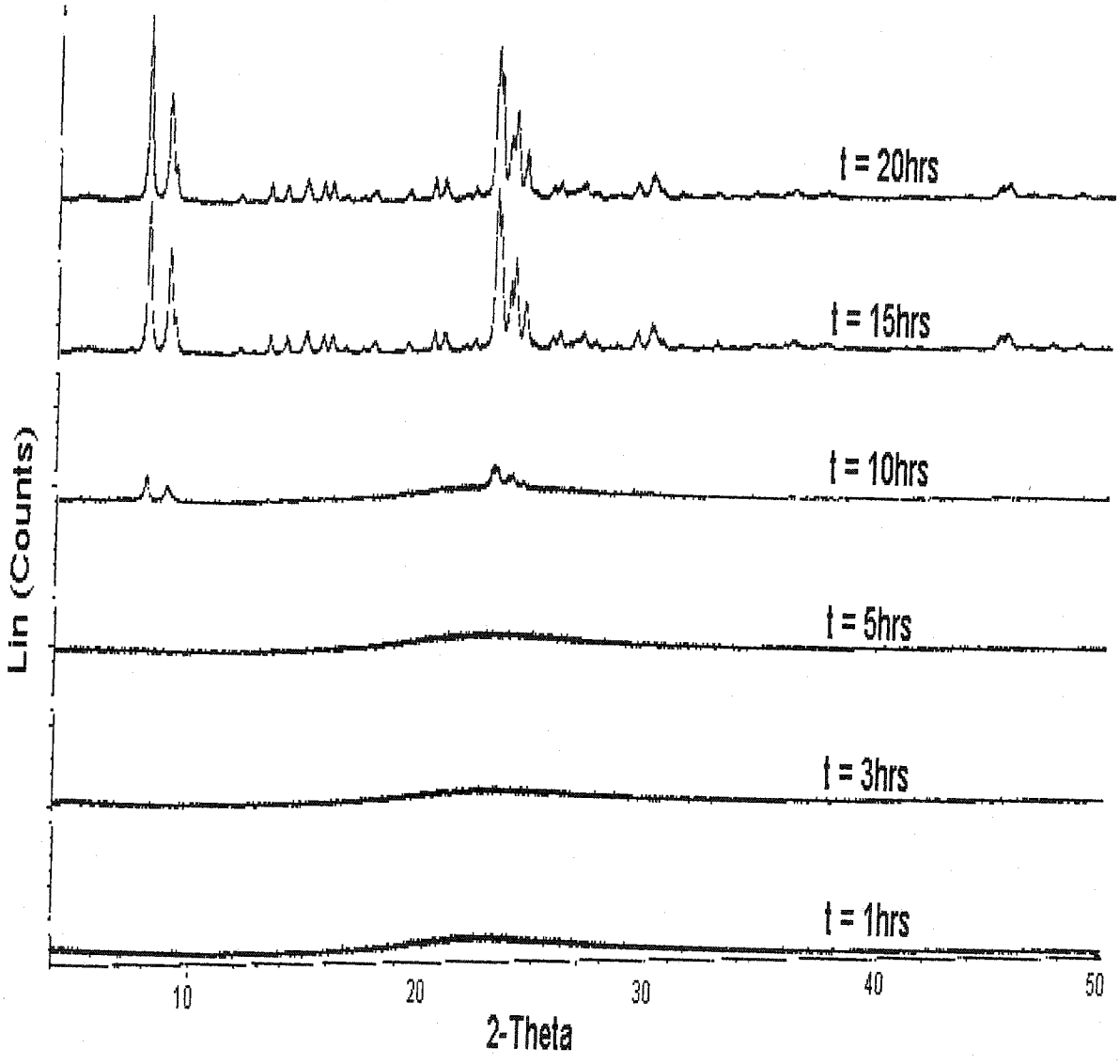

Figure 4.6: Powder X-ray diffraction pattern of DEA templated samples.

4.4 Benzene Adsorption

Benzene adsorption on some of the TPABr templeted samples gives rise to type I isotherm that is typical of microporous materials such as zeolites. The adsorption isotherms (figure 4.7) show that the amount of benzene adsorbed increases with increase in synthesis time. Though both X-ray and IR have shown T-345 to be partially crystalline but the amount benzene adsorbed is comparable to the amount absorbed by fully crystalline T-20hours. This probably explains its high cracking activity, which is comparable to that of pure ZSM-5.

The adsorption properties not only confirmed that T-3, T-3.4, T-3.45 and T-20 are material are microcrystalline but also can be utilized to follow the curse of crystallization.

4.5 Activity of *n*-Hexane Cracking

It is well known that the cracking rate is first order in n-hexane and the curve of $-\ln(1-x)$ in which x is the fractional conversion (%) of n-hexane, as a function of the contact time is expected to be linear. Thus the apparent rate constant can be calculated from the well-known formula $k = -\ln(1-x) * F/V$, in which F is flow rate and V is the volume of the catalyst. The activity plots of $-\ln(1-x)$ Vs contact time of all the catalysts at five different temperatures are provided in figure 4.8. Generally, a linear increase of $-\ln(1-x)$ when the contact time increases was observed even at the lower temperature 300°C. This however suggests that the n-hexane cracking activity of all the catalyst tested is first order in n-hexane.

For each of the catalyst tested, the rate constant (k) was obtained from the slope of the first order plot of $-\ln(1-x)$ against contact time at a given temperature. Table 4.3

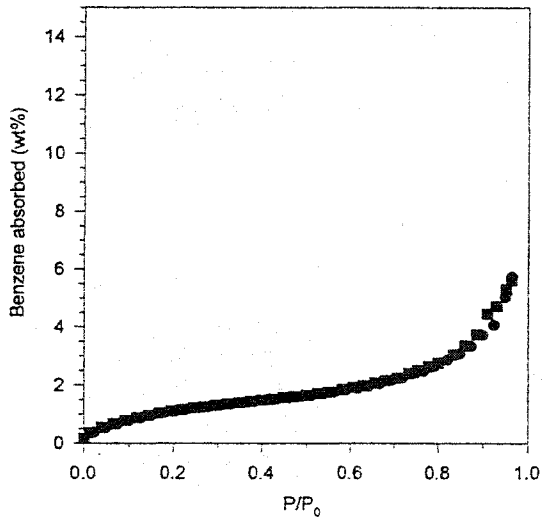

Figure 4.7a: Benzene adsorption isotherm of T-3 sample.

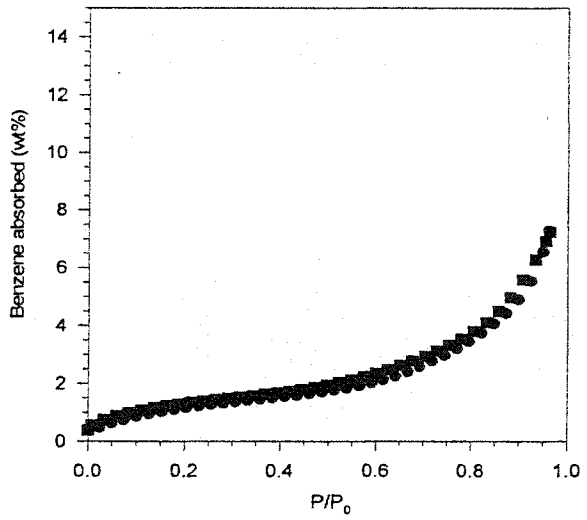

Figure 4.7b:Benzene adsorption isotherm of T-3.4 sample

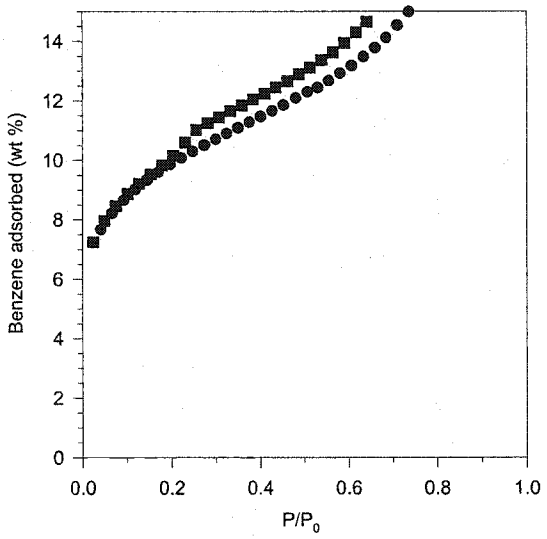

Figure 4.7c: Benzene adsorption isotherm of T-345 sample.

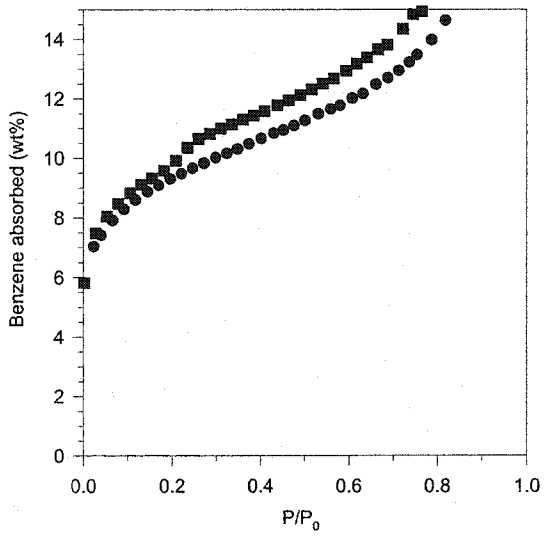

Figure 4.7d: Benzene adsorption isotherm of T-5 sample.

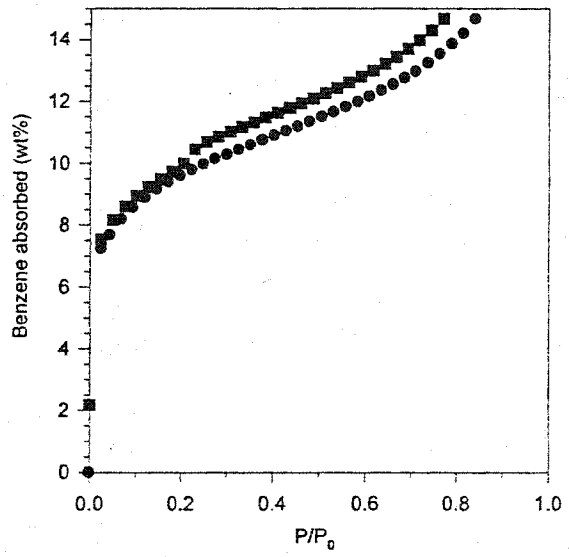

Figure 4.7e: Benzene adsorption isotherm of T-15 sample

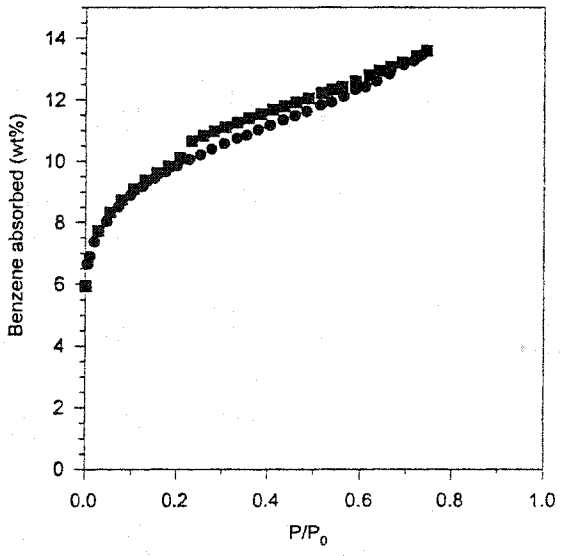

Figure 4.7f: Benzene adsorption isotherm of T-20sample

summaries typical kinetic parameters and rate constant for n-hexane cracking over series of catalysts tested at 500°C and 300°C. For all the TPABr templated precursors, the n-hexane cracking rate was found to satisfy first order kinetics over all the temperature range of 300 to 500°C. It should be noted that no significant deactivation occurred in the experimental conditions used, which involves the increase in flow rate at fixed temperature. This was confirmed by randomly repeating some run under the same flow rate.

A comparison between the n-hexane cracking rate constant (column 3 and 4 of table 4.3) shows that the T-345 catalyst has an activity comparable to that of pure ZSM-5. Among the other precursor the rate constant increases with synthesis time. However, the TPABr templated catalyst with synthesis time of 3hours and below which are infrared and X-ray amorphous are almost completely inactive under our experimental conditions. It is probable that the amorphous silica-alumina may be buried in the inaccessible sites and that a fraction of them are not tetrahedrally coordinated. This behavior is in agreement with the observation that pure silica-alumina catalysts have very low activity. Therefore, it can be concluded the *n*-hexane cracking activity exhibited by the partially crystalline T-3.4, T-3.5 and T-345 catalyst is definitely not due to amorphous matrix in which small crystals are imbedded.

Since, both X-ray and infrared confirmed the presence of microcrystalline ZSM-5 in these TPABr templated samples, it can be concluded that the zeolite component of the catalyst may be the locus of the *n*-hexane cracking. Hence, their rate constants increase with crystallinity (ZSM-5 content). Similarly, all the DEA-mediated samples that are both X-ray and IR amorphous were also found to be inactive in *n*-hexane cracking due to the weak acid strength of amorphous materials.

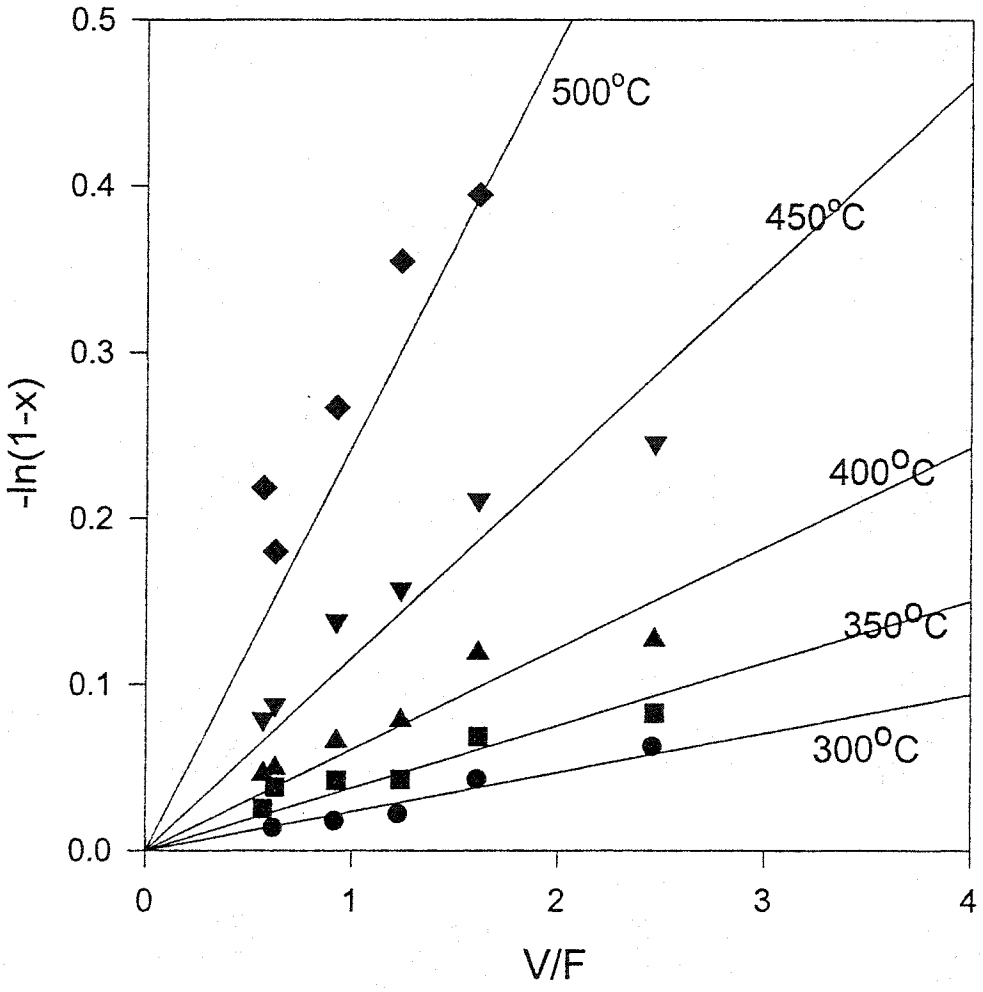

Figure 4.8a: Rate of cracking of *n*-hexane over T-3.4 catalyst as a function of contact time

Table 4.3: Kinetics Parameters and Rate Constant for *n*-hexane Cracking over Various catalyst tested*

Sample Code	Crystallization Time	Rate at 300°C	Rate at 500°C	ln k_o	E_a (kcalmol^{-1})	$\frac{A_{550}}{A_{450}}$	Benzene Adsorption
T-3	3 hours		0.0352		-	0.35	0.30
T-3.4	3hrs: 15mins	.02347	0.2443	4.95	10.1	0.42	0.50
T-3.5	3hrs: 30mins	0.0241	0.4485	7.49	12.9	0.46	-
T-345	3hrs: 45mins	0.0683	1.0650	7.51	11.6	0.64	7.2
T-5	5 hours	0.0259	0.5938	8.29	13.6	0.70	7.1
T-15	15 hours	0.0690	1.1346	8.62	13.1	0.70	7.2
T-20	20 hours	0.1120	1.4880	7.85	11.9	0.70	7.2
E-10	10 hours	-	0.0375		-	0.38	-
E-20	20 hours	0.1155	1.6300	8.089	11.9	0.70	-

*Assuming first order kinetics $r = k\,P_{\text{n-hexane}}$, where $k = k_o e^{-Ea/RT}$ and $P_{\text{n-hexane}}$ is the partial pressure of *n*-hexane.

In addition, T-3 and E-10 that are shown to be partially crystalline by both X-ray and IR were also found to be almost inactive at our experimental conditions, but E-20 being fully crystalline shows interesting catalytic activity comparable to that of fully crystalline TPABr templated sample. It could be inferred that certain level of crystallinity may be a prerequisite or condition for a relatively good catalytic activity of a zeolite catalyst.

Furthermore, from figure 4.8 it is obvious that the *n*-hexane cracking activity increases with temperature due to the increase acid strength and decrease in contact time. The same trend was observed for all the catalyst tested and this observation is in agreement with what is previously reported in the literature. It should be noted that, at elevated temperatures thermal cracking is an important pathway for the conversion of hydrocarbon feedstock. However, the pyrolysis of hydrocarbons is generally much slower than catalytic cracking at catalytic cracking temperature and in most cases one can readily arrange to study catalytic cracking in isolation by choosing an appropriate temperature. Blank run using inert carborandom in place of the catalyst at our experimental conditions showed that thermal cracking effect is negligible (less than 2%).

As the *n*-hexane cracking reaction is acid catalyzed and occurs either by monomolecular protolytic mechanism and or by the classical bimolecular carbenium ion chain mechanism (β-scission), the low activity of the pure silica-alumina samples indicates that the sites associated to the tetrahedral aluminum cation on the amorphous silica-alumina surface are less active in causing the primary reaction. It can be easily envisaged that if hydride transfer for reaction between carbenium ion and n-hexane molecule is indeed the rate limiting step for the classical cracking route, a second order dependence of the cracking rate of the *n*-hexane concentration will be expected.

However, our results can be described more closely by first order model. On the basis of the mechanism, there is no doubt that the product distribution observed during the cracking of paraffins will depend on the relative contribution of two mechanisms. Then, if the most of the cracking occurs through a bimolecular β-scission, high yield of branched products will be obtained. On the contrary, if protolytic cracking prevails, then more linear paraffins, methane, ethane and hydrogen will be produced. Though the prevalence of the two mechanisms could be obtained more precisely from Paraffin/Olefin ratio, Cracking mechanism Ratio, Constraint Index. However, the product selectivities data and the first order pressure dependence confirm to a large extend that *n*-hexane cracking over the series of catalyst tested can be describe by monomolecular reaction mechanism.

4.6 Activation Energy

The values of activation energies E_a obtained from an Arrhenius plot of ln k against T^{-1} for different catalyst tested are given in table 4.4. An Arrhenius plot figure 4.9, of the observed rate constant with temperature range of 300 to 500°C suggests similar apparent activation energies between 10 to 13.6kcalmol^{-1} on a number of catalyst tested in spite of differences in relative level of activity and this is approximate value for the pure ZSM-5. It has been suggested that the low activation energies for the cracking over the catalyst indicated that the reaction rate was inhibited by diffusion[163].

Different values of activation energy has been reported in the literature, a low value of 14.6kcalmol^{-1} for *n*-hexane cracking over HZSM-5 was reported earlier by Borade et al[164]. For a variety of cracking catalyst Wang et al[68] reports values from 15 to 30kcalmol^{-1}. Some years latter Miale et al[163] reported activation energy of 30kcal mol^{-1} on

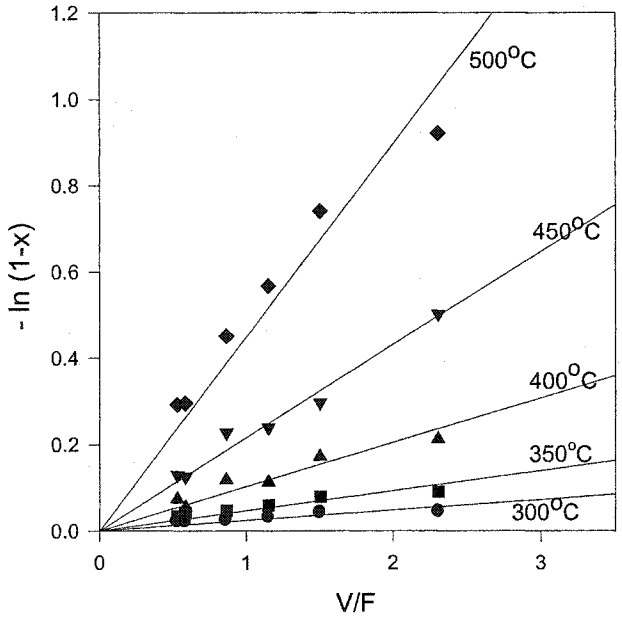

Figure 4.8b: Rate of *n*-hexane cracking over T-3.5 catalyst as a function of contact time

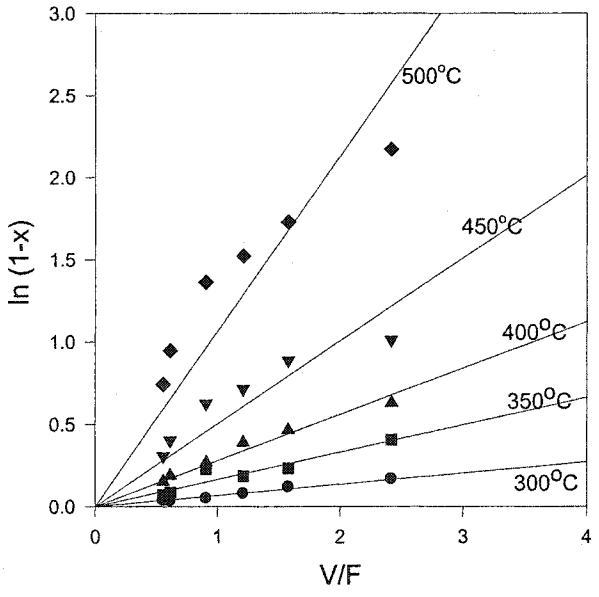

Figure 4.8c: Rate of *n*-hexane cracking over T-345 catalyst as function of contact time.

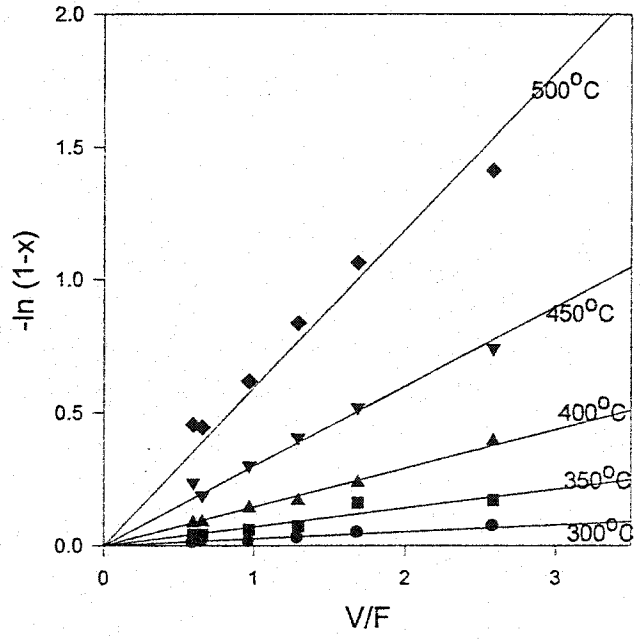

Figure 4.8d: Rate of *n*-hexane cracking over T-5 as a function of contact time

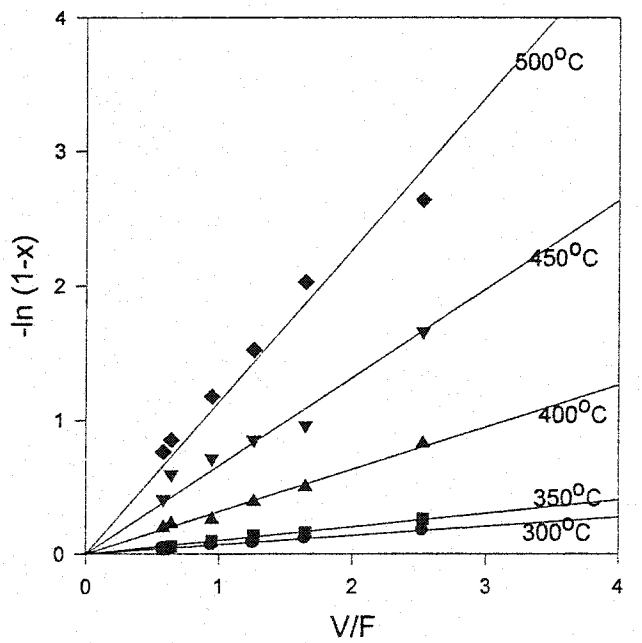

Figure 4.8e: Rate of *n*-hexane cracking over T-15 as a funtion of contact time.

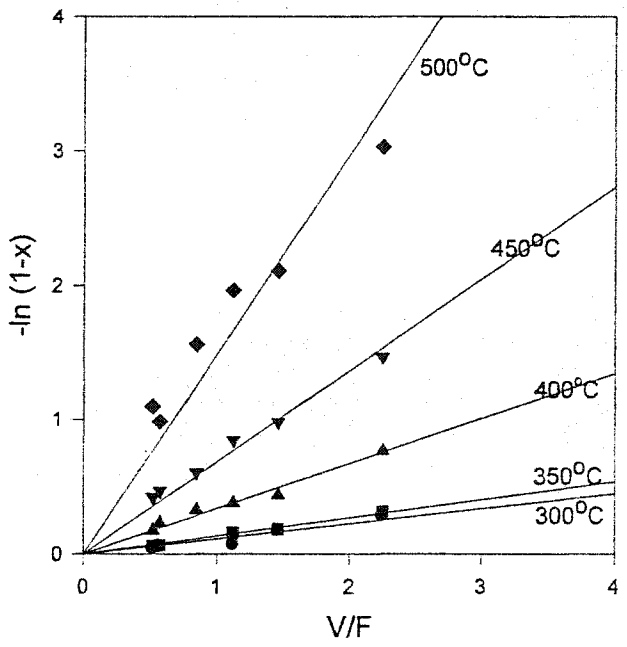

Figure 4.8f: Rate of *n*-hexane cracking over T-20 as a function of contact time.

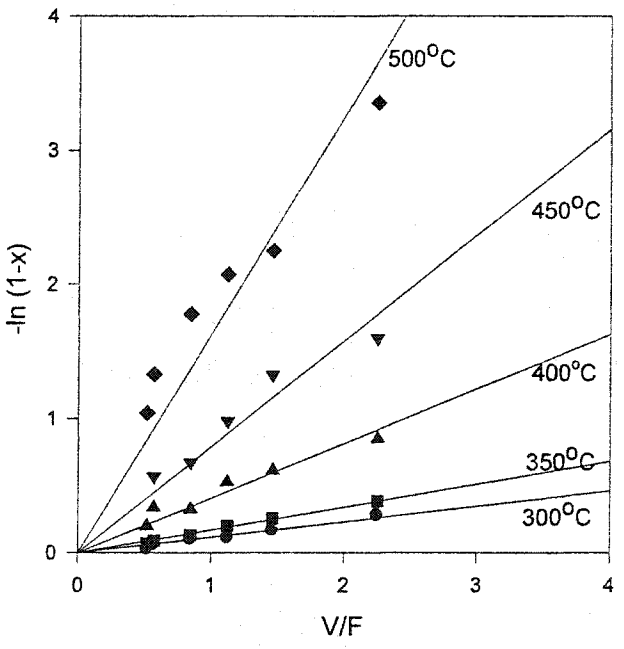

Figure 4.8g: Rate of *n*-hexane cracking over E-20 as function of contact time.

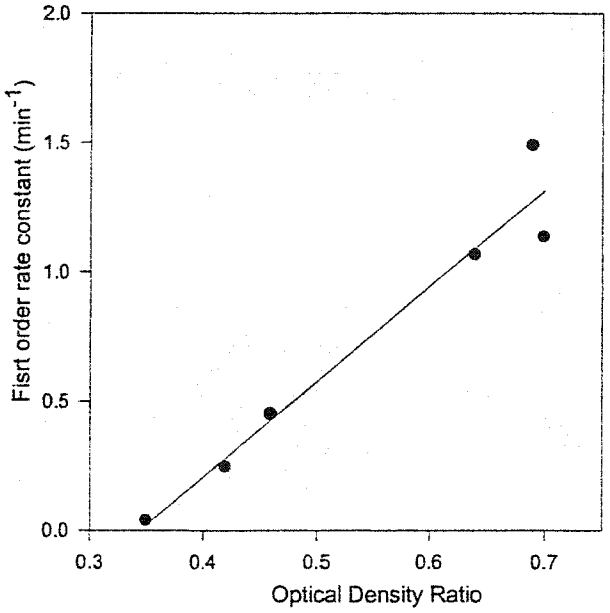

Figure 4.9: Correlation between rate constant and IR crystallinity.

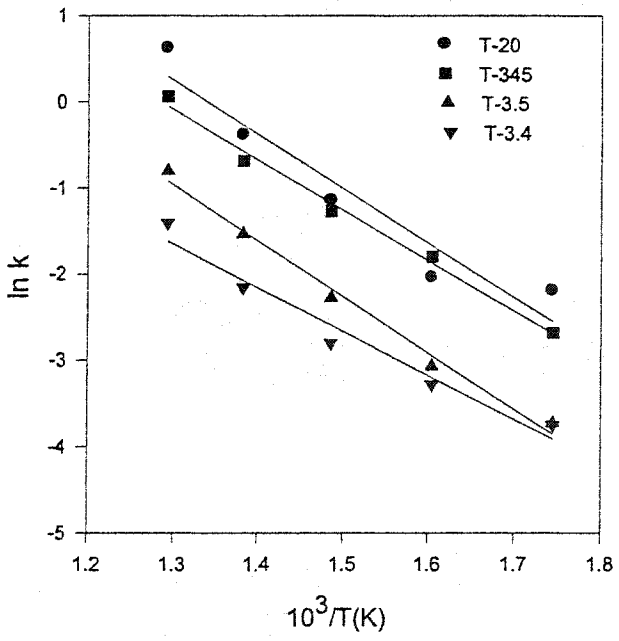

Fig. 4.10a: Arrhenius plot for *n*-hexane cracking over T-3.4, T-3.5, T-345, T-20 catalysts

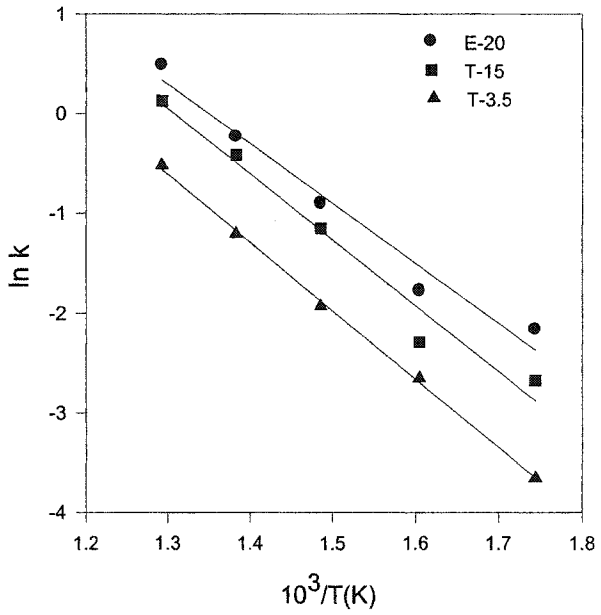

Figure 4.10b: Arrhenius plot for *n*-hexane cracking over T-15, T-3.5, and E-20 catalysts

Table 4.4 Activation energies of the catalyst tested at temperature range of 300 to 500°C

Sample Code	**Crystallization Time**	E_a **(kcalmol^{-1})**
T-3	3 hours	-
T-3.4	3hrs: 15mins	10.1
T-3.5	3hrs: 30mins	12.9
T-345	3hrs: 45mins	11.6
T-5	5 hours	13.6
T-15	15 hours	13.1
T-20	20 hours	11.9
E-20	20 hours	11.9

zeolite A while offretite produced a value of approximately 15kcalmol^{-1}. These workers attributed the differences to diffusion inhibition. Olson et al[131] have also noted that *n*-hexane cracking over ZSM-5 zeolite is diffusion inhibited.

More recently, Wielers et al[155] and Yarlagadda et al[165]. reported an apparent activation as low as 7.2kcal mol^{-1} and 10.1kcal mol^{-1} over aluminum reach MFI zeolites. In addition Wieler and co-workers reported that activation energy decreases with decrease in reaction temperature and increase in aluminum content. Since Cracking Mechanism Ratio (CMR) value also decrease in parallel, they inferred that the protolytic occurring at high temperature required a high energy of activation where as the bimolecular hydride transfer reaction, considered, as the main reaction required a low energy of activation. However, Jolly et al[155] suggested that the reported variations in the energy of activation as a function of the reaction temperature most probably reflected the change in the reaction mechanism and kinetics of the protolytic mechanism of *n*-hexane cracking rather than the intervention of the hydride transfer reactions.

Therefore the values of 7.2kcal mol^{-1}and 21.5kcal mol^{-1} at low and high temperature should be attributed to the activation energies of protolytic mechanism of *n*-hexane cracking of MFI zeolites at low at high temperature.

Thus the similar activation energies obtained suggest a similar *n*-hexane cracking reaction mechanism over all the catalyst tested, predominantly protolytic cracking route as we mentioned earlier on.

4.7 Cracking Mechanism Ratio

The result in figures 4.10 shows that CMR value for *n*–hexane over all the catalyst tested generally increases with temperature and contact time. Based only on product

distribution obtained, some authors have made a proposal to evaluate the contribution of both types of cracking mechanism taking place on a given catalyst and with a given reactant. However, a deep consideration of all the reactions occurring during the cracking mechanism of paraffins indicates that, when more than four carbon atoms are used, it becomes impossible to determine the exact contribution of the protolytic and β-scission mechanism to the final product distribution obtained if only product data are used in the procedure.

In order to indicate the relative contributions of the two different cracking mechanism for n-hexane cracking we use the " Cracking Mechanism Ratio" CMR, which is defined[155] as the ratio $(C_1 + \Sigma C_2)/ iC_4$ where C_1, ΣC_2, and iC_4 denote the selectivities to methane, total C_2 hydrocarbons, and isobutane, respectively. Methane and ethane are formed in the *n*-hexane protolytic cracking steps proceeding via the formation of non-classical pentacordinated carbonium ion $n\text{-}C_6H_{15}^+$) as the reaction transition state. Isobutane is formed (see the reaction scheme below) only in the steps of hydride transfer from *n*-hexane to tert-butyl carbenium ($i\text{-}C_4H_9^+$), the latter is produced by isomerization of the secondary butyl carbenium ion, which proceeds rapidly in comparison with the *n*-hexane transformation.

$$C_6H_{14} + H^+ \longrightarrow C_6H_{15}^+ \qquad \textit{Protolysis}$$

$$C_6H_{15}^+ \longrightarrow CH_4 + C_5H_{11}^+ \qquad \textit{Monomolecular}$$

$$C_6H_{15}^+ \longrightarrow C_2H_6 + C_4H_9^+ \qquad \textit{Monomolecular}$$

$$n\text{-}C_4H_9^+ \longrightarrow i\text{-}C_4H_9^+ \qquad \textit{Isomerization}$$

$$i\text{-}C_4H_9^+ + C_6H_{14} \longrightarrow i\text{-}C_4H_{10} + C_6H_{13}^+ \qquad \textit{Bimolecular}$$

Based on the experimental condition used, high CMR value greater than unity observed in most cases reflects the significant contribution of protolytic cracking route. A low CMR value 0<CMR<1 indicative of bimolecular mechanism were observed at low temperature (300°C) and low contact time. This observation is consistent with the evidence that the activation energy was higher for the protolytic than β-scission mechanism. Thus, it can be expected, as observed in our case, that the monomolecular mechanism will predominate at high reaction temperature.

Furthermore, since bimolecular hydride transfer leading to a β-scission mechanism involves large transition state than the unimolecular protolytic cracking, it appears that the pore size of a zeolite used as a catalyst can introduce a shape selectivity effect that will control the relative extension of the protolytic and β-scission mechanism. It can be visualized from our CMR values that *n*-hexane cracking proceeds predominately via monomolecular mechanism for all the catalyst tested.

The ratio of the protolytic versus β-scission mechanism is important not only from fundamental standpoint, but has important implications for the real FCC unit. Indeed, the product distribution obtained by purely protolytic cracking will be very similar to that obtained by a radical type mechanism, i.e. large H_2, CH_4, C_2 and olefin/paraffin production. Moreover, it will produce less branched products and lower selectivity to gasoline and diesel. On the other hand, the bimolecular mechanism will give less dry gas, more gasoline and diesel oil. Hence, it is obvious that the introduction of ZSM-5 zeolite additive should, contribute to increase the ratio of protolytic versus β-scission cracking, augment the olefinicity of LPG and gasoline, but decrease the gasoline yield.

The CMR value is considered a useful parameter to reveal in a qualitative manner the extent to which the two acid catalyzed cracking mechanisms prevail. On the other hand, the value of CMR can only be used as a quick guide since the cracking mechanism is too complicated.

4.8 Nature of the Zeolite Precursors

Most of the zeolite precursor tested have shown interesting catalytic in n-hexane cracking trend similar to that of pure ZSM-5 material. Microporous zeolite such as ZSM-5 material have been shown in literature to have good catalytic activity in *n*-hexane cracking while mesoporous MCM-41 have been reported to have low catalytic activity in n-hexane cracking reaction possible due to absence of strong Bronsted acid sites. It therefore follows that the observed cracking activity of our precursor materials may be due to their microcrystalline nature.

n-hexane cracking reaction on zeolites generally proceeds via monomolecular protolytic cracking and bimolecular β-cracking mechanism. The bimolecular hydride transfer leading to a β-cracking mechanism involves large transition state compared with unimolecular protoytic cracking; it appears that the pore size of zeolite used as a catalyst can introduce the relative extension of the protolytic and β-cracking. Since we have earlier suggested based on CMR that the *n*-hexane cracking mechanism over pure ZSM-5 and all the precursors tested is predominantly protolytic, it can be concluded that these zeolite precursors are microcrystalline material with structure similar to that of ZSM-5. This conclusion is consistent with the report of Haag and Dessau[140] who proposed that protolytic cracking is more favorable in 10 membered ring zeolite such as ZSM-5 than in

12 membered ring zeolite such as faujusite. This is also supported by Miratos and Barthomeuf[166] who reported that protolytic cracking is favored when small pore zeolites are used.

As a matter of fact, both the infrared spectroscopy and the X-ray diffraction pattern of the precursors material reveal that these zeolite precursors are microcrystalline materials having structure similar to that of pure ZSM-5 embedded in amorphous. This was confirmed by their benzene adsorption property, which is typical of microcrystalline material. It is interesting to note that though both infrared spectroscopy and X-ray diffraction pattern have shown T-345 to be partially crystalline, but its n-hexane cracking activity is comparable to that of pure ZSM-5. This could be explains by its high adsorption property which is also comparable to that of pure ZSM-5 material.

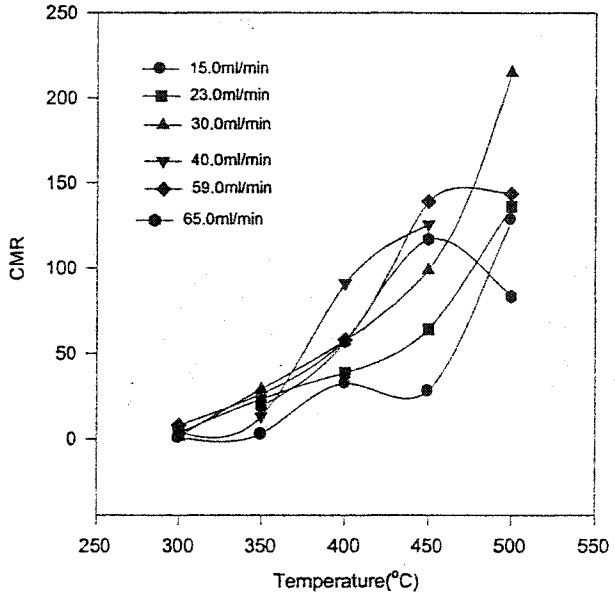

Figure 4.11a: Variation of selectivity of T-3.4 with reaction temperature

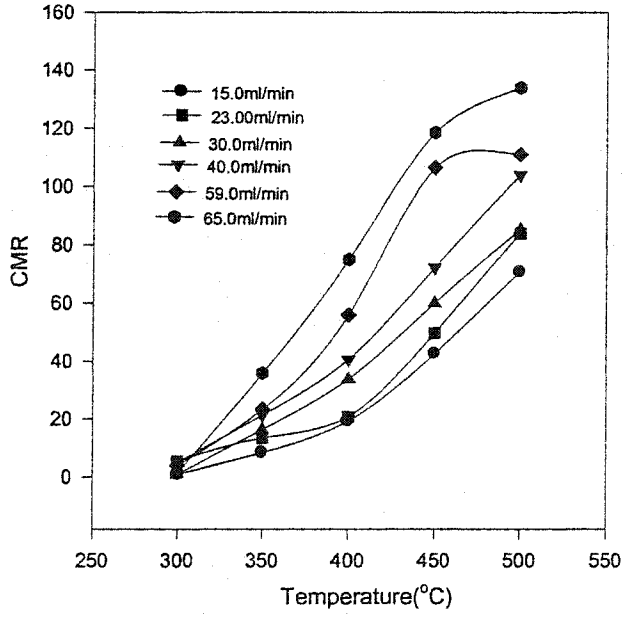

Figure 4.11b: Variation of selectivity of T-3.5 with reaction temperature

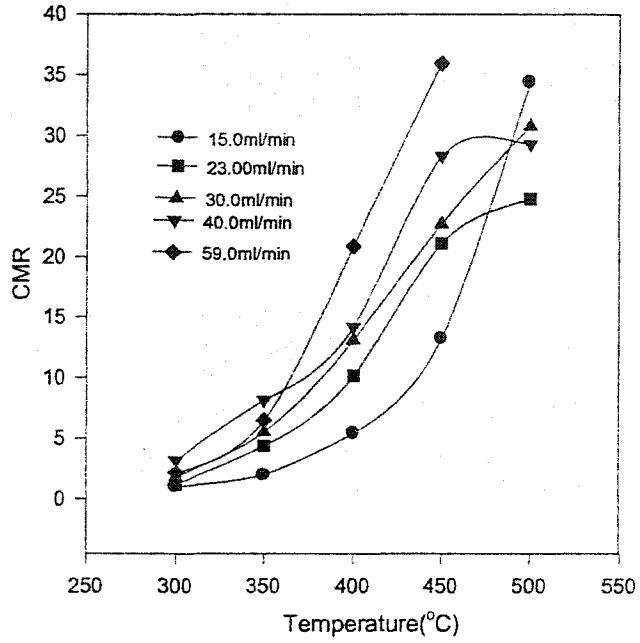

Figure 4.11c: Variation of selectivity of T-345 with reaction temperature

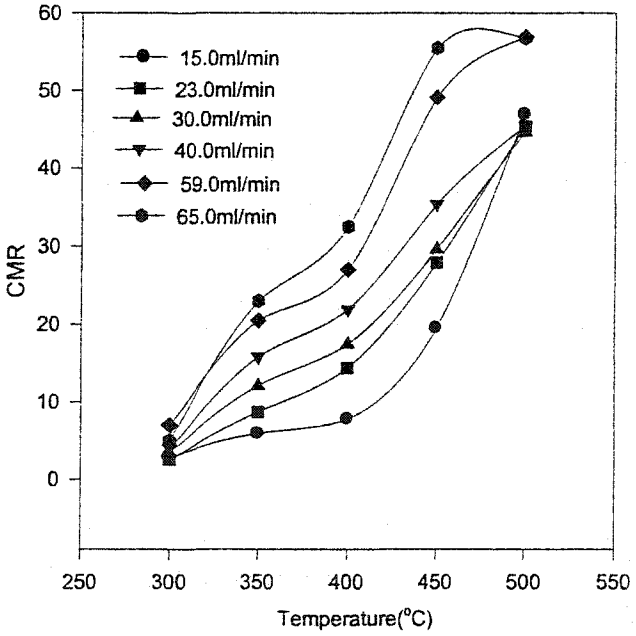

Figure 4.11d: Variation of selectivity of T-5 with reaction temperature

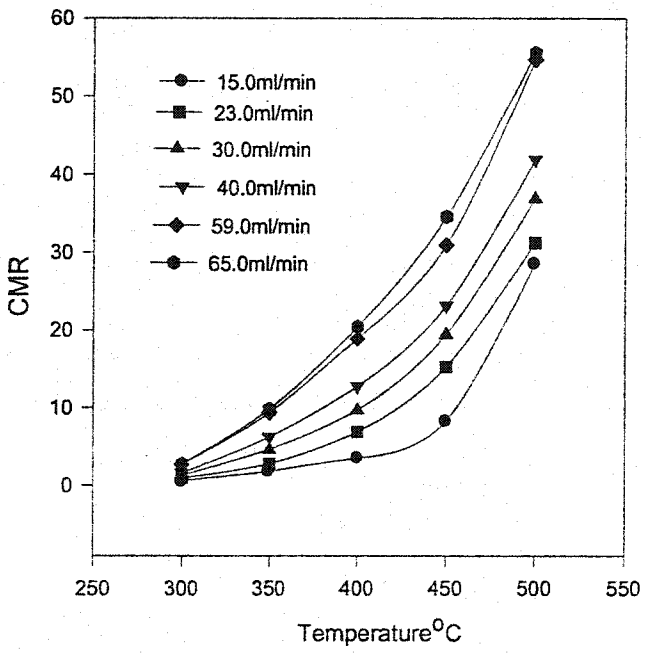

Figure 4.11e: Variation of selectivity of T-15 with reaction temperature

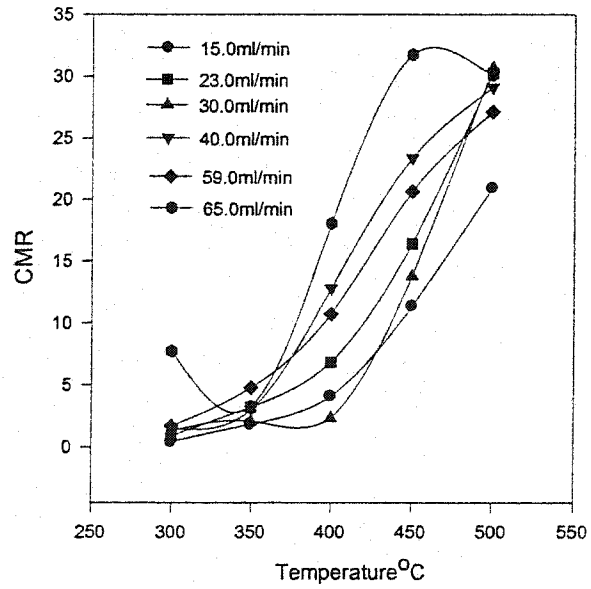

Figure 4.11f: Variation of selectivity of T-20 with reaction temperature

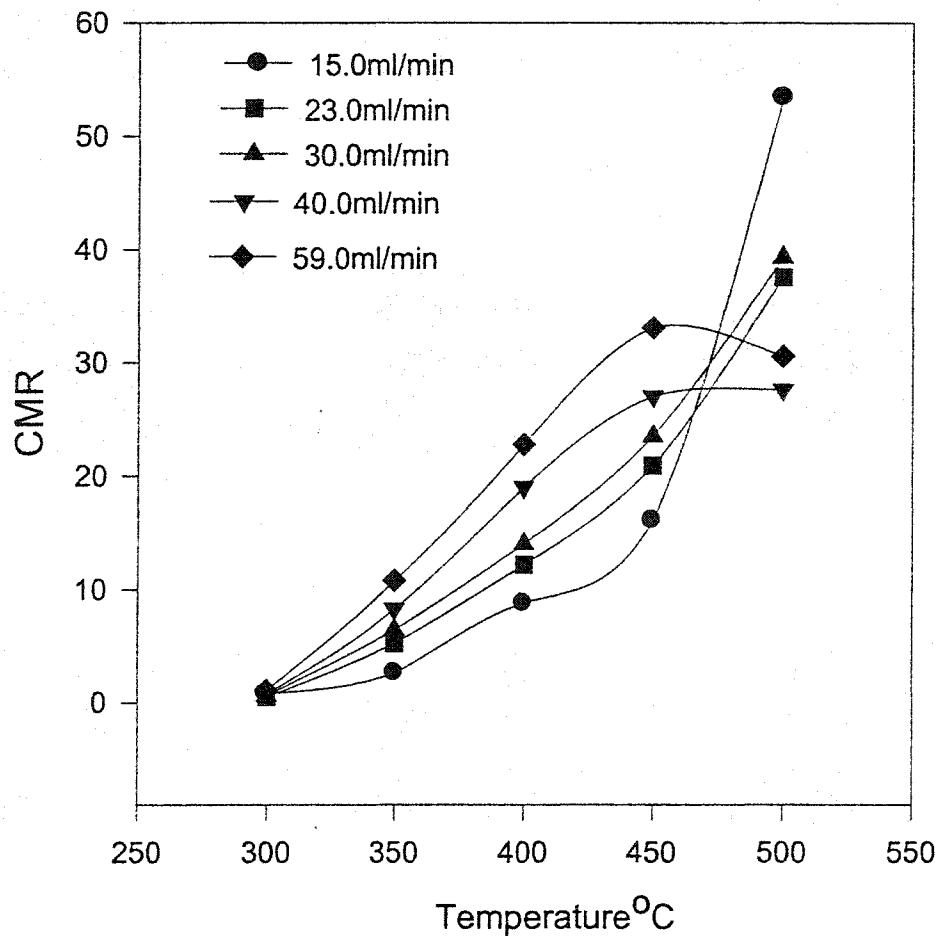

Figure 4.11g: Variation of selectivity of E-20 with reaction temperature

CHAPTER 5

CONCLUSIONS AND RECOMMENDATIONS

5.1 Summary and Conclusions

The results of the investigation suggest the following.

- The syntheses were generally characterized by period of induction, crystal growth, and full crystallization. The shorter induction period of TPABr samples may be attributed to their better structure directing ability (templating effect).
- Three different phases were identified in the synthesis namely Amorphous, Composite, and pure crystalline ZSM-5.
- Both X-ray and IR confirmed that the Zeolite precursor of both TPABr and DEA templated systems are microcrystalline zeolitic materials having structure similar to ZSM-5 embedded in amorphous matrix.
- Certain level of crystallinity may be required for a good catalytic performance of the sample tested.
- The cracking temperature, crystallinity and the contact time are the factors that affect the catalytic activity.
- The n-hexane activity of the precursor increases with crystallinity and the apparent activation energies were remarkably similar in spite of the differences in relative level of activity suggesting a similar cracking mechanism.
- Though T-345 is shown to be a composite material by both the X-ray and IR but it high adsorption property comparable to that of pure ZSM-5 is consistent with it's high catalytic.

- It can be visualized from the CMR values that *n*-hexane cracking proceeds predominantly via monomolecular protolytic mechanism for all the catalyst tested.

5.1 Recommendations

The following are the recommendations for future work.

- The effect of zeolite composition should be studied.
- The effect pf crystal size and synthesis method should be investigated.
- The studies should be extended to other zeolites.
- Structural characterization could be extended to other physical methods.

APPENDIX

Table A-4.5

Selectivities of *n*-hexane cracking as a function of temperatures at V/F (ml/ml min^{-1})

2.25, 1 atm, over 1.00g of T-3.4

Temperature (°C)	300.00	350.00	400.00	450.00	500.00
CMR	0.81	2.68	32.43	27.75	128.25
iC_4/nC_4	0.88	1.00	0.15	0.18	0.05
Conversion (wt%)	5.99	7.92	11.88	21.77	41.44
Selectivity (wt%)					
C_1	0.83	0.51	1.35	1.61	2.29
C_2	2.67	2.27	8.84	9.37	10.86
C_2=	6.18	4.67	8.92	9.42	11.61
C_3	20.20	9.97	17.34	17.46	14.14
C_3=	16.69	19.07	34.43	31.56	34.24
iso-C_4	12.02	2.78	0.59	0.73	0.19
n-C_4	13.69	2.78	3.96	4.13	4.08
trans-C_4=	3.67	16.54	3.03	3.08	2.65
1-C_4=	0.67	2.78	0.84	0.96	0.94
iso-C_4=	2.17	3.28	3.87	3.86	4.25
cis-C_4=	1.67	2.90	1.85	2.02	1.81
iso-C_5	2.00	2.02	0.08	0.09	0.07
n-C_5	3.01	0.63	1.18	2.53	0.05
ΣC_5=	1.00	5.05	1.26	5.24	1.81

Table A-4.6

Selectivities of *n*-hexane cracking as a function of temperatures at V/F (ml/ml min^{-1})

1.61, 1 atm, over 1.00g of T-3.4

Temperature (°C)	300.00	350.00	400.00	450.00	500.00
CMR	3.57	0.70	38.60	64.17	136.00
iC_4/nC_4	0.41	0.45	0.13	0.09	0.05
Conversion (wt%)	4.08	6.61	11.20	19.04	32.61
Selectivity (wt%)					
C_1	0.74	0.30	1.61	1.89	2.82
C_2	1.23	1.21	8.04	9.82	11.50
C_2=	4.17	1.97	7.59	8.51	10.70
C_3	23.04	1.21	11.88	12.76	12.48
C_3=	15.69	12.86	33.84	36.55	35.39
iso-C_4	1.72	4.99	0.45	0.32	0.18
n-C_4	4.17	11.04	3.39	3.41	3.68
trans-C_4=	2.70	1.66	3.21	3.99	3.62
1-C_4=	0.74	0.76	0.89	1.42	1.38
iso-C_4=	2.45	0.91	4.29	5.72	5.58
cis-C_4=	1.72	0.76	2.05	3.05	2.42
iso-C_5	0.98	0.00	0.63	0.95	0.06
n-C_5	1.23	0.00	0.27	2.52	2.09
ΣC_5=	5.15	5.90	0.80	0.89	0.55

Table A-4.7

Selectivities of *n*-hexane cracking as a function of temperatures at V/F (ml/ml min^{-1}) 1.24, 1 atm, over 1.00g of T-3.4

Temperature (°C)	300.00	350.00	400.00	450.00	500.00
CMR	1.25	29.00	6.33	98.67	215.00
iC_4/nC_4	0.92	0.11	0.75	0.07	0.03
Conversion (wt%)	2.08	4.18	7.53	14.54	29.85
Selectivity (wt%)					
C_1	0.48	0.96	1.06	2.68	2.61
C_2	1.92	2.15	6.91	8.87	10.35
C_2=	4.81	3.83	7.17	8.80	8.64
C_3	12.98	4.78	11.55	9.83	12.13
C_3=	21.15	24.16	36.79	31.91	34.87
iso-C_4	5.77	0.24	2.39	0.21	0.10
n-C_4	6.25	2.15	3.19	2.82	3.82
trans-C_4=	3.37	2.39	3.85	3.99	4.52
1-C_4=	0.96	0.48	1.20	1.38	1.81
iso-C_4=	4.33	2.15	4.91	5.30	6.37
cis-C_4=	2.40	1.67	2.52	2.68	2.91
iso-C_5	0.96	2.87	0.27	0.07	0.07
n-C_5	1.92	0.72	1.99	1.65	1.84
ΣC_5=	3.85	0.96	1.99	0.83	0.64

Table A-4.8

Selectivities of *n*-hexane cracking as a function of temperatures at V/F (ml/ml min^{-1})

0.93, 1 atm, over 1.00g of T-3.4

Temperature (°C)	300.00	350.00	400.00	450.00	500.00
CMR	3.67	13.00	91.00	125.50	34.20
iC_4/nC_4	0.38	0.30	0.07	0.04	0.17
Conversion (wt%)	1.71	4.14	6.35	12.89	23.42
Selectivity (wt%)					
C_1	0.58	0.72	1.26	1.71	2.18
C_2	1.75	3.14	6.46	9.46	10.93
C_2=	4.09	5.56	6.61	8.30	8.80
C_3	52.63	13.77	9.45	11.09	12.51
C_3=	17.54	30.19	38.27	38.32	36.46
iso-C_4	1.75	0.72	0.16	0.16	0.64
n-C_4	4.68	2.42	2.36	3.72	3.76
trans-C_4=	2.92	2.90	6.30	4.65	4.91
1-C_4=	0.58	0.72	1.73	1.63	1.96
iso-C_4=	2.92	2.90	4.57	5.82	6.75
cis-C_4=	1.75	1.69	2.52	3.03	3.25
iso-C_5	0.58	0.24	0.16	0.54	0.17
n-C_5	1.17	0.24	0.79	1.24	1.92
ΣC_5=	5.26	4.59	1.10	1.32	0.94

Table A-4.9

Selectivities of *n*-hexane cracking as a function of temperatures at V/F (ml/ml min^{-1})

0.63, 1 atm, over 1.00g of T-3.4

Temperature (°C)	300.00	350.00	400.00	450.00	500.00
CMR	8.00	1.67	58.00	139.00	143.50
iC_4/nC_4	0.33	2.57	0.11	0.04	0.04
Conversion (wt%)	1.31	3.75	4.83	8.37	16.46
Selectivity (wt%)					
C_1	0.76	0.53	1.04	1.79	1.76
C_2	2.29	2.67	4.97	8.00	9.11
C_2=	3.05	4.80	6.00	6.81	6.56
C_3	12.21	5.07	7.25	9.32	10.33
C_3=	16.03	27.47	34.78	36.80	31.23
iso-C_4	0.76	4.80	0.21	0.12	0.12
n-C_4	2.29	1.87	1.86	2.75	3.28
trans-C_4=	2.29	2.40	6.83	4.54	6.56
1-C_4=	1.53	0.80	1.24	1.67	2.55
iso-C_4=	2.29	2.67	3.11	5.14	6.93
cis-C_4=	1.53	1.60	3.11	3.46	4.74
iso-C_5	2.29	0.27	0.00	1.08	0.24
n-C_5	2.29	0.53	1.04	0.60	2.67
ΣC_5=	7.63	5.33	1.45	2.27	1.03

Table A-4.10

Selectivities of *n*-hexane cracking as a function of temperatures at V/F (ml/ml min^{-1})

0.57, 1 atm, over 1.00g of T-3.4

Temperature (°C)	350.00	400.00	450.00	500.00
CMR	19.00	57.00	117.00	83.33
iC_4/nC_4	0.25	0.11	0.06	0.07
Conversion (wt%)	2.50	4.50	7.60	19.63
Selectivity (wt%)				
C_1	0.40	0.89	2.50	2.24
C_2	2.80	5.56	6.58	6.06
C_2=	4.40	6.22	6.32	4.43
C_3	10.40	6.22	7.89	6.78
C_3=	30.00	37.78	33.55	25.17
iso-C_4	0.40	0.22	0.13	0.15
n-C_4	1.60	2.00	2.37	2.14
trans-C_4=	3.20	4.00	4.34	3.52
1-C_4=	1.20	1.56	1.58	1.53
iso-C_4=	2.00	4.00	4.87	4.28
cis-C_4=	2.00	2.67	3.55	2.45
iso-C_5	0.40	0.22	0.79	0.15
n-C_5	0.40	0.89	0.13	0.87
ΣC_5=	5.20	2.67	2.11	0.66

Table A-4.11

Selectivities of *n*-hexane cracking as a function of temperatures at V/F (ml/ml min^{-1}) 2.31, 1 atm, over 1.00g of T-3.5

Temperature (°C)	300.00	350.00	400.00	450.00	500.00
CMR	0.88	8.44	19.30	42.52	70.77
iC_4/nC_4	1.78	0.44	0.23	0.14	0.11
Conversion (wt%)	4.39	8.65	19.2	39.47	60.24
Selectivity (wt%)					
C_1	0.68	1.04	1.61	2.03	2.86
C_2	2.05	5.78	10.36	11.60	11.29
C_2=	3.64	10.75	11.15	13.30	16.40
C_3	10.48	23.01	21.67	17.94	15.44
C_3=	14.58	33.41	32.97	34.66	31.87
iso-C_4	7.29	2.08	1.20	0.63	0.43
n-C_4	4.10	4.74	5.21	4.66	4.00
trans-C_4=	2.51	2.89	2.71	3.09	2.37
1-C_4=	0.46	0.81	0.83	1.14	0.95
iso-C_4=	2.51	2.89	4.17	4.36	4.08
cis-C_4=	1.59	1.73	1.77	2.05	1.66
iso-C_5	0.68	0.92	0.47	0.18	0.13
n-C_5	1.37	0.81	0.26	1.39	1.59
ΣC_5=	0.91	2.54	0.36	0.66	0.88

Table A-4.12

Selectivities of *n*-hexane cracking as a function of temperatures at V/F (ml/ml min^{-1})

1.50, 1 atm, over 1.00g of T-3.5

Temperature (°C)	300.00	350.00	400.00	450.00	500.00
CMR	5.50	13.44	20.80	49.67	83.88
iC_4/nC_4	0.40	0.35	0.23	0.11	0.08
Conversion (wt%)	4.15	7.56	15.87	25.71	52.36
Selectivity (wt%)					
C_1	0.72	0.93	1.45	2.14	2.16
C_2	1.69	5.69	9.58	10.66	11.67
C_2=	2.89	9.39	8.63	10.39	13.41
C_3	6.75	17.59	16.64	15.29	14.38
C_3=	13.98	36.90	34.78	36.25	36.02
iso-C_4	0.96	1.19	0.95	0.47	0.32
n-C_4	2.41	3.44	4.10	4.36	4.07
trans-C_4=	2.17	2.51	3.47	4.12	3.27
1-C_4=	0.72	0.79	1.20	1.56	1.38
iso-C_4=	2.41	2.25	5.23	6.18	5.39
cis-C_4=	1.69	2.38	2.21	2.88	2.25
iso-C_5	3.13	5.56	0.00	0.43	0.10
n-C_5	2.41	0.00	1.39	1.13	1.45
ΣC_5=	2.89	2.38	1.83	1.05	0.23

Table A-4.13

Selectivities of *n*-hexane cracking as a function of temperatures at V/F (ml/ml min^{-1})

1.15, 1 atm, over 1.00g of T-3.5

Temperature (°C)	300.00	350.00	400.00	450.00	500.00
CMR	1.00	16.40	33.83	60.00	85.25
iC_4/nC_4	1.50	0.29	0.14	0.09	0.07
Conversion (wt%)	3.00	5.74	10.68	21.29	43.30
Selectivity (wt%)					
C_1	0.00	0.87	1.50	1.69	2.22
C_2	1.00	5.40	9.64	9.77	10.74
C_2=	2.00	8.01	7.87	8.27	10.67
C_3	4.00	14.46	15.82	13.15	14.25
C_3=	10.67	36.59	37.08	34.05	35.20
iso-C_4	3.00	0.87	0.56	0.33	0.28
n-C_4	2.00	2.96	4.12	3.85	4.06
trans-C_4=	1.67	2.44	4.31	5.03	4.32
1-C_4=	0.33	0.87	1.50	1.88	4.09
iso-C_4=	1.67	1.92	6.55	6.67	6.49
cis-C_4=	1.00	1.57	2.90	3.15	2.70
iso-C_5	0.33	0.87	0.00	0.38	0.00
n-C_5	1.00	0.35	1.12	0.94	1.45
ΣC_5=	8.00	3.14	0.84	0.61	0.88

Table A-4.14

Selectivities of *n*-hexane cracking as a function of temperatures at V/F (ml/ml min^{-1}) 0.87, 1 atm, over 1.00g of T-3.5

Temperature (°C)	300.00	350.00	400.00	450.00	500.00
CMR	5.00	21.33	40.60	72.17	104.00
iC_4/nC_4	0.50	0.21	0.13	0.07	0.06
Conversion (wt%)	2.47	4.58	11.12	20.35	36.28
Selectivity (wt%)					
C_1	0.00	1.09	1.44	2.01	2.40
C_2	0.81	5.46	9.53	10.96	10.75
C_2=	1.21	7.42	7.28	8.30	9.79
C_3	2.83	13.76	15.02	13.86	12.02
C_3=	9.72	37.99	38.04	37.44	33.05
iso-C_4	0.40	0.66	0.45	0.29	0.22
n-C_4	0.81	3.06	3.51	4.18	3.72
trans-C_4=	2.02	2.40	4.41	4.96	4.08
1-C_4=	0.40	0.87	1.62	1.97	1.79
iso-C_4=	2.02	1.97	6.56	7.32	6.34
cis-C_4=	1.21	1.75	2.88	3.34	2.87
iso-C_5	0.00	0.66	0.00	0.34	0.47
n-C_5	0.00	1.75	0.81	0.29	2.18
ΣC_5=	0.40	3.93	0.90	0.88	0.33

Table A-4.15

Selectivities of *n*-hexane cracking as a function of temperatures at V/F (ml/ml min^{-1}) 0.59, 1 atm, over 1.00g of T-3.5

Temperature (°C)	300.00	350.00	400.00	450.00	500.00
CMR	1.50	23.50	56.00	106.50	111.00
iC_4/nC_4	0.50	0.17	0.09	0.05	0.05
Conversion (wt%)	2.1	4.04	5.34	11.83	25.57
Selectivity (wt%)					
C_1	0.00	1.49	1.41	1.61	2.35
C_2	0.48	4.46	8.16	9.55	11.11
C_2=	0.95	5.69	6.19	6.85	8.25
C_3	2.38	8.66	11.67	12.93	12.71
C_3=	7.14	35.15	35.16	35.25	35.78
iso-C_4	0.95	0.50	0.28	0.17	0.20
n-C_4	1.90	2.97	3.09	3.63	3.99
trans-C_4=	1.43	2.23	4.22	5.41	5.20
1-C_4=	0.48	0.74	1.55	2.28	2.42
iso-C_4=	1.90	1.98	6.05	8.71	7.70
cis-C_4=	0.95	1.73	2.81	4.90	3.75
iso-C_5	0.00	1.98	0.14	0.17	0.55
n-C_5	0.48	0.99	0.70	0.68	1.88
ΣC_5=	10.48	3.96	1.69	2.28	0.94

Table A-4.16

Selectivities of *n*-hexane cracking as a function of temperatures at V/F (ml/ml min^{-1}) 0.53, 1 atm, over 1.00g of T-3.5

Temperature (°C)	300.00	350.00	400.00	450.00	500.00
CMR	4.00	35.93	75.00	118.50	133.93
iC_4/nC_4	0.33	0.14	0.06	0.05	0.04
Conversion (wt%)	2.13	3.34	5.34	2.16	25.34
Selectivity (wt%)					
C_1	0.00	0.90	1.12	1.81	2.33
C_2	0.94	4.49	6.93	10.61	10.69
C_2=	0.94	5.39	5.99	7.07	8.41
C_3	2.35	8.68	10.67	12.34	12.51
C_3=	8.45	34.13	29.40	36.51	34.81
iso-C_4	0.47	0.30	0.19	0.16	0.16
n-C_4	1.41	2.10	3.00	3.62	4.06
trans-C_4=	10.33	2.40	4.31	5.35	5.52
1-C_4=	3.76	0.90	1.87	2.22	2.60
iso-C_4=	4.69	2.10	7.30	7.40	7.93
cis-C_4=	6.57	1.80	3.56	3.62	4.30
iso-C_5	0.47	0.00	0.00	0.33	1.50
n-C_5	0.47	0.60	0.94	1.07	0.47
ΣC_5=	0.94	4.79	3.18	1.40	0.51

Table A-4.17

Selectivities of *n*-hexane cracking as a function of temperatures at V/F (ml/ml min^{-1}) 2.42, 1 atm, over 1.00g of T-345

Temperature (°C)	300.00	350.00	400.00	450.00	500.00
CMR	1.02	1.98	5.42	13.19	34.40
iC_4/nC_4	0.85	0.83	0.65	0.58	0.42
Conversion (wt%)	15.45	33.38	46.71	63.60	88.60
Selectivity (wt%)					
C_1	1.68	0.87	1.11	2.34	3.51
C_2	2.14	4.34	7.34	12.37	13.08
C_2=	5.95	9.20	12.55	21.78	25.34
C_3	25.24	31.73	26.12	23.88	17.55
C_3=	14.56	18.75	25.22	31.93	27.33
iso-C_4	9.58	7.28	3.87	2.77	1.22
n-C_4	11.26	8.75	5.95	4.78	2.92
trans-C_4=	3.56	3.62	2.85	2.64	1.50
1-C_4=	0.97	0.96	0.98	1.01	0.60
iso-C_4=	4.27	4.43	4.32	3.90	2.34
cis-C_4=	1.75	1.80	1.95	1.71	1.05
iso-C_5	0.32	1.32	0.47	0.33	0.12
n-C_5	2.85	1.23	0.54	0.27	0.41
ΣC_5=	1.36	1.77	1.82	1.31	0.51

Table A-4.5

Table A-4.18

Selectivities of *n*-hexane cracking as a function of temperatures at V/F (ml/ml min^{-1})

1.58, 1 atm, over 1.00g of T-345

Temperature (°C)	300.00	350.00	400.00	450.00	500.00
CMR	1.22	4.40	10.16	21.11	24.81
iC_4/nC_4	0.99	0.61	0.44	0.35	0.30
Conversion (wt%)	11.16	20.80	37.21	58.81	82.23
Selectivity (wt%)					
C_1	0.45	0.96	2.02	2.06	2.80
C_2	2.33	5.00	7.66	10.61	11.12
C_2=	7.17	10.53	12.17	16.41	20.18
C_3	21.33	26.01	21.47	18.18	15.20
C_3=	18.73	26.92	30.18	32.85	29.62
iso-C_4	8.15	3.75	2.15	1.38	1.37
n-C_4	8.24	6.11	4.84	3.89	4.56
trans-C_4=	3.32	3.27	3.52	2.87	1.99
1-C_4=	0.99	1.01	1.24	1.19	0.91
iso-C_4=	5.56	5.14	4.94	4.39	3.14
cis-C_4=	2.33	2.31	2.12	2.06	1.37
iso-C_5	0.90	0.82	0.27	0.32	0.12
n-C_5	1.79	0.96	0.30	0.20	0.91
ΣC_5=	1.16	1.63	2.07	1.16	1.08

Table A-4.19

Selectivities of *n*-hexane cracking as a function of temperatures at V/F (ml/ml min^{-1})

1.21, 1 atm, over 1.00g of T-345

Temperature (°C)	300.00	350.00	400.00	450.00	500.00
CMR	1.86	10.81	13.10	22.72	30.79
iC_4/nC_4	0.77	0.26	0.37	0.28	0.29
Conversion (%)	7.48	16.80	32.35	51.06	78.20
Selectivity (%)					
C_1	0.53	0.77	1.24	1.72	2.57
C_2	3.07	4.23	7.67	9.77	11.28
C_2=	5.35	8.51	11.34	13.87	18.04
C_3	15.64	21.01	19.63	16.69	15.74
C_3=	16.84	27.98	31.38	34.00	33.73
iso-C_4	4.81	1.25	1.55	1.12	1.04
n-C_4	6.28	4.76	4.17	3.94	3.53
trans-C_4=	3.07	3.10	3.21	3.33	2.33
1-C_4=	1.07	1.07	1.24	1.37	1.05
iso-C_4=	5.35	4.64	5.10	4.88	3.81
cis-C_4=	2.41	2.02	2.32	2.25	2.48
iso-C_5	0.94	0.42	0.46	0.29	0.12
n-C_5	1.60	0.48	0.43	0.57	1.04
ΣC_5=	5.21	4.88	2.44	1.00	0.56

Table A-4.20

Selectivities of *n*-hexane cracking as a function of temperatures at V/F (ml/ml min^{-1})

0.91, 1 atm, over 1.00g of T-345

Temperature (°C)	300.00	350.00	400.00	450.00	500.00
CMR	3.20	10.81	14.19	28.33	29.30
iC_4/nC_4	0.60	0.26	0.35	0.23	0.28
Conversion (wt%)	4.88	20.39	23.57	46.50	74.40
Selectivity (wt%)					
C_1	0.41	0.64	2.16	1.98	2.50
C_2	2.25	3.48	7.21	10.04	11.37
C_2=	7.17	7.01	9.29	12.34	16.45
C_3	16.60	17.31	16.93	15.89	15.24
C_3=	24.18	23.05	33.43	37.10	36.22
iso-C_4	3.07	1.03	1.32	0.86	1.03
n-C_4	5.12	3.92	3.78	3.68	3.67
trans-C_4=	3.69	2.55	3.56	3.57	2.66
1-C_4=	1.64	0.88	1.23	1.53	1.24
iso-C_4=	6.35	3.83	5.30	5.35	4.40
cis-C_4=	2.25	1.67	2.29	2.43	1.91
iso-C_5	2.25	0.34	0.25	0.13	0.08
n-C_5	1.43	0.39	0.34	0.41	1.25
ΣC_5=	6.76	4.02	3.48	2.15	0.77

Table A-4.21

Selectivities of *n*-hexane cracking as a function of temperatures at V/F (ml/ml min^{-1}) 0.62, 1 atm, over 1.00g of T-345

Temperature (°C)	300.00	350.00	400.00	450.00	500.00
CMR	2.18	6.50	0.50	35.95	32.65
iC_4/nC_4	1.00	0.54	41.81	0.18	0.21
Conversion (wt%)	3.27	8.31	17.26	33.21	61.23
Selectivity (wt%)					
C_1	0.61	0.72	1.45	2.10	2.11
C_2	2.14	4.21	8.00	9.76	10.26
C_2=	4.59	6.02	9.91	9.73	12.17
C_3	18.04	12.88	15.59	13.87	13.49
C_3=	22.02	32.25	0.64	37.47	36.24
iso-C_4	3.36	1.68	38.76	0.60	0.75
n-C_4	3.36	3.13	0.93	3.39	3.53
trans-C_4=	3.06	2.89	3.36	4.02	3.22
1-C_4=	1.22	1.08	3.65	1.77	1.57
iso-C_4=	5.50	4.21	5.85	6.00	5.13
cis-C_4=	3.98	1.93	2.78	2.76	2.25
iso-C_5	0.61	0.24	0.70	0.00	0.10
n-C_5	1.22	0.84	0.52	0.33	1.08
ΣC_5=	2.75	3.85	4.58	2.04	0.75

Table A-4.22

Selectivities of *n*-hexane cracking as a function of temperatures at V/F (ml/ml min^{-1})

0.56, 1 atm, over 1.00g of T-345

Temperature (°C)	300.00	350.00	400.00	450.00	500.00
CMR	8.80	2.92	9.77	34.31	31.42
iC_4/nC_4	0.56	1.24	0.37	0.17	0.19
Conversion (wt%)	3.56	6.86	14.14	26.50	52.48
Selectivity (wt%)					
C_1	6.18	0.73	1.13	1.85	1.96
C_2	2.53	3.94	6.93	9.58	10.00
C_2=	3.65	6.41	7.14	9.28	10.79
C_3	9.27	12.10	14.99	14.04	13.15
C_3=	17.98	32.80	35.22	39.85	36.68
iso-C_4	1.40	3.79	1.56	0.60	0.72
n-C_4	2.53	3.06	4.24	3.62	3.73
trans-C_4=	4.49	2.92	3.61	4.53	3.94
1-C_4=	1.12	1.02	5.66	2.00	1.94
iso-C_4=	4.49	4.37	2.76	6.79	5.81
cis-C_4=	1.97	2.04	0.71	3.13	2.61
iso-C_5	0.28	0.58	0.00	0.53	0.13
n-C_5	0.56	0.87	0.64	1.06	1.18
C_5=	1.69	6.71	4.60	1.40	0.44

Table A-4.23

Selectivities of *n*-hexane cracking as a function of temperatures at V/F (ml/ml min^{-1}) 2.59, 1 atm, over 1.00g of T-5

Temperature (°C)	300.00	350.00	400.00	450.00	500.00
CMR	2.85	5.90	7.76	19.46	46.89
iC_4/nC_4	0.77	0.61	0.42	0.30	0.20
Conversion (wt%)	6.89	15.64	32.53	52.31	75.62
Selectivity (wt%)					
C_1	0.58	0.70	1.26	1.66	2.99
C_2	1.60	3.26	6.33	9.42	11.40
C_2=	11.47	10.74	11.50	15.69	19.10
C_3	17.71	17.84	23.79	20.07	15.62
C_3=	19.88	25.00	27.48	31.03	32.76
iso-C_4	4.79	2.49	2.46	1.38	0.71
n-C_4	6.24	4.09	5.81	4.59	3.56
trans-C_4=	3.19	2.49	3.35	3.33	3.05
1-C_4=	0.87	0.96	1.14	1.30	1.45
iso-C_4=	4.93	3.84	4.89	4.55	4.10
cis-C_4=	2.03	1.85	2.21	2.24	2.14
iso-C_5	2.18	0.77	0.40	0.32	0.12
n-C_5	2.32	7.80	0.86	0.23	0.54
ΣC_5=	3.34	3.77	2.80	1.93	0.79

Table A-4.24

Selectivities of *n*-hexane cracking as a function of temperatures at V/F (ml/ml min^{-1}) 1.69, 1 atm, over 1.00g of T-5

Temperature (°C)	300.00	350.00	400.00	450.00	500.00
CMR	2.57	8.69	14.37	27.89	45.41
iC_4/nC_4	0.91	0.58	0.28	0.21	0.17
Conversion (wt%)	4.75	14.89	21.05	40.46	65.35
Selectivity (wt%)					
C_1	0.63	0.87	1.14	1.68	2.37
C_2	1.68	4.16	7.13	10.03	10.79
C_2=	9.05	11.89	10.17	13.10	15.33
C_3	12.00	16.25	19.48	18.31	14.69
C_3=	20.84	36.87	34.06	35.66	35.58
iso-C_4	4.42	1.95	1.28	0.89	0.63
n-C_4	4.84	3.36	4.56	4.23	3.70
trans-C_4=	2.95	2.89	3.80	3.76	3.50
1-C_4=	0.84	1.07	1.38	1.53	1.62
iso-C_4=	4.42	4.63	5.42	5.41	3.41
cis-C_4=	2.11	1.88	2.38	2.55	2.48
iso-C_5	1.47	0.40	0.00	0.17	0.09
n-C_5	2.32	0.74	0.52	0.20	0.66
ΣC_5=	4.42	3.96	1.52	1.63	1.97

Table A-4.25

Selectivities of *n*-hexane cracking as a function of temperatures at V/F (ml/ml min^{-1})

1.29, 1 atm, over 1.00g of T-5

Temperature (°C)	300.00	350.00	400.00	450.00	500.00
CMR	3.50	12.11	17.44	29.65	44.64
iC_4/nC_4	0.73	0.45	0.24	0.16	0.15
Conversion (wt%)	2.81	7.02	15.57	33.68	56.65
Selectivity (wt%)					
C_1	0.71	1.00	1.16	1.51	2.10
C_2	1.42	4.13	7.26	8.70	10.68
C_2=	7.83	10.40	9.51	10.04	13.22
C_3	9.61	13.53	17.92	15.02	14.47
C_3=	23.49	39.03	37.25	33.22	35.45
iso-C_4	2.85	1.28	1.03	0.68	0.58
n-C_4	3.91	2.85	4.37	4.25	3.76
trans-C_4=	2.85	2.99	3.98	4.31	3.95
1-C_4=	1.07	1.14	1.41	2.26	0.00
iso-C_4=	4.63	4.70	5.84	5.58	5.60
cis-C_4=	1.42	2.14	2.70	2.94	2.77
iso-C_5	2.14	0.43	0.51	0.98	0.11
n-C_5	2.85	0.57	0.39	0.36	0.53
ΣC_5=	5.34	2.85	1.35	2.43	1.04

Table A-4.26

Selectivities of *n*-hexane cracking as a function of temperatures at V/F (ml/ml min^{-1}) 0.98, 1 atm, over 1.00g of T-5

Temperature (°C)	300.00	350.00	400.00	450.00	500.00
CMR	4.00	15.80	21.91	35.38	45.46
iC_4/nC_4	0.50	0.38	0.22	0.15	0.13
Conversion (wt%)	1.58	5.75	13.18	25.98	46.11
Selectivity (wt%)					
C_1	1.27	0.70	1.29	1.66	1.95
C_2	0.00	3.65	7.66	9.74	10.24
C_2=	3.80	9.39	9.33	10.39	11.47
C_3	4.43	10.43	16.24	15.86	13.81
C_3=	12.03	37.22	40.82	37.68	37.13
iso-C_4	1.27	0.87	0.83	0.62	0.52
n-C_4	2.53	2.26	3.79	4.08	3.99
trans-C_4=	2.53	2.96	4.86	4.58	4.90
1-C_4=	1.27	1.04	1.67	2.00	2.41
iso-C_4=	3.16	4.52	6.30	6.51	6.38
cis-C_4=	1.90	2.09	2.73	3.19	3.54
iso-C_5	1.27	0.17	0.00	0.00	0.13
n-C_5	1.90	0.35	0.00	0.42	0.67
ΣC_5=	3.16	4.35	0.91	1.23	0.78

Table A-4.27

Selectivities of *n*-hexane cracking as a function of temperatures at V/F (ml/ml min^{-1})

0.98, 1 atm, over 1.00g of T-50.66, 1 atm, over 1.00g of T-5

Temperature (°C)	300.00	350.00	400.00	450.00	500.00
CMR	7.00	20.50	27.00	55.50	56.93
iC_4/nC_4	0.25	0.29	0.19	0.11	0.11
Conversion (wt%)	1.34	4.11	8.51	17.22	36.55
Selectivity (wt%)					
C_1	0.75	0.73	1.29	2.50	2.00
C_2	1.49	2.92	6.82	11.96	10.43
C_2=	2.99	6.33	7.76	11.32	9.74
C_3	2.99	7.06	12.69	15.97	13.02
C_3=	12.69	34.31	40.19	47.15	36.72
iso-C_4	0.75	0.49	0.59	0.46	0.39
n-C_4	2.99	1.70	3.17	4.30	3.64
trans-C_4=	2.24	2.68	4.94	5.11	4.76
1-C_4=	1.49	1.22	2.00	2.50	2.53
iso-C_4=	2.24	3.89	6.23	7.67	6.76
cis-C_4=	1.49	1.95	2.82	3.72	3.39
iso-C_5	0.75	0.24	0.24	0.00	1.20
n-C_5	2.24	0.49	0.35	0.58	0.45
ΣC_5=	6.72	1.95	1.29	3.14	0.83

Table A-4.28

Selectivities of *n*-hexane cracking as a function of temperatures at V/F (ml/ml min^{-1})

0.60, 1 atm, over 1.00g of T-5

Temperature (°C)	300.00	350.00	400.00	450.00	500.00
CMR	5.00	23.00	32.52	49.14	56.77
iC_4/nC_4	0.50	0.29	0.16	0.11	0.10
Conversion (w%)	1.17	3.99	8.22	21.11	36.25
Selectivity (w%)					
C_1	0.85	0.75	1.34	1.33	1.94
C_2	0.85	3.51	6.93	7.53	46.59
C_2=	2.56	7.27	7.66	7.44	41.24
C_3	3.42	7.77	11.92	11.23	62.65
C_3=	12.82	38.35	40.63	30.70	163.63
iso-C_4	0.85	0.50	0.49	0.33	1.58
n-C_4	1.71	1.75	3.04	2.98	15.94
trans-C_4=	1.71	2.76	4.74	3.79	21.53
1-C_4=	0.85	1.25	1.70	1.75	11.80
iso-C_4=	3.42	4.26	5.72	5.45	30.90
cis-C_4=	2.56	2.01	2.55	2.75	15.21
iso-C_5	0.85	0.25	0.00	0.00	0.00
n-C_5	1.71	0.25	0.00	0.00	1.82
ΣC_5=	59.83	2.51	0.97	3.46	3.53

Table A-4.29

Selectivities of *n*-hexane cracking as a function of temperatures at V/F (ml/ml min^{-1}) 2.53, 1 atm, over 1.00g of T-15

Temperature (°C)	300.00	350.00	400.00	450.00	500.00
CMR	0.57	1.76	3.45	8.26	28.52
iC_4/nC_4	0.91	0.79	0.83	0.40	0.49
Conversion (w%)	15.98	23.08	56.14	80.95	92.84
Selectivity (w%)					
C_1	0.56	0.74	1.37	2.61	3.23
C_2	1.75	3.51	6.95	8.04	12.03
C_2=	4.94	8.58	11.83	14.38	24.98
C_3	27.60	29.77	30.64	18.64	17.22
C_3=	9.82	18.24	19.72	24.97	26.96
iso-C_4	12.83	7.28	5.84	3.03	1.41
n-C_4	14.14	9.23	7.07	7.66	2.89
trans-C_4=	2.63	3.42	2.85	2.38	1.96
1-C_4=	0.50	0.69	0.75	1.42	0.65
iso-C_4=	4.26	4.85	4.03	3.32	2.73
cis-C_4=	1.63	2.04	1.76	2.32	1.27
iso-C_5	3.69	1.47	0.94	0.68	0.12
n-C_5	4.38	1.60	0.71	0.73	0.32
ΣC_5=	2.63	2.56	2.80	1.52	0.62

Table A-4.30

Selectivities of *n*-hexane cracking as a function of temperatures at V/F (ml/ml min^{-1}) 1.65, 1 atm, over 1.00g of T-15

Temperature (°C)	300.00	350.00	400.00	450.00	500.00
CMR	0.93	2.77	6.88	15.24	31.22
iC_4/nC_4	0.80	0.70	0.56	0.44	0.37
Conversion (wt%)	11.04	14.90	39.37	61.74	86.85
Selectivity (wt%)					
C_1	0.54	0.74	1.32	1.77	2.82
C_2	1.90	3.56	7.19	9.62	11.55
C_2=	5.89	8.52	13.16	16.50	23.02
C_3	24.37	23.83	25.50	19.26	16.70
C_3=	14.67	24.16	26.62	30.27	31.01
iso-C_4	8.97	4.63	3.15	1.83	1.20
n-C_4	11.14	6.64	5.66	4.13	3.26
trans-C_4=	3.44	3.76	3.30	3.16	2.51
1-C_4=	0.72	0.94	1.04	1.07	0.88
iso-C_4=	5.98	5.64	4.80	4.79	3.45
cis-C_4=	2.08	2.28	2.13	2.45	1.66
iso-C_5	2.36	0.74	0.48	0.29	0.14
n-C_5	3.17	1.01	0.46	0.19	0.07
ΣC_5=	3.80	2.48	2.26	1.31	1.27

Table A-4.31

Selectivities of *n*-hexane cracking as a function of temperatures at V/F (ml/ml min^{-1})

1.27, 1 atm, over 1.00g of T-15

Temperature (°C)	300.00	350.00	400.00	450.00	500.00
CMR	1.27	4.62	9.69	19.44	36.88
iC_4/nC_4	0.73	0.54	0.45	0.35	0.28
Conversion (wt%)	8.15	12.98	32.46	57.42	78.23
Selectivity (wt%)					
C_1	0.49	0.77	1.11	1.69	2.57
C_2	1.84	4.16	6.22	9.44	11.21
C_2=	5.77	8.94	10.87	14.94	20.63
C_3	20.98	22.73	19.59	17.66	15.72
C_3=	16.93	30.59	26.03	32.32	34.02
iso-C_4	6.38	3.00	1.88	1.34	0.93
n-C_4	8.71	5.55	4.22	3.80	3.32
trans-C_4=	3.68	4.01	4.19	3.62	2.88
1-C_4=	0.86	1.16	2.99	1.57	1.04
iso-C_4=	6.38	6.24	5.24	5.68	3.95
cis-C_4=	2.21	2.47	2.37	3.24	1.89
iso-C_5	1.72	0.46	0.31	0.23	0.42
n-C_5	2.45	0.77	0.31	0.19	0.17
ΣC_5=	3.80	2.23	1.29	1.15	0.78

Table A-4.32

Selectivities of *n*-hexane cracking as a function of temperatures at V/F (ml/ml min^{-1})

0.95, 1 atm, over 1.00g of T-15

Temperature (°C)	300.00	350.00	400.00	450.00	500.00
CMR	1.58	6.20	12.73	23.14	41.88
iC_4/nC_4	0.75	0.48	0.35	0.30	0.22
Conversion (wt%)	6.72	9.24	22.73	51.04	69.16
Selectivity (wt%)					
C_1	0.60	0.76	1.06	1.74	2.39
C_2	2.23	4.33	6.03	9.58	10.84
C_2=	6.10	8.33	9.72	14.07	18.26
C_3	20.24	19.91	16.81	16.91	14.98
C_3=	20.54	34.09	28.90	35.05	36.63
iso-C_4	5.65	2.16	1.32	1.10	0.75
n-C_4	7.59	4.55	3.78	3.70	3.41
trans-C_4=	4.02	4.11	3.26	3.43	3.27
1-C_4=	1.04	1.19	1.28	1.25	1.24
iso-C_4=	7.29	6.39	5.41	6.43	4.53
cis-C_4=	2.53	2.60	2.11	3.62	2.18
iso-C_5	1.19	0.00	0.26	0.20	0.00
n-C_5	1.79	0.54	0.26	0.20	0.38
ΣC_5=	5.65	1.73	4.62	1.12	0.58

Table A-4.33

Selectivities of *n*-hexane cracking as a function of temperatures at V/F (ml/ml min^{-1})

0.64, 1 atm, over 1.00g of T-15

Temperature (°C)	300.00	350.00	400.00	450.00	500.00
CMR	2.70	9.33	18.89	30.94	54.66
iC_4/nC_4	0.59	0.38	0.29	0.23	0.16
Conversion (wt%)	3.99	5.16	20.27	44.78	57.38
Selectivity (wt%)					
C_1	0.50	0.71	1.13	1.74	2.21
C_2	1.75	3.39	6.51	9.74	10.23
C_2=	4.51	5.88	9.13	12.01	15.18
C_3	13.53	13.37	14.75	14.98	13.25
C_3=	19.55	30.12	34.73	39.12	38.04
iso-C_4	2.51	1.07	0.89	0.76	0.51
n-C_4	4.26	2.85	3.06	3.33	3.12
trans-C_4=	3.26	3.21	3.21	3.89	4.50
1-C_4=	0.75	0.89	1.13	1.92	2.14
iso-C_4=	5.76	4.99	4.69	5.83	5.05
cis-C_4=	2.01	2.14	2.07	2.81	2.54
iso-C_5	0.50	0.36	0.00	0.20	0.09
n-C_5	1.25	0.71	0.00	0.13	0.35
ΣC_5=	3.51	3.92	1.13	0.76	0.63

Table A-4.34

Selectivities of *n*-hexane cracking as a function of temperatures at V/F (ml/ml min^{-1})

0.58, 1 atm, over 1.00g of T-15

Temperature (°C)	300.00	350.00	400.00	450.00	500.00
CMR	2.75	9.83	20.43	34.57	55.54
iC_4/nC_4	0.57	0.42	0.27	0.21	0.16
Conversion (wt%)	3.67	3.56	17.93	33.56	53.4
Selectivity (wt%)					
C_1	0.00	3.65	1.12	1.85	2.17
C_2	1.63	8.15	6.36	9.95	10.15
C_2=	4.36	1.97	8.48	11.89	14.72
C_3	11.44	4.21	13.78	14.72	13.20
C_3=	19.07	10.96	34.58	40.70	38.50
iso-C_4	2.18	1.40	0.78	0.69	0.49
n-C_4	3.81	3.30	2.84	3.34	3.13
trans-C_4=	3.00	2.53	4.02	3.90	3.80
1-C_4=	0.82	1.40	2.45	1.43	1.91
iso-C_4=	5.18	3.65	5.19	5.54	4.98
cis-C_4=	1.91	1.97	2.23	2.53	2.43
iso-C_5	0.82	0.00	0.00	0.27	0.00
n-C_5	1.09	1.69	0.28	0.57	0.34
ΣC_5=	5.18	7.58	1.12	0.80	0.64

Table A-4.35

Selectivities of *n*-hexane cracking as a function of temperatures at V/F (ml/ml min^{-1}) 1.47, 1 atm, over 1.00g of T-20

Temperature (°C)	300.00	350.00	400.00	450.00	500.00
CMR	0.89	3.19	6.82	16.39	30.25
iC_4/nC_4	0.84	0.59	0.55	0.42	0.36
Conversion (wt%)	15.95	16.82	35.44	62.45	87.86
Selectivity (wt%)					
C_1	2.19	0.71	1.27	1.87	2.96
C_2	2.13	4.10	7.00	10.15	11.75
C_2=	5.39	8.26	11.74	16.85	21.80
C_3	25.64	25.21	23.11	19.30	16.29
C_3=	12.92	23.66	24.94	30.07	31.08
iso-C_4	10.97	4.10	2.93	1.76	1.21
n-C_4	13.04	6.90	5.30	4.16	3.35
trans-C_4=	3.01	4.52	3.13	3.19	2.45
1-C_4=	0.69	1.13	0.96	1.01	0.80
iso-C_4=	5.08	5.77	4.40	4.42	3.39
cis-C_4=	1.82	2.44	2.23	2.05	1.58
iso-C_5	2.76	1.01	0.85	0.30	0.14
n-C_5	3.45	0.24	0.34	0.19	0.61
ΣC_5=	4.26	3.45	2.26	1.43	0.89

Table A-4.36

Selectivities of *n*-hexane cracking as a function of temperatures at V/F (ml/ml min^{-1}) 1.13, 1 atm, over 1.00g of T-20

Temperature (°C)	300.00	350.00	400.00	450.00	500.00
CMR	1.26	2.05	2.32	13.79	30.69
iC_4/nC_4	0.64	0.90	1.07	0.48	0.32
Conversion (wt%)	6.75	14.59	31.58	57.01	85.99
Selectivity (wt%)					
C_1	0.44	0.96	0.70	1.58	2.70
C_2	1.93	3.50	3.93	8.09	11.76
C_2=	5.63	5.96	6.24	12.59	19.80
C_3	20.74	16.93	11.78	14.56	15.98
C_3=	13.78	21.04	15.67	25.78	34.54
iso-C_4	6.37	5.07	4.69	1.61	1.12
n-C_4	9.93	5.62	4.37	3.39	3.44
trans-C_4=	3.41	3.98	1.99	2.75	2.78
1-C_4=	0.74	2.95	0.66	0.86	0.97
iso-C_4=	5.78	0.82	2.79	3.75	3.90
cis-C_4=	2.22	1.78	1.39	1.79	1.78
iso-C_5	2.37	0.62	0.00	3.30	0.00
n-C_5	3.41	16.24	0.00	0.35	0.55
ΣC_5=	4.89	2.06	0.73	1.77	0.44

Table A-4.37

Selectivities of *n*-hexane cracking as a function of temperatures at V/F (ml/ml min^{-1})

0.84, 1 atm, over 1.00g of T-20

Temperature (°C)	300.00	350.00	400.00	450.00	500.00
CMR	1.53	3.00	12.80	23.38	29.12
iC_4/nC_4	0.67	0.61	0.39	0.27	0.30
Conversion (wt%)	8.1	6.45	28.08	45.42	79.02
Selectivity (wt%)					
C_1	0.49	0.00	1.32	1.74	2.47
C_2	1.98	2.48	7.55	9.47	11.30
C_2=	5.68	4.03	11.18	13.50	17.55
C_3	21.36	11.47	18.66	16.07	15.36
C_3=	17.28	23.26	32.83	32.98	36.08
iso-C_4	5.31	2.17	1.57	1.06	1.08
n-C_4	7.90	3.57	4.02	3.85	3.59
trans-C_4=	3.46	2.95	3.17	3.59	3.11
1-C_4=	0.86	0.00	1.03	1.14	1.08
iso-C_4=	6.30	4.50	4.59	4.87	3.11
cis-C_4=	2.35	2.64	2.03	2.31	4.35
iso-C_5	0.25	2.33	0.21	0.22	2.02
n-C_5	1.23	1.55	0.28	2.00	0.10
ΣC_5=	2.84	2.17	1.42	1.61	0.57

Table A-4.38

Selectivities of *n*-hexane cracking as a function of temperatures at V/F (ml/ml min^{-1})

0.57, 1 atm, over 1.00g of T-20

Temperature (°C)	300.00	350.00	400.00	450.00	500.00
CMR	1.68	4.78	10.73	20.65	253.43
iC_4/nC_4	0.81	0.53	0.43	0.31	0.28
Conversion (wt%)	5.23	6.26	20.61	37.32	62.65
Selectivity (wt%)					
C_1	0.38	0.48	1.07	1.74	2.30
C_2	1.91	2.88	6.26	9.32	0.11
C_2=	4.78	3.51	8.30	11.07	0.14
C_3	15.49	10.54	14.26	14.20	0.14
C_3=	18.74	19.49	29.55	35.88	0.37
iso-C_4	4.21	1.44	1.46	1.07	0.01
n-C_4	5.16	2.72	3.40	3.43	0.04
trans-C_4=	3.25	4.15	3.06	4.07	0.04
1-C_4=	0.76	0.80	1.16	1.90	0.01
iso-C_4=	5.74	3.83	4.27	5.23	0.05
cis-C_4=	2.10	1.76	1.99	2.41	0.02
iso-C_5	0.76	0.32	0.05	0.00	0.00
n-C_5	1.34	0.96	0.29	0.24	0.01
ΣC_5=	5.54	12.14	1.16	0.48	0.01

Table A-4.39

Selectivities of *n*-hexane cracking as a function of temperatures at V/F (ml/ml min-1) 0.52, 1 atm, over 1.00g of T-20

Temperature (°C)	300.00	350.00	400.00	450.00	500.00
CMR	2.45	3.28	18.07	31.75	30.09
iC_4/nC_4	0.58	0.95	0.28	0.20	0.25
Conversion (wt%)	4.3	5.73	15.93	34.35	66.59
Selectivity (wt%)					
C_1	0.00	1.57	1.13	1.69	2.24
C_2	1.86	4.19	6.65	9.52	10.87
C_2=	4.42	4.54	8.10	10.98	13.10
C_3	12.56	11.87	13.50	14.26	13.88
C_3=	17.21	26.53	32.20	37.03	38.37
iso-C_4	2.56	3.14	0.88	0.70	0.87
n-C_4	4.42	3.32	3.14	3.44	3.48
trans-C_4=	3.26	3.14	3.20	3.70	3.83
1-C_4=	0.93	0.87	1.13	1.25	1.40
iso-C_4=	6.05	4.89	4.58	5.12	5.33
cis-C_4=	2.09	2.09	2.13	2.45	2.49
iso-C_5	0.70	2.09	0.00	0.29	0.69
n-C_5	1.40	14.83	0.31	0.29	0.47
ΣC_5=	3.02	3.14	1.76	0.79	0.83

REFERENCES

1. Gates, B.C, Katzer, J. R and Schuit G. C. A, "Chemistry of Catalytic Process". MeGraw, New York, 1979.

2. Weisz, P.B., Pure Appl. chem., **52** 2091(1980)

3. Chen, N.Y and Garwood, W. E Catal. Rev.-Sci. Eng., **28**, 185(1986)

4. Holderich, W.F., Pure Appl. Chem., **58**, 1383(1986).

5. Bekkum, H.V. and Kouwenhowen, Stud. Surf. Sci. Catal., **41**, 45(1988).

6. Jacobs, P.A.; Jacobs J. M. and R. Parton, in "Proc. Int. Symp. On Zeolites as catalyst, sorbents, and detergent builders"; Wurburg FRC 1988 Elsvier, Amsterdam 163 1989.

7. Greensfelder, B. S.; Voge, H. H.; Good, G. M., Ind. Eng. Chem., **41**, 2573(1949).

8. Poutsma, M. L.; Zeolite Chemistry and Catalysis eds: (Rabo, J. A.), ACS Monography Washington DC 117, 1976.

9. Maxwell, I. E., Stud. Surf. Sci. Catalysis, **58**, 571(1991)

10. Barrer, R. M. Hydrothermal Synthesis of Zeolites, Academic Press New York, 1982.

11. Smith. J.V., Origin and structure of zeolites in zeolite chemistry and catalysis, Rabo, J. A. Ed., Am. Chem. Soc. Monogr. 171, 1976.

12. Avelini Corma, from microporous to mesoporous molecular sieve and their use in catalysis, Chemical Reviews, 1997, **97**(6), 2373-2419.

13. Kokotailo, G. T.; Lawton, et al.; Structure and synthetic zeolite ZSM-5. Nature, **272**, 437-438(1978).

14. Chang, C. D.; Catal. Rev.-Sci. Eng., **25**, 1-118(1983).

15. Kiem, K. H.; Maziuk, J.; Tonnessmann, A.; Er dol.; Kohle Er dgas., Petrochem., **37**, 558-562 (1984).

16. Yanik, S. Y; Dammel, E. J.; Humphries A. P. and R.J Campagna, Oil Gas J. 83 **19**, 108-117(1985).

17. Weisz, P. B., Proc. 7th Int. Congr. Catalysis, Tokyo, paper PI, 1980.

18. Jacobs, Peter A.. J. Chem. Soc. Chem. Comm., 591-593(1991).

19. G. Bellusi; et al, Stud. Surf. Sci, and Catalysis, **84**, 85-92(1994).

20. Cronstedt, Acad. Handl. Stockholm **17** 120(1756).

21. Lowenstien, N.; Am. Mineral, **39**, 92(1954)

22. Breck, D.W., Zeolite Molecular Sieves: Structure Chemistry and Use, John Wiley, London, 1974.

23. Wilson, S. T.; Lok, B. M.; Messina, C.A.; Cannan, T.R.; Flanigen, E.M.; J. Am. Chem. Soc. 1982, **104**, 1146-1147.

24. Lok, B. M.; Messina, C.A.; Lyle Patton, R.; Gajek, R. T.; Cannan, T.R; Flanigen, E.M; J Am Chem. Soc. **106**, 6092-6093 (1984).

25. Wilson, S. T. and Flanigen, E. M., ACS Symp. Ser., 398, 329(1989)

26. Flanigen, E. M; Lok, B. M.; Patton, R.L.; Wilson, S. T. Pure & Appl. Chem., **58** 1351 (1986).

27. Barrer, R. M. J. Chem. Soc., 127, 1948.

28. Barrer, R. M. and Denny, P. J., J. Chem. Soc., 971, 1961.

29. Kerr, G. T. and Kokotailo, G. T., J. Am. Chem. Soc., **83**, 4675(1961).

30. Kerr, G. T. Inorganic Chem., **5**, 1537(1966).

31. Wadlinger, R. L.; Kerr, G. T. and Rosinki, E. J.,US Patent 3, 308, 069 (1967)

32. Kokotailo, G. T.; Chu, P.; Lawton, S. L., Nature, **275**, 119-120(1978).

33. Argauer, R.G. and Landolt, G. R. U. S. Patent 3, 308, 069(1972).

34. Flanigen, E. M.; Bennett, J. M.;. Grose, R. W; Cohen, J. P.; Patton, R. L.; Kirchner, R. M.; Smith, J. V. Nature, **271**, 512(1978).

35. Davis, M. E.; Saldarriaga, C.; Montes, C.; Garces J. and Crowder, C. Nature **331**, 698, (1988).

36. Estermann, M.; McCusker, L. B.; Bacerlocher, Ch.; Merrouche, A. and Kesslaer, H, Nature **352**, 320, 1991.

37. Jones, R. H.; Thomas, J. M.; Chen, J.; Xu, R.; Huo, Q.; Li, S.; Ma, Z.; Chippindale, A.M. J. Stat. Chem. **102**, 204, (1993).

38. Freyhardt, C.C; Tsapatsis, M.; Lobo, R.F.; Balkus, K. J., Jr.; Davies, M.E. Nature **381**, 295(1996).

39. Vaughan, D.E. W and Lussies, R. J., in Proc. of the 5th Int. Conf. on Zeolites (L.V. C. Rees eds.) Heyden London 1980. 94.

40. Occelli, M. L.; Takolama, K.; Yokoyama, M. and Hirao, S., in Expanded Clays and Other Microporous Materials (M. L. Occelli, and H. Robson, eds) Van Nostrand New York, 1992, 57.

41. Sing, K.S.W.; Everelt, D. H.; Haul, R.H.W.; Moscou, L.; Pierotti, R.A.; Rouquerol, J.; Siemieniewska, T., Pure Appl. Chem. **57**, 603 (1985).

42. Cartilidge, S.; Nissen, H. V.; Wessieken, R. Zeolites, **9**, 346(1989).

43. Beryerlain, R. A.; Choi-feng, C.; Hall, J. B.; Huggins, B. J.; Ray, G. J. ACS Symp. Series, **571**, 81(1994).

44. Corma, A. Stud. Surf. Sci. Catal, **49**, 49(1989).

45. Yangisawa, T.; Sohimizu, T.; Kiroda, K.; Kato, G.; Bull. Chem. Soc. Japan, **63**, 988-992(1990).

46. Beck, J. S et al J. Am. Chem. Soc., **114**, 10834-10843(1992).

47. Kresge, C.T.; Leonowicsz, M. E.; Roth, W. J.; Vartuli, J. C.; Beck, J.S.; Nature, 359,710-712(1992). (b). Zhao, X. S; Lu, G. Q. and Millar, G. J Ind. Eng. Chem. Res. **35**, 2075-2090(1996)

48. Zhao, S. U. et. al Ind. Eng. Chem. Res. **35**, 2075-2090(1996).

49. Meier, W.M., Molecular Sieve, Society for Chemical Industry, London, 10 (1968).

50. Kokotailo, G. T.; Lawton, S.L. and Olson, D.H., Nature **272**, 437-438(1978).

51. Meier, W. M., and Olson, D. H., Atlas of Zeolite Structure and Types, 2nd ed., Butterworths, 1987.

52. Derouane, E. G., and Gabelica, J. Catal., **65**, 486(1980).

53. Dejaifre, P.; vedrine, J. C. and Derouane, E. G., J. Catal., **63**, 331(1980).

54. Thomas, J. M. ; Millward, G. R., J. Chem. Soc. Chem. Commun., 1380(1982).

55. Csicsery, S. M., Zeolites, **4**, 202(1984).

56. Derouane, E. G., and Gabelica, J. Catal., **65**, 486(1980).

57. Chen, N. Y., and Garwood, W.E., Catal. Rev.-Sci. Eng., **28**, 185(1986).

58. Chen, N. Y., and Garwood, W.E., J. Catal., **52**, 453(1978).

59. Frilette, V.J.; Haag, W. O. and Lago, R. M. J. Catal., **67**, 218(1981).

60. Inui, T.; Suzuki, T.; Inoue, M.; Murakamo, Y. ;Takegami, Y., Structure and Reactivity of Modified Zeolites. Jacobs et al eds., Elsevier, Amsterdam 1984, 201.

61. Derouane, E.G.; Dejaifue, P.; Gabelica, Z.; Vedrine, J.C., Disc. Faraday Soc., **72**,331(1981).

62. Vedrine, J.C.; Auroux, A.; Coudurier, G.; Engelhard, P.; Gallez, J.P; Szavbo, G., Proc. 6th Int. Conf. on Zeolites, Bisio eds. Butterworth Guildford, V. K 497(1984).

63. Auroux, A.; Wierzchowski, P.; Gravelle, P. C., Thermchim Acta. **32**, 165, 1979.

64. Sayed, M. B.; Cooney, R.P. Aust. Chem., **35**, 2483, 1982.

65. Anderson, J. R.; Foger, K.; Mole, T.; Rajadlyaksha, R.; Sanders, J.V., J. Catal. **58**, 114(1979).

66. Nayak, V.S; Choudhary, Y. R., Appl. Catal., **4** 33, 1982.

67. Bibby, D. M.; Aldridge, L. P.; Milestone, N. B., J. Catal., **72**, 373, 1981.

68. Wang, I.; Chen, T.; Chao, K.; Tsai, T., J. Catal., **60** 140 1979.

69. Rajakhyksha, R. A.; Anderson, J.R., J. Catal., **63** 510 1980.

70. Chu, C. T.; Chang, C. D., J. Phys. Chem. **89**, 1569, (1985).

71. Uytterhoeven, J. B.; Jacobs, P. A;. Makay, K; Schoonheydt, R., J. Phys. Chem. 72 1768.

72. Barrer, R. M., J. Chem. Soc., 2340(1950); Nature 164 112(1949).

73. Barrer, R. M., and Kanellopoulos, A. G., J. Chem. Soc. A, 775(1970).

74. Chang, C. D.; Chu, C. T.; Miale, J. N.; Bridger, R. F.; Calvert, R. B., J. Am. Chem. Soc., **106**, 8143(1984).

75. Jacobs, P. A.; von Ballmoos, R., J. Phys. Chem., **86**, 3050 (1982).

76. Bibby, D.M.; Dale, M. P., Nature, **317**, 157(1985).

77. Dai, F. Y.; Suzuki, M.; Takahashi H. and Saito, Y., Stud. Surf. Sci. Catal., **28**, 223(1986).

78. Derouane, E. G.; and Gabelica, Z., J. Solid State Chem. **64**, 296(1986).

79. Jacobs, P. A., and Martens, J. A., "Synthesis of High-Silica Aluminosilicate Zeolites", Elsevier, The Netherlands, 1986.

80. Szostak, R., "Molecular Sieves: Principle of Synthesis and Identification", Van Nostrand Reinhold Catalysis series, 1989.

81. Erdem, A.; Sand, L. B.; J. Catal. **60**, 241(1971).

82. Lecluze, V. and Sand, L. B., Recent. Progress Report. 5th Int. Conf. Zeolites, Naples, R. Sersale C. Colella, R. Aiello, eds., 41(1980).

83. Rollmann, L. D., "Zeolites: Science and Technology", F. R. Ribeiro, A. E. Rodrigues, L. D. Rollmann and C. Naccache, eds., M. Nijhoff, Den Haag, 109(1984).

84. V. N. Romannikov, V. M. Mastikhin, S. Hocevar and B. Drzaj, Zeolites **3**, 311(1983).

85. Chao K. J.; Tasi, T.S. Chen, M. S.; Wang, I., J. C. S. Faraday I **3** 547-555(1981).

86. Chen, N. Y.; Miale, J. N., and Reagan, W. J., U.S.P. 4,112,056 (1978).

87. Kukarni, S. B. et al., Zeolites, **2**, 313(1982).

88. Wilkosz, J.; Stobiecka, E. and Dudek, B.; Cryst. Res. Technol., **25**(3), 251(1990).

89. Kukarni, S. J.; H. Hattori, and K. Tenabe, Applied catalysis **49**, 27-44(1989).

90. Lok, B. M.; Cannan, T. R. and Messina, C. A. Zeolites, **3**, 282, (1983).

91. Rollmann, V Adv. Chem. Ser., **173**, 131(1979).

92. Draya, A. and Lowe, B. M., Zeolites, **6**, 111-118(1986).

93. van Santen, R. A.; Keijsper, J. Ooms. G., Stud. Surf. Sci. Catal., **28**, 196(1986).

94. Mostowicz, R., and Sand, L. B., Zeolites, **2**, 143(1982).

95. Ueda, S.; Kageyama, W. and Koizumi, M.; Proc. 6th int. Zeolite Conf., 1984, 905.

96. Barrer, R. M.; Baynham, J. W.; Bulfitude, F. W and Meier, W. M. J. Chem. Soc., 195(1959).

97. Kerr, G. T. J. Phys. Chem., **70**, 1047(1966).

98. Kerr, G. T. J. Phys. Chem., **72**, 1385(1968).

99. Culfas, A. and Sand, L. B., Molecular sieves, Adv. Chem. Ser., **121** 140(1973).

100. Cournoyer, R.A.; karnick, W. L.; and Sand L.B., J. Phys. Chem., **79**, 1578(1975).

101. Freund, E. F.; J. Crystal Growth, **34**, 11(1976).

102. Wang, I. J., J. Chem. Soc., Faraday 1, **77**, 547(1981).

103. Zhadanov, S. P., Adv. Chem. Ser., **100**, 20(1971).

104. Zhadanov, S. P. and Samulevich, N. N., in Proceed. 5th Int., Zeolite Conf., Ed. L. V. Rees, Heyden London, 75, 1980.

105. Kacirek H. and Lechert, H., J. Phys. Chem., **79**, 1975, 1589.

106. Testa, F.; Szostak, Chiappeta, R.; Aiello, R.; Fonseca, A. and Nagy, J.B., Zeolites, **18**, 106(1997).

107. Breck, D.W.; Flanigen, E.N., Molecular Sieves, Soc. Chem. Ind. London, 42(1968).

108. McNicol, B. D.; Pott, G. T.; Loos, K. R. and Mulder, N., Molecular Sieves, Adv. Chem. Ser., **121**, 152(1973).

109. Xu W.; Li, J.; Li, W.; Zhang H. and B. Liang, Zeolites, **9**, 468(1989).

110. Mostowicz, R.; Sand, L. B., Zeolites **2**, 143(1982)

111. Ghamami. M.; Sand, L. B., Zeolites, **3**, 155(1983).

112. Zelimir Gabelica and Eric G. Derouane, ACS Symposium Series 248 Catalytic Material: Relationship Between Structure and Reactivity. Am. Chem. Soc., 220-251(1984).

113. Derouane, E. G.; Detremmerie, S.; Gabelica, Z and Blom, N. Appl. Catalysis, **1**, 201-224(1981).

114. Iton, L. E. ; Trouw, F.; Brun, T. O. and Epperson, J. E. Langmuir, **8**, 1045(1992).

115. Bodart, P.; Nagy, J.B.; Gabelica, Z.; Derouane, E.G., J. Chim. Phys.1986, **83**, 777.

116. Flanigen, E. M., Proc. 5th Int. Conf. Zeolites, L.V.C Rees, Editor, Heyden, London, 1980, page 760.

117. Gies, H. and Marler, B. Zeolites, **12**, 42(1992).

118. Burkett, S. L. and Davis, N.E. J. Am. Chem. Soc., **117**, 3766(1995).

119. Frank, H. S. and Evans, M. W. J. Chem. Phys., **13**, 50(1945).

120. Muller, N.; Acc. Chem. Res., **23**, 23(1990).

121. Mintova, S.; Valtchev, V. ; Vultcheva, E.; Veleva, S.; Zeolites, **12**, 210-215, 1992.

122. Jacobs, P. A.; in Zeolite Microprous Solids: Synthesis, Structure and Reactivity, Eds. E. G. Derouane, F.lemos, C. Naccache and F. R. Ribeiro, NATO ASI ser. 352, Kluwer Academic Publishers, Dordrecht, 3, 1992.

123. Zhadanov, S. P. and Samulevich, N. N. ; in Proceed. 5th Int., Zeolite Conf., Ed. L. V. Rees, Heyden London, 75, 1990.

124. Gulfaz, A. and Sand, L. Adv. Chem. Ser., **121**, 1973, 140.

125. Chao, Kuei-Jung ; Tasi, Tseng Chang and Chen, Mei-shu; J. Chem. Soc., Faraday Trans. 1, 1981, 77, 547-555.

126. Barret, P. Heterogeneous Reaction Kinetics, Mir Moscow, 195,1976.

127. Gult, J. L. ; Caullet, P. ; Seive, A. ; Patarin, J. and Delprato, F.; in Guidelines for Mastering the Properties of Molecular Sieves, EDS. Barthomeuf et al., Plenum Press New York, 69, 1990.

128. McCormick , A.V. and Bell, A. T. Catalysis. Rev-Sci. Eng **31**(1 and 2) 97, 1989.

129. Scholle, K. F.M. G.; Veeman, W. S.; Franken, P.; Velden, G. P. M.; Vander, Applied Catalysis, **17** (1985), 233-259.

130. Coudurier, G. ; Naccache, C.; Verdrine, J. C.; J. C. S. Chem., Comm. (1982) 1413.

131. Oslon, D. H.; Haag, W.O, and Logo, R.M., J. Catal., **61**, 390(1980).

132. Abbot, J. and Wojciechowski, B. W., J. Catal., **113**, 353 (1988).

133. Wieler, A.F. H.; Vaarkamp. M.; Post; M. F. M; J.of Catalysis, (1991) **127**, 51-66.

134. Lukyanov, D.B.; J. Catal. **145**, 54(1994).

135. Lukyanov, D.B.; Shtral, V. I.; Khadzhiev, S. N.; J. Catal. **146**, 87(1994).

136. Greenfelder. B. S. and Voge, H. H., Ind. Eng. Chem. 37, 983, 1038(1945)

137. Thomas, C. L. Ind. Eng. Chem. **41**, 2564(1949).

138. Hattori, H.; Takahashi, O.; Tagaki, M. and Tanabe, K.; J. Catal., 68, 132,1981.

139. Haag, W. O.; Lago, R. M.; and Weisz, P. B.; Nature, **309**, 589, 1984.

140. Haag, W.O.; Dessau, R. M., Proceed. of 8th Int. Congr. on Catalysis, Dechema, Berlin **2** 305(1984).

141. Shertukde, P. V.; Marcelin, G.; Sill, G. A.; Hall, W. K.; J. Catal., **136**, 446, 1992.

142. Lambardo, E. A.; Pierantozzi, R. and Hall, W. K.; J. Catal., **110**, 171, 1988.

143. Lambardo, E. A., and Hall, W. K., J. Catal., **112**, 171 ,1988.

144. Olah, G.A.; Halpern, Y.; Shen, J. and Mo, K.; J. Am. Chem. Soc., **95**, 4960(1973).

145. Whitemore, F. C., Ind. Eng. Chem. **26**, 94, 1934.

146. March, J., "Advanced Organic Chemistry." Wiley, New York, 1985.

147. Pansing, W. F., J. Phys. Chem., **69**, 392, 1966.

148. Narbeshuber, T.F; Brait, A.; Seshan, K.; Lercher, J. A.; Appl. Catal. A: Gen **146**, 119(1996).

149. Brait, A.; Koopmans, A.; Weinstabe, H.; Ecker, A.; Seshan, K.; Lercher, J. A.; Ind. Eng. Chem. Res., **37**, 873(1998).

150. Tung, S. E.; McIninch, E. J.; J. Catal. **16**, 166(1968).

151. Corma, A.; Fornes, V.; Martinez, A.; Orchilles, A. V.; ACS Symp. Ser. **368**, 542(1988).

152. Corma, A.; Monton, J. B.; Orchilles, A. V.; Appl. Catal. **23**, 255(1986).

153. Corma A; Planeless ,J.; Sanchez-marin, J.; Thomas F; *J. of Catal.* **93**, 30(1985).

154. Abbot ,J.; and Wojchechowski, B.W; Canad. J. of Eng. **66**, 825(1988).

155. Jolly, S; Saussey, J.; Bettahar, M. M.; Lavelly, J. C.; and Benazzi, E., Appl. Catal A: General **156**, 71-96(1997).

156. Wojchechowski, B.W.; Catal., Rev. Sci. Eng **40**(3), 209-328(1998).

157. Varlagadda, P.; Lund, C.R.F and Ruckenstein, E., *J. Catal.* **60**, 28-41.

158. Riekert, L and Zhou, J.; J. Catal. **137**, 437(1992).

159. Rao, C.N.R; Chemical Application of Infrared Spectroscopy; Academic Press Lodon, 533-550(1963).

160. Jasense, J. C. ; vander Gaag, F. F. and Bekkum, H. Zeolites, 4, 369-372(1984).

161. Jacobs, P. A.; Bayer, H. K. and Valyon, J. Zeolites. 1, 161(1981).

162. Shukla, D. B. and Pandya, V. P., J. Chemical Tech. Boitech. 44, 147(1989).

163. Miale, J. N; Chen, N.Y; and Wiesz, P. B., J. Catalysis 60, 390(1980)

164. Borade, R. B,; Hedge, S.G; Kulkarni, S. B; and Ratrasamy, P. Applied Catal. 13, 27(1984).

165. Yarlagada, Prasad ; Carl, R. F. ; Ruckenstein, E. ; J. Catal. 133, 28-41(1992)

166. Mirodatos, C. and Barthomeuf, D., J. Catal. **114**, 121(1989).

VITA

- Yunusa Umar
- Born in Sunkuso, Nigeria.
- Received Bachelor of Science in Chemistry at Ahmadu Bello University, Zaria, Nigeria in November 1995.
- Joined King Fahd University of Petroleum and Minerals (KFUPM), Dhahran Saudi Arabia in 1998 as a Research Assistant.
- Received Master of Science degree in Chemistry at KFUPM in May 2001.